Open Conference Proceedings
1 | 2022

Vision and Strategies for Reinforcing Additively Manufactured Concrete Structures

4 November 2021 – Dresden, Germany

Editors:

Asko Fromm

Viktor Mechtcherine

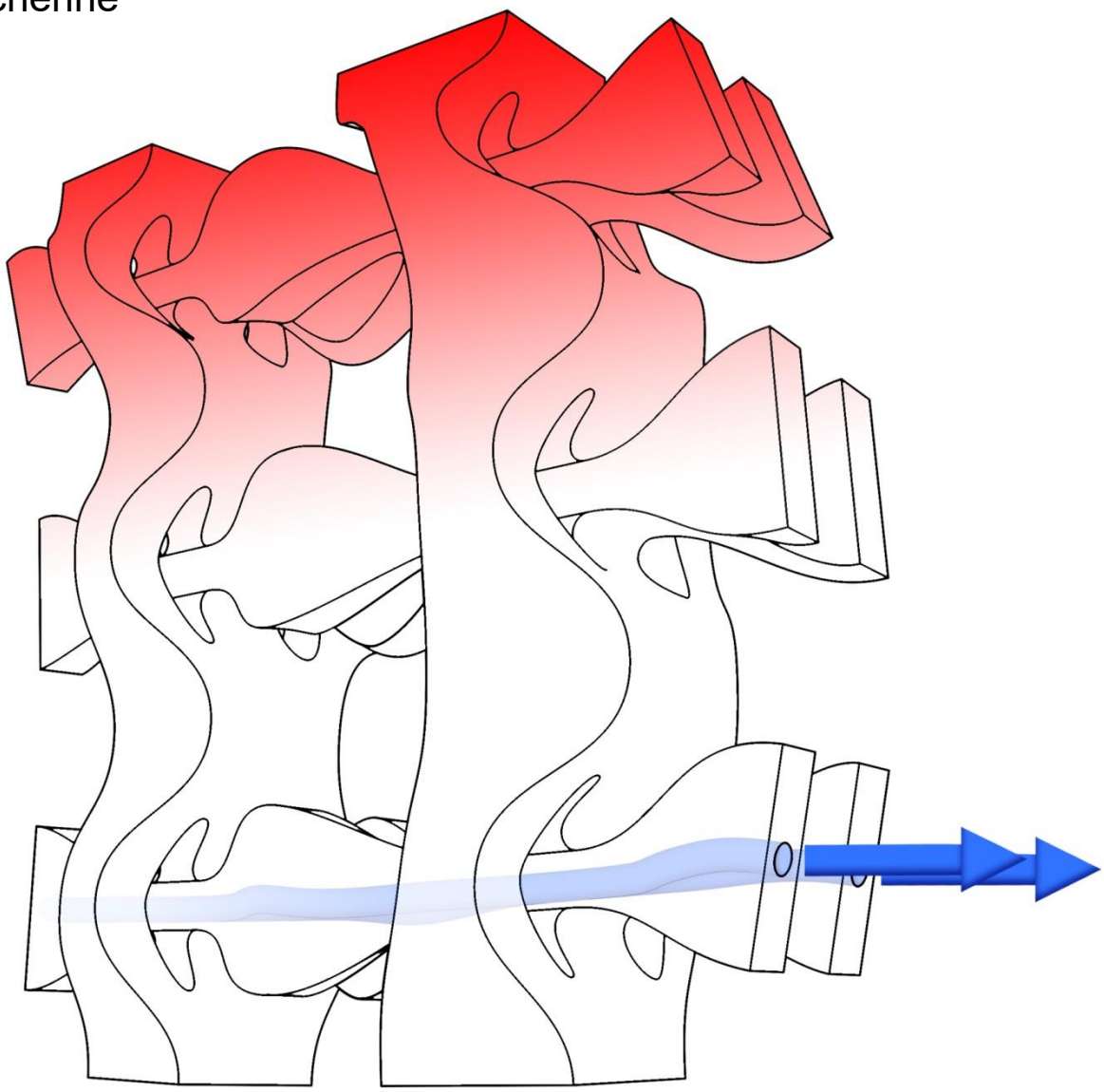

TIB OPEN PUBLISHING

Open Conference Proceedings

Open Conference Proceedings (OCP) is an open series dedicated to publish proceedings from various conferences, workshops, symposia, and other academic events.

ISSN (online): 2749-5841

Open Conference Proceedings (OCP) is published by by TIB Open Publishing (Technische Informationsbibliothek, Welfengarten 1 B, 30167 Hannover).

Volume 1

Vision and Strategies for Reinforcing Additively Manufactured Concrete Structures

4 November 2021 – Dresden, Germany

Preface

Fromm	Preface	1

Architecture and Reinforcement

Block	No Reinforcement – Compression-Only Structures: The Striatus Footbridge	3
Ahmed et al.	A framework for large-scale structural applications of 3D printed concrete: the case of a 29 m bridge in the Netherlands	5
Anton net al.	Strategies for Integrating Straight Rebar in 3DCP Columns and Shear Walls	21

Reinforcing Methods

Ivaniuk et al.	Strategies for integrating reinforcement into 3D concrete printing at TU Dresden	23
Dittel et al.	Digital Concrete Production With Vertical Textile Reinforcement – First Trials	35
Gantner et al.	Reinforcement Strategies for Additive Manufacturing in Construction based on Dynamic Fibre Winding: Concepts and Initial Case Studies	45

Reinforcing Materials

Straßer et al.	Combining Wire and Arc Additive Manufacturing and Selective Paste Intrusion for Additively Manufactured Structural Concrete – Fundamental Investigations on the Effect of Heat Exposure by WAAM on the Rheological and Intrusion Behavior of Cement Paste in the Particle Bed During Selective Paste Intrusion	61
Neef & Mechtcherine	Simultaneous Integration of Continuous Mineral-bonded Carbon Reinforcement into Additive Manufacturing with Concrete	73
Freund & Lowke	Interlayer Reinforcement in Shotcrete-3D-Printing –The Effect of Accelerator Dosage on the Resulting Bond Behavior of Integrated Reinforcement Bars	83

Visions

Orlinski et al.	Optimizing Reinforcement – Structural Analysis, Challenges and Strategies	97
Ledderose et al.	Magnetic Alignment of Microsteel Fibers as Strategy for Reinforcing UHPFRC	99
Becker	Felt-Concrete Composites in Architecture and Design	115

https://doi.org/10.52825/ocp.v1i

Editors

Prof. Dr.-Ing. Asko Fromm, Hochschule Wismar

Univ. Prof. Dr.-Ing. Viktor Mechtcherine, TU-Dresden

Review process

The contributions (max. 10 A4 pages) undergo a double-blind review process via Open Conference Proceedings.

Financing

Funding for the publication of this volume is provided by the DFG-funded Scientific Network: Adaptive Armierung geometrisch komplexer zementgebundener Formkörper. Project identifier: German Research Foundation (DFG) - Project number 326129619.

Vision and Strategies for Reinforcing Additively Manufactured Concrete Structures

Preface

https://doi.org/10.52825/ocp.v1i.86

Submitted: 1 Feb. 2022 | Published: 15 Feb. 2022

Preface

Asko Fromm[1][https://orcid.org/0000-0003-1592-0857]

[1] Hochschule Wismar, Philipp-Müller-Str. 14, 23966 Wismar, Germany

On November 4, 2021, the symposium "Vision and Strategies for Reinforcing Additively Manufactured (AM) Concrete Structures" scientific network "Adaptive Reinforcement of Geometrically Complex Cementitious Shaped Structures" (DFG project number 326129619) was hosted at the Technical University of Dresden to conclude the funding period.

The aim of this network, which is funded by the German Research Foundation (DFG), was to increase the design freedom in the use of cementitious materials through the use of end-to-end digital processes.

The complexity of this task was reflected in the group of participants, which included architects and civil engineers as well as computer scientists and materials scientists.

In addition to its many positive properties, the cement material, which is important for architecture, has clear weaknesses, particularly in the transmission of tensile forces. Without the addition of reinforcement, the potential of the material is significantly limited. Processing in an automated process such as so-called 3D printing does not initially change this. Regardless of the design, economic and ecological advantages associated with AM processes, the mechanical properties may even deteriorate without the integration of reinforcement. The known reinforcement methods, i.e. the use of rods and mats, usually cannot be integrated into the automated processes. In order to be able to use the mentioned potentials nevertheless, new reinforcement methods have to be developed for this purpose.

During the symposium, various approaches, methods and materials were presented, as well as solutions for the complete elimination of reinforcement.

Vision and Strategies for Reinforcing Additively Manufactured Concrete Structures
Architecture and Reinforcement
https://doi.org/10.52825/ocp.v1i.82

Submitted: 30 Nov. 2021 | Published: 15 Feb. 2022

No Reinforcement – Compression-Only Structures:

The Striatus Footbridge

Philippe Block[1]

[1] ETH Zurich, Switzerland

Abstract. This talk presented Striatus, an arched, unreinforced masonry footbridge composed of 3D-printed concrete blocks assembled without mortar. Exhibited at the Giardini della Marinaressa during the Venice Architecture Biennale through November 2021, the 16x12-metre footbridge was the first of its kind, combining traditional techniques of master builders with advanced computational design, engineering and robotic manufacturing technologies. The name “Striatus” reflects its structural logic and fabrication process. Concrete was printed in layers orthogonal to the main structural forces to create a “striated” compression-only funicular structure that required no reinforcement.

Keywords: 3D-Printed Concrete, Structural Design, Computational Design, Compression-Only, Funicular, Unreinforced

Conference presentation video: https://doi.org/10.5446/56106

Data availability statement

For further information, full project credits, project fact sheet, and any potential forthcoming publications, please see: https://www.block.arch.ethz.ch/brg/project/striatus-3d-concrete-printed-masonry-bridge-venice-italy-2021.

Competing interests

The author declares no competing interests.

Funding

This project was made possible by Holcim.

Acknowledgement

Project by the Block Research Group (BRG) at ETH Zurich and Zaha Hadid Architects Computation and Design Group (ZHACODE), in collaboration with incremental3D (in3D).

Vision and Strategies for Reinforcing Additively Manufactured Concrete Structures

Architecture and Reinforcement

https://doi.org/10.52825/ocp.v1i.74

Submitted: 30 Sept. 2021 | Accepted: 13 Jan. 2022 | Published: 15 Feb. 2022

A framework for large-scale structural applications of 3D printed concrete: the case of a 29 m bridge in the Netherlands

Zeeshan.Y. Ahmed[1][https://orcid.org/0000-0001-7250-9752], Rob J.M. Wolfs[1][https://orcid.org/0000-0001-7897-433X], Freek P. Bos[1] [https://orcid.org/0000-0002-6666-2395] and Theo .A.M. Salet[1]

[1] Eindhoven University of Technology, department of the Built Environment

Abstract. In this work, a framework for large-scale structural applications of 3D printed concrete is presented, which serves as an important step to develop a regulatory basis for approval in the Netherlands. The steps in this framework, consisting of a design phase, testing phase and manufacturing phase, towards a final output were presented and discussed theoretically. The framework was then applied to the case of a 29 m 3D printed bridge, funded by Rijkswaterstaat Major Projects and Maintenance, constructed in the Netherlands. The full application of the framework illustrates that despite the absence of standards, it is possible to safely apply 3D printed structures in practice. With the gradual increase of testing data expected to become available over the coming years, the extent of the application of the framework can be reduced step-by-step.

Keywords: 3D concrete printing, bridge, protocol, testing, mock-up

Conference presentation video: https://doi.org/10.5446/56115

1. Introduction

The digitization and industrial automation of various production stages have supported productivity growth in the manufacturing industries [1,2]. Over the past decade, many manufacturing industries have reaped the benefits of the process and product innovations from the fourth industrial revolution (Industry 4.0) and implemented novel digital technologies such as augmented reality, 3D scanning, robotics, and additive manufacturing (AM) [2]. The latter, also popularly known as 3D printing, has been adopted by key manufacturing industries such as the automobile and aerospace industries to improve capital gains through material optimization with product customization [3]. The potential of AM has been recognized by the architecture, engineering & construction (AEC) industry, too, as a method to fulfil the industry's inherent demands for a higher productivity, and reduced environmental impact. In the AEC industry, AM can be applied to manufacture structural and non-structural elements with various materials such as concrete, wood, ceramics, steel, polymers, foam, glass, and other building materials [4]. At the moment, concrete is the most widely used 3D printable material in the construction industry [5-7].

However, scaling up the 3D concrete printing (3DCP) technology to apply it in the construction of houses or infrastructure projects comes with its own set of challenges. Despite all the progress made over a short period by various research groups and companies the world over, the application of 3DCP in the AEC industry is still in its infancy: current (showcase) projects demonstrate the potential, but cannot yet compete economically and

there is much to be gained in terms of environmental footprint. The issues related to the scaling of objects and standardization of the technology need to be addressed by codes and protocols with high priority [8], as existing regulations are not directly applicable to 3DCP without further consideration. Technology-specific characteristics such as the lack of compaction by vibration, or the layering and associated anisotropy, are not considered. Specimen sizes and geometries are not always suitable. Moreover, the consistency of structural properties when printing under varying conditions, with different equipment or operators, is mostly unknown. International associations such as RILEM, ASTM, and *fib* have only recently begun addressing these developments. Standardization requires sufficient, reliable data and a sound understanding based on actual project experiences. In this latter area, in particular, there is a dire lack of publicly available information.

To address this gap and start developing protocols for standardization, Rijkswaterstaat (the executive body of the Dutch Ministry of Infrastructure and Water Management) Major Projects and Maintenance together with the Eindhoven University of Technology (TU/e) has initiated an experimental valorization project. The project aims to study the challenges of applying 3DCP technology in an actual structure of significant size, namely a bicycle and pedestrian bridge with a total span of 29 m, in the city of Nijmegen. In addition to common requirements of bridge performance, two project specific demands were set. Firstly, the bridge would feature a size and design freedom that constituted a significant improvement over a previously realized 3DCP bicycle bridge constructed in the Netherlands [9]. This required the development of a process for the bridge design, which could fulfil the design requirements within the limitations of 3D concrete printing technology. Secondly, the bridge was to be used as a case to study the effects of scaling up 3DCP technology and its performance in a real-life project open to public use. A validation methodology had to be developed for the generic design and construction of similar projects in the future, which facilitates the approval process by authorities.

The current paper presents the design and mock-up phase of this bridge, with the aim to further demonstrate the viability of the applied design concept to realize moderately sized bridge structures with additive manufacturing of concrete by extrusion layering, in addition to previous studies [9-11], but on a larger level of scale. On a more general level, this paper intends to contribute to the development of generalized methods for design, calculation, testing, and approval of such structures, by presenting an overall framework of design and structural validation, in which the work has taken place.

2. Framework for the design methodology

Although it is obvious the extrusion-based 3DCP technology provides a wealth of hitherto unfeasible geometrical design opportunities, which can be used for aesthetical, functional, or structural purposes, it still does have specific limitations as to what is and what is not possible to make. An extensive discussion of these limitations falls outside the current paper's scope, but the shape-making method based on continuous linear stacked filaments dictates a certain design logic that has to be adhered to [7]. Considering this from the design start significantly reduces extensive redesign mid-stream that could weaken the original design intent. Therefore, an explicit design and validation framework was developed that could be applied to this project, as well as similar ones. It allowed for a relatively efficient design and approval process without excessive trial-and-error and is schematically represented in Figure 1. The framework is broadly divided into four blocks:

- Data,
- Design,
- Production, and
- Realization.

They are further detailed in the following subsections.

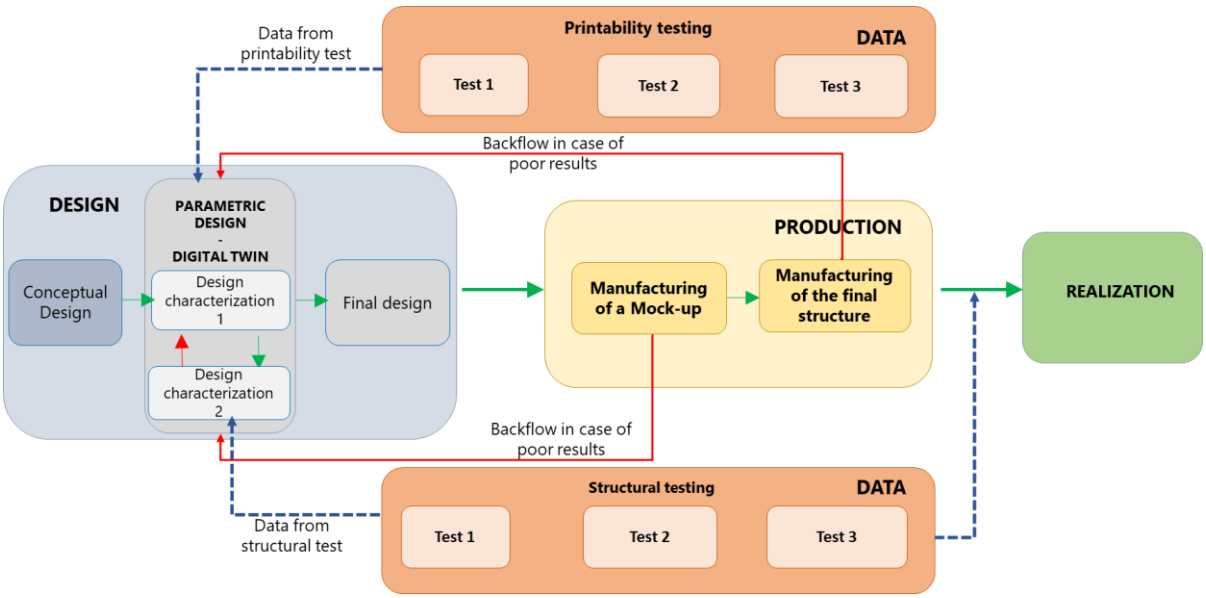

Figure 1. Framework illustrating the validation methodology for 3DCP structures.

2.1. Data

In comparison to conventional construction projects, the framework is characterized by the data blocks, one related to aspects of printability and the other to mechanical properties. Covering information on printability on the one hand (top block in Figure 1), and mechanical properties data on the other (bottom block in Figure 1), they inform the design block with the data needed to develop the design. While such information is normally readily available from codes, guidelines, supplier data sheets, text books and so on, this needs to be explicitly established for the 3DCP method. At the start of the project, some data on both was already available, but in order to develop an increasingly efficient design methodology, the data block is supplied with additional testing data from the production and realization blocks during the project.

2.2. Design

The design starts with formulating and outlining the structure's requirements regarding functionality, aesthetics, structural performance, budget and so on. Similar to conventional construction, the discussions on the requirements are translated into a conceptual design idea in the form of a 3D computer-aided model (CAD) model for the structure. However, much more than in conventional processes, the construction method (3D printing), the material behaviour and geometric design should be considered in an integral fashion in this digital model, as they influence each other and thereby the quality of both the printing process and that of the final, printed result. The model of the conceptual design should thus consider various technological limitations, structural, printability, and material requirements. In this framework, the digital model is developed through an iterative process based on a parametric design platform. This avoids a trial-and-error design of the overall structure. The data underlying this model (stored in the data blocks) can be acquired through mixed approaches and methods based on mainstream experimental testing on printable concrete, empirical observations, previously conducted research projects. This allows for a more robust understanding of learning environments [12-14].

Existing data on the parameters are fed into the parametric model to create boundary conditions within which the structure can be realized. Based on the structure's required design characterizations, the parametric model can provide design iterations until a satisfactory result is achieved. Besides providing a manufacturable design, the parametric model also provides a digital platform to store the data from the tests on the structure. Furthermore, the model offers the possibility to store data from every project, by updating the established correlations between printing strategy, material behaviour and structural behaviour of the printed object in the parametric tool, thereby making the model more efficient with each project.

2.3. Production

Although the results from printability and mechanical testing provide a basis to estimate the manufacturability of the full-scale objects, this can only definitely be established in the production phase itself. As the design is developed based on data from generic tests, project-specific and scaling issues [15] might arise (e.g. material quality deviations due to prolonged printing, plastic deformations in large elements, compatibility with other construction materials). Hence the production is divided into two stages.

The one-to-one scale construction of a mock-up in the first phase helps to identify any unforeseen parameters related to manufacturing in the design phase. As mock-ups are intensive both in terms of associated costs and efforts, the appropriate item of which to make a mock-up of, has to be carefully selected through engineering judgment, based on what part of the structure is considered governing in complexity and structural performance, and what mock-up design is expected to provide the most information relative to the cost. The mock-up construction provides the opportunity to combine and test the learning from various printability test and design decisions from previous projects. The other significant activities carried out during the mock-up construction is to document and develop protocols. Documentation of conditions such as temperature, time, and humidity, which may impact printing the elements, assembly, and logistics, is essential to provide learning for future projects. Studying the influence of the conditions related to the mock-up construction also provides the opportunity to develop quality control protocols during the structure's final realization. Upon completing the mock-up, various tests associated with validating the mock-up's performance are carried out.

If satisfactory results are achieved from the mock-up testing, the protocols developed during the mock-up construction are followed to manufacture the final structure. However, in case of unsatisfactory results from the mock-up test, the whole process is reviewed and redesigned starting from the parametric design phase to either construct a new mock-up or proceed to develop the final structure in case of minor corrections from the mock-up construction. During the manufacturing of the final structure, the process related to documentation and quality control should be carried out to improve the data associated with the manufacturability of 3DCP structures. Over time, the necessity for a mock-up should reduce and eventually become obsolete with increasing data becoming available from previous projects.

2.4. Realization

Fulfilling the *'living laboratory'* role of the bridge, it will be subjected to on-site testing before final placement as well as to in-use monitoring to provide additional input to the data blocks which will help to develop standards and codes of practice for scaling up 3DCP technology in general.

3. The case of a 3D printed bridge

The framework will be illustrated for the case of the 3D printed bridge in Nijmegen. In this work, the design, manufacturing and testing of a mock-up is considered. The full-scale pro-

duction and assembly of the bridge was performed by the industrial parties involved in the project, based on the findings reported in this study (but not discussed here).

Figure 2. Design for the bridge designed by Michiel van der Kley [16].

The bridge's design (Figure 2) was developed by Michiel van der Kley, and TU/e performed the research on the printing process and structural testing. The structural design of the bridge was developed by Witteveen+Bos consulting engineers, for which Summum Engineering developed a parametric design tool. Finally, the bridge's manufacturing and assembly are realized by the joint venture 3D printing facility of Saint-Gobain Weber Beamix and BAM constructions.

3.1. Conceptual design of the bridge

The bridge design is based on a double curved deck that spans across tapered columns, which appear to be sprouting out of the deck. This nature-inspired shape illustrates the freedom of geometry enabled through 3D printing, near impossible to manufacture efficiently by traditional construction techniques.

3.2. Structural principle

Like the 3D printed concrete bridge realized in Gemert, the structural principle is based on the assembly of multiple printed elements joined together by prestressing tendons. This principle eliminates the necessity of passive reinforcement along the bridge span, as the prestress level is selected such that exclusively compressive stresses remain active in each section due to occurring bending moments. The 29m span of the bridge was divided into five simply-supported parts, each spanning between 4.5 to 6.5 m, resulting in a configuration of multiple statically determinate girders. Each of these five girders is enclosed by two anchor blocks, which introduce the prestressing force into the 3D printed concrete. The five girders were further subdivided into smaller elements due to manufacturing and logistic constraints. Contrary to the previous bridge project, each element's geometry is unique due to the bespoke, double-curved bridge design. As such, each element has a width of 3500 mm, and a height varying between 700 to 1200 mm (Figure 3). These elements are glued together in the assembly stage.

The cross-section of each of the elements consists of a series of connected bottle shapes, alternatively positioned upside down illustrated in fig. 5. The exact geometry (e.g. number of bottle shapes, size) followed parametrically from each element's dimensions and was designed to resist occurring shear forces. All ‘bottles’ are connected via a continuous line at the bottom. This principle of non-solid sections has already proven its value in the previous bridge project of Gemert and allows for a reduction of material use and weight while simultaneously providing openings along the bridge span for the prestress tendons to run through.

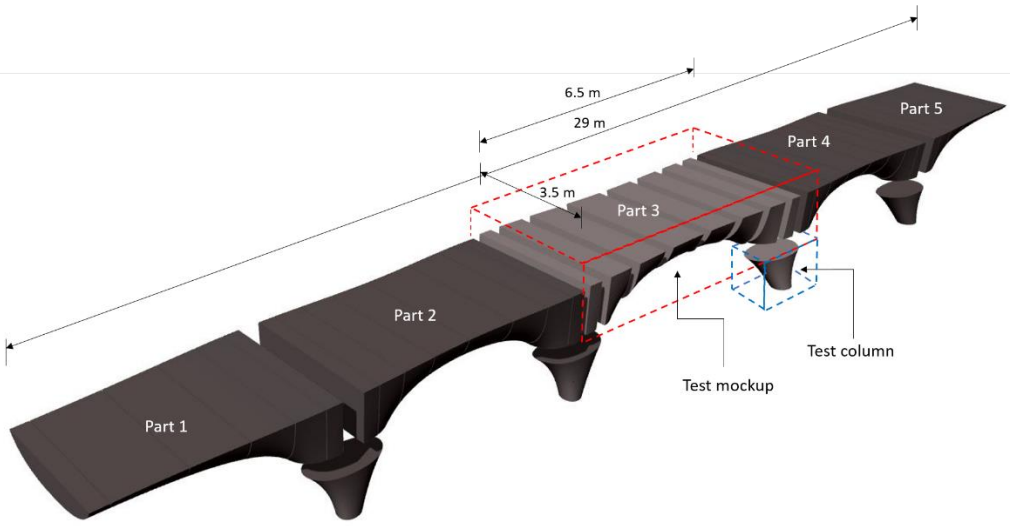

Figure 3. Tessellation of the Nijmegen bridge.

Each part consisting of multiple elements, as shown in figure 3, is enclosed by two anchor blocks at the ends. These blocks consist of conventional reinforced concrete, cast into a 3D printed concrete 'lost formwork' to achieve a consistent texture appearance. Unlike the cross-section of the girder segments, the anchor blocks were realized as solid sections to distribute the prestress force into the printed element evenly and prevent high stress concentrations in the relatively slender, printed layers.

The anchor blocks rest on four pairs of columns along the bridge span and two traditional abutments at the bridge ends. The columns are designed as reinforced concrete elements and are, like the anchor blocks, cast into 3D printed lost formwork. These columns are fixed to a pile foundation. From a structural engineering perspective, they may be treated as conventional reinforced concrete columns and are therefore excluded from structural testing and further discussion.

3.3. Structural validation

Structural engineering consultancy throughout the project was provided by Witteveen+Bos consulting engineers. Using Finite Element Analysis (FEA), the bridge girders were as modelled as 3-dimensional structures built from curved shell elements (rather than volume elements, to reduce modelling effort and computational time). In projects, such as this, where 3DCP elements are applied as part of the main load-bearing structure, data on structural material properties are limited, particularly concerning the interaction with process parameters, which is significant [17]. Scale effects may also occur [15] and suitable reinforcement technologies are still under development [18]. The print mortars themselves generally contain a high amount of cement and only small aggregates, resulting in a high shrinkage and low friction resistance in cracks. The layered structure may introduce anisotropy and variations in print settings can influence the properties of the printed product. The lack of formwork printed objects requires specific attention to curing conditions. Furthermore, the topology of 3DCP elements, characterized by relatively thin-walled parts with open space in between, introduces a number of potential structural risks unfamiliar to conventional concrete structures. It may lead to local instability phenomena and a loss of load redistribution capability (and hence susceptibility to stress concentrations, geometrical accuracy, and deviations between structural models and reality). Furthermore, it is likely these geometries result in differential shrinkage due to uneven dehydration and temperatures throughout an element. In turn, this may cause forced deformations and thus cracking.

Current structural codes and guidelines do not take these effects into account, and are thus an insufficient basis for structural design and approval. In recognition of the need to provide innovations with a potential path to the construction market, articles 4.2 and 5.2 of the Eurocode 0 *Basis of Design* [19] allow the possibility to develop structural designs partially based on project-specific experimental testing, rather than generalized calculation rules alone. Annex D 'design by testing' further details the type of experiments that can be performed and regulations on the statistical evaluation of results. It distinguishes 7 categories of tests that can be applied, but due to the necessarily general nature of this Annex, it only provides minimal instructions on the embedment of such experiments into the design and validation process. Based on the possibilities thus offered by the Eurocode to deviate from generalized calculation rules, a testing protocol was developed containing the following approach.

Initially, a set of mechanical tests was performed to obtain relevant structural material properties (Annex D, category b) such as the compressive strength, flexural strength, and modulus of elasticity of the material. The characteristic mechanical properties of the applied material, a commercially available print mortar (Weber 3D 145-2), have been established in an extensive experimental program [17] and further expanded with additional tests on samples from new batches of the same material, according to the same methods. The tests were performed in multiple directions, on printed samples. The data (stored in the 'data' block of the framework) were used to define the final dimensions of the bottle-shaped cross-section and the required prestress level of the tendons. The ultimate limit state (ULS) has been calculated based on the common load factors in NEN-EN 1992-1-1 and the mechanical properties.

Subsequently, a full-scale mock-up was prepared (as part of the 'production' block of the framework). New material samples were prepared during the printing of the mock-up elements, and subjected to additional mechanical tests to verify the previously obtained material properties (category b/e). The mock-up itself was subjected to a full-scale destructive test (category a/d), which is discussed in Section 5. After evaluating the material and full-scale tests, the production could be approved. Since all of the girders were designed following the same structural logic, only one representative part of the full bridge was considered for the mock-up testing, designated as 'Part 3' in Figure 3.

The protocol further specifies that material samples are again taken at the final element production for verification (category e), while the final bridge is to be subjected to a diagnostic test (i.e. a loading until the ultimate limit state load) before being taken into use (category g). Material samples are cubes of 40 x 40 x 40 mm and prisms of 40 x 40 x 160 mm, in accordance with mortar testing codes, as the print material mostly resembles a mortar rather than a concrete, and these dimensions are furthermore appropriate for the typical wall thickness of 3DCP elements (40 – 80 mm). The behaviour of the bridge will furthermore be monitored during its service life, to timely recognize potential long-term degradations and adjust the prestress in the tendons if necessary (category g). The successful completion of this protocol formed the basis for approval by the local building authorities. To reduce uncertainties in future projects, all material tests (initial, mock-up, production) were collected to extend the database on material properties.

3.4. Printable design

The structural design of the bridge was further refined following conditions related to the bridge's printability. The capabilities and limitations associated with the 3D concrete printing system at Eindhoven University of Technology (TU/e) defined printing and manufacturing constraints for the bridge design. For example, considering logistics and lifting capacity, the segmentation of the bridge girders into smaller elements was based on the limit value of 4000 kg. The TU/e 3DCP system has been extensively discussed in [7], based on which printing strategies were developed to overcome the printing limitations and improve the degree of design freedom according to the bridge's design ambitions.

With regard to the print process parameters, basic printing settings had to be recalibrated to the larger scale of the project. Normally, the 3DCP printing facility of the TU/e is used to print filament widths of 40 – 60 mm, and 10 mm height. To obtain the 80 mm wide filament required in this project, the print mouth opening was redesigned and consequently settings such as print head travel speed and pump frequency had to be reset to obtain a smooth filament. In relation to the filament width, the minimum radius of in-plane curves was re-established. Most importantly, a method using a granular inner support material was developed to print doubly curved geometries in the u,w-plane (separately published as [20]). The results of these tests served as input for the development of a printable design, particularly for the parametric model used during the design. When initial designs for the various bridge parts had been developed based on these studies, full scale trial prints were performed as some effects cannot be simulated on a small scale. This resulted in some adjustments of the design (see Section 4).

Following the constraints of the general strategy of 3D concrete printing by stacking layers vertically, the bridge girder and column elements had to be printed with different printing directions compared to the direction of final assembly on site. Like the 3DCP bridge at Gemert [9], the girder elements have been printed along the cross-section and were rotated 90° after printing for assembly. The columns were positioned by flipping them 180° to the direction of printing. However, to maintain continuity in the bridge design's double curved form, the transition between girder and column required special attention since the angle of curvature at the connection was relatively large.

4. Manufacturing of the mock-up

The mock-up manufacturing was conducted in three phases: printing a column, printing the girder segments, and constructing the anchor blocks. Finally, the overall assembly of the mock-up and quality control protocols developed during the printing phases are discussed. All mock-up printing was performed using Weber 3D 145-2 printable mortar, and a 60 x 12 mm backflow-flow nozzle. The geometrical shape and properties of the nozzle are discussed in [9]. The extruded filament's width was increased to 80 mm, compared to the nozzle opening, by reducing the print speed and increasing the extrusion rate, with the aim to improve the object stability during the printing process.

4.1. Column printing

A mock-up column was printed to evaluate the significantly cantilevering geometry's buildability, calibrate the corresponding print settings, and test the infill support material. Only after the geometrical limits had been established, and were incorporated into the parametric design tool, the final shape of column as well as of the connecting girder could be defined.The column layering was horizontal, but the column was printed upside down (i.e. from top to bottom) such that the infill material would support the internally cantilevering shape.

However, despite the application of a temporary support material, the initial column design was still susceptible to failure during printing, as one side of the column was partly straight and even slightly curved outwards, and thus unsupported. Due to the relatively small column circumference, and corresponding rapid vertical building rate, the fresh material was loaded (too) quickly and failed due to object instability at the unsupported part during printing, illustrated in Figure 4, left.

Figure 4. Failure during printing of the initial column design (left) and successful printing of the adjusted column design (right).

Following analysis of the failure mode, the geometrical restrictions were fed back into the parametric model and the design of the column was updated, such that the infill material would support the column across its full height. Subsequently, the column was printed successfully as shown in Figure 4, right.

4.2. Printing of girder elements

Considering the maximum lift capacity of the printing facility, the girder was tessellated into six separate segments which were printed individually. Each segment had comparable weight, and since the print path length per layer varied, thus a varying overall height. These bridge segments had significant curvatures along their outer geometry, which, despite the relatively long contour length, could lead to similar failure as observed in the column printing trials. To address this issue, the segments were positioned such that any cantilevering would occur inwards and could thus be supported by infill material. The straight parts on the other side of the elements (i.e. along the bridge deck) were not supported to minimize additional labour. A close-up during printing and an overview of a printed segment is shown in Figure 5.

Figure 5. Printing of a girder segment with support material.

The printing settings were selected such that, similar to the column, the filament width of the girder segments was equal to 80 mm. The heartline distance between print paths in the horizontal (print) plane was, however, reduced to 65 mm to create an overlap in the printed filaments. This was done to avoid cavities in the printed geometry and maintain adequate bonding between two horizontally adjacent layers. Such overlap does result in collection of fresh concrete in front of the nozzle during printing, which had to be removed periodically by hand. The girder segment's print path strategy was based on following a spiral-based continuous contour of closed-loop layers over the whole printed segment. Each layer was composed of the required bottled shaped print path to support the structural design requirements of the

internal geometry. The (vertical) transition between each layer is achieved by gradually moving the print path from the first layer to the layer above to maintain a smooth layer transition.

Based on this manufacturing strategy, each of the six girders' segments was printed successfully. After printing, each element was covered in plastic sheets for a curing process of approximately one week. The foil was only temporarily removed to lift the elements from the print bed, which took place at least 48 hours after they had been manufactured.

It should be noted that, while the adopted support material strategy improves the printing freedom, adding the material manually during the printing process is a tedious process, in particular for large geometries such as the girder segments. For industrial applications, it is recommend to develop an automated system to introduce the support material instead.

4.3. Construction of anchor blocks

The anchor blocks are positioned at both sides of the (six) printed segments and were composed out of conventional, reinforced cast concrete, to withstand splitting tensile forces caused by the prestress tendons. To maintain consistent overall appearance, the anchor blocks were poured in a 3D printed mould that acts as a lost formwork, similar to the column strategy discussed above. Locally, the 3D printed concrete formwork was removed such that the poured concrete of the anchor block was resting directly on the poured concrete of the columns. This way, any peaks stresses caused by the layered textured of the printed lost formwork were avoided.

4.4. Assembly of the girder

The assembly process of the girder segments and the anchor blocks was carried out following the procedure developed for the construction of the 3DCP bridge at Gemert [9]. The elements were flipped 90^{o} from the printing direction and assembled horizontally in the direction to be placed on site. However, due to the girder's double curve shape (contrary to the straight elements of the Gemert bridge) a temporary scaffold following the curvature of the bridge girder had to be constructed upfront. The elements were placed one after another on the scaffold and assembled. Each interface between two adjacent segments was glued with a synthetic epoxy-based resin to level out the uneven top surface of a printed segment and avoid local stresses once loaded.

Like the Gemert bridge, the mock-up was prestressed by straight, unbonded post-tensioning tendons. Due to the curvature of the bottom side of the girder, the prestressing tendons were concentrated in the top part of the cross section, such that the tendons could pass through the internal bottled shaped structure of all the mock-up segments without touching the printed layers. The tendons were placed in two rows, nine prestressing tendons in the top and six tendons in the bottom. The final step was to lift the assembled girder and place it in a testing rig for the large-scale mock-up test.

4.5. Data collection and quality control

Developing protocols for data collection and quality control is an integral part of the design and manufacturing in this bridge project. Hence, during the manufacturing, different quality control checks were performed to document the quality of the process and that of the final product. During the printing process, sensors were placed on the printing system to collect temperature data. For relatively long printing times, as is the case for the bridge girders, large fluctuations in temperature could affect the quality of printed concrete as discussed in [21]. Similarly, the environmental conditions such as relative humidity were logged. For manufacturing of the bridge mock-up, these values were found to be approximately constant during individual printing sessions, and between printing days (all performed within the time span of two weeks).

To validate the expected structural performance of the girder segments, during printing, the filament dimensions were measured periodically, as changes in the layer dimension might influence both the global resistance and the self-weight of the bridge mock-up (which is the dominant load case on this bridge). Where needed, to maintain the required layer dimension, countermeasures are adopted by adjusting the printing speed and the extrusion rate to achieve the desired layer dimensions. Moreover, following the protocol for structural validation, material samples were taken during printing of the girder segments to validate expected material properties.

5. Structural test of the mock-up

To assess the structural performance of the 3D printed bridge and validate its compliance to the safety regulations, one 3D printed and pre-stressed girder of the bridge spanning between columns was subjected to an experimental testing program on a 1:1 scale, designated as the 'mock-up test'. A single girder, with a total length of 5875 mm, was subjected to a four-point bending test, whereby the distance between the loading and support points was varied in two configurations, to validate the bridge resistance towards both bending moment and shear stresses.

The test set-up of the bridge girder is illustrated in Figure 6. In the first configuration (designated as T1700), the distance between the support and loading points a = 1700 mm, such that b = 2475 mm, to assess the girders resistance towards the applied bending moment. In the second configuration (T1000), a = 1000 mm and b = 3875 mm, thereby increasing the ratio between shear and bending stresses, which allows for an assessment of the shear resistance of the girder.

For both configurations, the applied loading was based on the ultimate limit state. For configuration T1700, this resulted in a maximum loading of 100 kN at each loading point, whereas for T1000 each point was loaded up to 115 kN. The loading was applied via two hydraulic jacks in steps of 25 kN at a loading rate of 0.25 kN/s per jack. The girders were fully unloaded in between steps, at a rate of 1.00 kN/s per jack, to evaluate whether damage has occurred in the structure. The top of the girder was locally capped with self-levelling mortar to evenly distribute the loading over its full width.

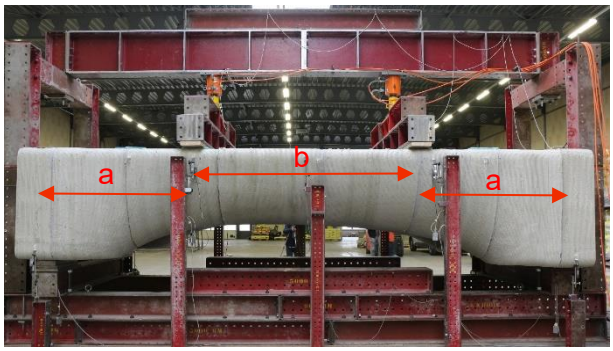

Figure 6. Setup of the structural mock-up test.

The test with configuration T1700 was performed first, after which the girder was fully unloaded, and the setup was changed to configuration T1000. Once the design load according to the ULS was then reached, the loading in this configuration was further increased to 345 kN per loading point. This additional step was performed to gain insight into the occurrence and type of damage, and the possible presence of warning signals before failure. Throughout both tests, the load was recorded by means of 350 kN load cells position at the loading points, and vertical deformations were measured at midspan on two sides of the girder by LVDT's. The prestress level was monitored at 4 tendons, two at the girder top, and two at the

bottom. This level was found to be constant over the duration of both tests, and is thus excluded from further discussion.

It is noted that due to this particular bridge design, a direct load transfer to the supports is not unlikely in the T1000 configuration. This will have a positive impact on the girders' shear capacity, and should be considered in the analysis of tests results, and in particular, when designing similar structures with larger span to depth ratios.

5.1. Results

Figure 7 shows the load-displacement curve of the tests in configuration T1700 and T1000, respectively. Here, the force per jack is plotted versus the averaged vertical deformation at midspan. The results of both tests show a perfect linear elastic behaviour throughout the complete loading-unloading sequence, up to the load level corresponding to the ultimate limit state (ULS). After each loading step, the curve returns to zero displacement, indicating that no damage, and thus no loss of stiffness, has occurred. For the regime beyond the ULS loading level, tested in configuration T1000, the linear elastic behaviour is observed up to approximately 260 kN per jack. From this point on, a slight non-linear deformation behaviour is observed up to the maximum applied load of 345 kN. No visible cracks were observed however. It is noted that this change in behaviour occurred well above the required minimum capacity. After reaching 345 kN per jack, the test was stopped, as three times the loading level of the ULS was reached without occurrence of failure. While it would have been insightful to observe which failure mode would have occurred, the limit of the measurement equipment was reached and the risk corresponding to sudden release of energy was too high.

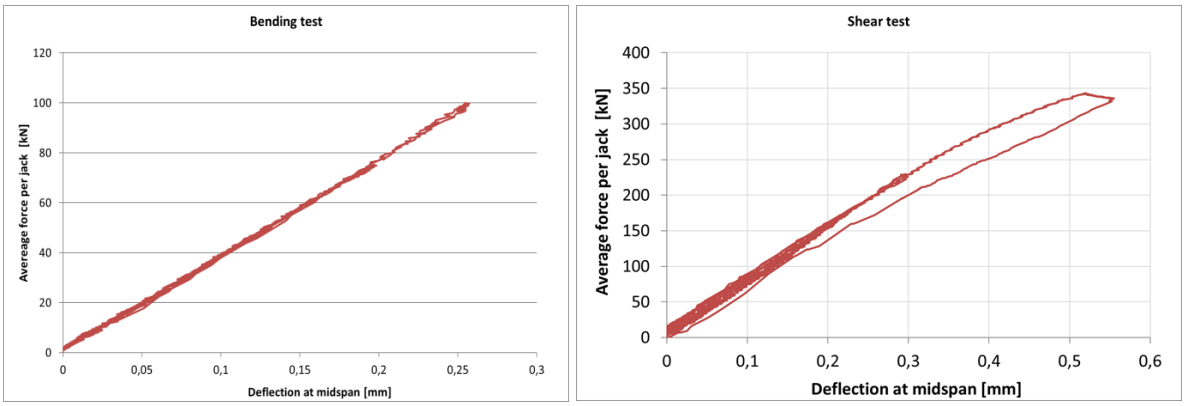

Figure 7. Load-displacement graphs of the two loading T1700 (left) and T1000 (right).

In configuration T1700, the loading points of 100 kN each resulted in a bending moment capacity of M_R of 170 kNm and an additional shear resistance capacity V_R of 100 kN for external loads. Similarly, in configuration T1000, the applied loads of 345 kN each resulted in a bending moment resistance capacity M_R of 345 kNm and an additional shear resistance capacity V_R of 345 kN for external loads, for this particular girder design.

From the experimental program, it may be concluded that the mock-up of the bridge performed well and that the structural capacity is sufficient. A bending of resistance of two times the ULS load was found, without failure occurring. Likewise, a shear resistance of three times the ULS load was achieved, although the contribution of direct load transfer is not known. The tests moreover confirmed that the serviceability limit state (SLS) requirements are well met, as the deflections in both configurations were minor.

6. Bridge assembly and diagnostic test

The satisfactory results of the mock-up test demonstrated that the bridge design fulfilled the structural requirement, and production of the full bridge was commissioned, and performed by the industrial parties involved in the project in correspondence with the manufacturing strategy applied for the production of the mock-up, illustrated in Figure 8. In accordance with the framework proposed here, the full 3D printed bridge has been subjected to an in-situ diagnostic test. The difference with the mock-up test is that this time the bridge girders are not loaded to failure, but to a load that gives enough valuable information about the safety, without causing unnecessary damage. Based on the structural response found in the mock-up test, it was chosen to load the bridge girders up to 100% of the ULS load, since a linear elastic response was found in the mock-up test and the same behaviour was expected here. Since each of the six girders can be considered as a simply supported, statically determinate system, they were all tested separately such that six diagnostic tests were performed. The loading was applied by means of water tanks, which were filled in steps of 25% of the full load. After each step, the deformation was measured at five points along the span, on both sides of the girder. A detailed description of the process of printing, assembling and testing of the full bridge falls beyond the scope of the present work.

7. Conclusions

In this work, a framework for large-scale structural applications of 3D printed concrete is presented. The steps in this framework, consisting of a design phase, testing phase and manufacturing phase, towards a final output were presented and discussed theoretically. The framework was then applied to the case of a 29 m 3D printed bridge, constructed in the Netherlands. The full application of the framework illustrates that despite the absence of standards, it is possible to safely apply 3D printed structures in practice. However, it is not desirable from the perspective of cost and material use to be required to conduct such large-scale tests for every 3DCP project. The framework now offers guidance for application, but as soon as the quality of 3D printing processes can be sufficiently assured, the intermediate mock-up test phase can be dispensed with. In this stage, a diagnostic test of final object will suffice to validate the expected structural performance.

Figure 8. Assembly of the final bridge on location

Eventually, once the structural behaviour of 3D printed concrete can be assessed, through analytical models, numerical analysis or via codes of practice, as is the case for conventional concrete structures, the diagnostic test can likewise be omitted. In this final stage, experimental characterization of the material quality will remain as part of the quality assessment of the 3D printing process. To support this transition, it is imperative that the relatively young community in the field of 3DCP shares the lessons learnt and results of these first illustrative projects. This contributes to the development of understanding of the structural behaviour of

printed structures, and provides a basis for standardization in the field. The framework discussed in this paper serves as a starting point to conduct this in a uniform manner.

Data availability statement

The testing report of the mock-up phase is available upon request.

Author contributions

Z.Y. Ahmed: Investigation, Methodology, Writing original draft. **R.J.M. Wolfs:** Conceptualization, Writing – review & editing. **F.P. Bos:** Conceptualization, Writing – review & editing. **T.A.M. Salet:** Conceptualization and Supervision

Competing interests

The authors declare no competing interests.

Acknowledgement

The Nijmegen bridge project is a collaboration between Rijkswaterstaat, Major Projects and Maintenance, Nijmegen municipality and omgevingsdienst Nijmegen (ODRN) and TU/e.

The authors would like to thank in particular D. Schaafsma, S. Fennis, E. Roijen and E. Drenth for their input to this contribution.

References

1. McKinsey Global Institute, “Reinventing Construction: A Route To Higher Productivity”, McKinsey Co., p20, 2017.
2. P.Gerbert, S. Castagnino, C. Rothballer, and A. Renz, “Shaping the Future of Construction”, World Econ. Forum, 1–64, 2016.
3. T. Ngo, A. Kashani, G. Imbalzano, K. Nguyen, and D. Hui, “Additive manufacturing (3D printing): A review of materials, methods, applications and challenges”, Composites Part B: Engineering, 143, 172–196, 2018, doi: https://doi.org/10.1016/j.compositesb.2018.02.012.
4. F. Craveiro, J. Duarte, H. Bartolo, and P. Bartolo, “Additive manufacturing as an enabling technology for digital construction: A perspective on Construction 4.0”, Autom. Constr., 103, 251–267, 2019, doi: https://doi.org/10.1016/j.autcon.2019.03.011
5. N. Labonnote, A. Rønnquist, B. Manum, and P. Rüther, “Additive construction: State-of-the-art, challenges and opportunities”, Automation in Construction, 72, 347–366, 2016, doi: https://doi.org/10.1016/j.promfg.2017.08.006.
6. B. Lu et al., “A systematical review of 3D printable cementitious materials”, Constr. Build. Mater. 207, 477–490, 2019, doi: https://doi.org/10.1016/j.conbuildmat.2019.02.144.
7. F. Bos, R. Wolfs, Z. Ahmed, and T. Salet, “Additive manufacturing of concrete in construction: potentials and challenges of 3D concrete printing”, Virtual Phys. Prototyp., 2016, doi: https://doi.org/10.1080/17452759.2016.1209867.
8. S. Paul, G. van Zijl, and I. Gibson, “A review of 3D concrete printing systems and materials properties: current status and future research prospects”, Rapid Prototyp. J. 24(4), 784–798, 2018, doi: https://doi.org/10.1108/RPJ-09-2016-0154.

9. T. Salet, Z. Ahmed, F. Bos, and H. Laagland, “Design of a 3D printed concrete bridge by testing”, Virtual Phys. Prototyp. 13(3), 222–236, 2018, https://doi.org/10.1080/17452759.2018.1476064.
10. G. Vantyghem, W. De Corte, E. Shakour, O. Amir, “3D printing of a post-tensioned concrete girder designed by topology optimization”, Autom. Constr. 112, 103084, 2020, doi: https://doi.org/10.1016/j.autcon.2020.103084.
11. K. Kinomura, S. Murata, Y. Yamamoto, H. Obi, and A. Hata, “Application of 3D Printed Segments Designed by Topology Optimization Analysis to a Practical Scale Prestressed Pedestrian Bridge”, In F. Bos, S. Lucas, R. Wolfs, & T. Salet (Eds.), Second RILEM International Conference on Concrete and Digital Fabrication: Digital Concrete 2020 (pp. 790-803). (RILEM Bookseries; Vol. 28), Springer, doi: https://doi.org/10.1007/978-3-030-49916-7_66.
12. F. Wang and M. Hannafin, “Design-based research and technology-Enhanced Learning Environments”, Educ. Technol. Res. Dev., 53(4), 5–23, 2005.
13. B. Ritland, “The role of design in research: The integrative learning design framework”, Educ. Res. 32, 21–24, 2003, doi: https://doi.org/10.3102/0013189X032001021.
14. B. Fishman, R. Marx, P. Blumenfeld, J. Krajcik, and E. Soloway, “Creating a Framework for Research on Systemic Technology Innovations”, J. Learn. Sci. 13(1), 43–76, 2004, doi: https://doi.org/10.1207/s15327809jls1301_3.
15. F. Bos, R. Wolfs, Z. Ahmed, and T. Salet, “Large Scale Testing of Digitally Fabricated Concrete (DFC) Elements”, 2018, doi: https://doi.org/10.1007/978-3-319-99519-9_12.
16. http://www.michielvanderkley.nl/bridge-project/ [Online] [Accessed: 24-Feb-2020].
17. R. Wolfs, F. Bos, and T. Salet, “Hardened properties of 3D printed concrete: The influence of process parameters on interlayer adhesion’, Cem. Concr. Res.119, 132–140 2019, doi: https://doi.org/10.1016/j.cemconres.2019.02.017.
18. D. Asprone, C. Menna, F. Bos, T. Salet, J. Mata-Falcón, and W. Kaufmann, ‘Rethinking reinforcement for digital fabrication with concrete’, Cem.Concr. Res., 112, 111–121, 2018, doi: https://doi.org/10.1016/j.cemconres.2018.05.020.
19. EN 1990: Eurocode - Basis of structural design’, 2002
20. Z. Ahmed A. Biffi, L. Hass, F. Bos, and T. Salet, 3D Concrete Printing - Free Form Geometries with Improved Ductility and Strength. In F. Bos, S. Lucas, R. Wolfs, & T. Salet (Eds.), Second RILEM International Conference on Concrete and Digital Fabrication: Digital Concrete 2020 (pp. 741-756). (RILEM Bookseries; Vol. 28). Springer, doi: https://doi.org/10.1007/978-3-030-49916-7_74.
21. F. Bos, R. Wolfs, L. Hermens, and T. Salet “The influence of material temperature on the in-print strength and stability of a 3D print mortar” In A. Zingoni (Ed.), Advances in Engineering Materials, Structures and Systems: Innovations, Mechanics and Applications - Proceedings of the 7th International Conference on Structural Engineering, Mechanics and Computation, 2019 (pp. 425-430). CRC Press/Balkema., doi: https://doi.org/10.1201/9780429426506-76.

Vision and Strategies for Reinforcing Additively Manufactured Concrete Structures
Architecture and Reinforcement
https://doi.org/10.52825/ocp.v1i.81

Submitted: 29 Nov. 2021 | Published: 15 Feb. 2022

Strategies for Integrating Straight Rebar in 3DCP Columns and Shear Walls

Ana Anton[1][https://orcid.org/0000-0002-3034-8978], Lex Reiter[2], and Eleni Skevaki[1][https://orcid.org/0000-0003-4820-4048]

[1] Digital Building Technologies, ETH, Switzerland

[2] Physical Chemistry of Building Materials, ETH, Switzerland

Abstract. 3D Concrete Printing (3DCP) is one of the most used digital fabrication processes with concrete as it allows the shaping of concrete into freeform geometries that optimize material use without the need for formworks. Despite the recent advancements of the technology, incorporating reinforcement remains one of its main shortcomings that obstruct it from being used in structural applications. The presented work proposes a diagonal grid of intersecting straight rebars as a reinforcement strategy for 3DCP. By acting as a guide for reinforcement in two directions, the resulting diagrid lattice offers structural efficiency and takes advantage of the geometric freedom of the fabrication process to integrate open channels during printing. Those can serve either as formwork for casting structural concrete or as channels for post-tensioning. The building components use less amount of concrete overall together with linear, inexpensive rebars. This design strategy was tested in a series of columns and a wall element and could be further extended to slabs. From a structural standpoint, the materialized prototypes should be tested and evaluated against existing structural systems for reinforced concrete.

Keywords: Digital Concrete, 3DCP, reinforcement

Conference presentation video: https://doi.org/10.5446/56114

Competing interests

The authors declare no competing interests.

Funding

This research was supported by the NCCR Digital Fabrication, funded by the Swiss National Science Foundation (NCCR Digital Fabrication Agreement #51NF40-141853). ETH Zürich Foundation supported this research under the project number: 2019-FE-202.

Acknowledgement

We acknowledge the contribution of Michael Lyrenmann, Philippe Fleischmann, Tobias Hartmann (Robotic Fabrication Lab) and Andreas Reusser (Concrete Lab) for the setup development and continuous support in robotics and concrete technology.

Vision and Strategies for Reinforcing Additively Manufactured Concrete Structures

Reinforcing Methods

https://doi.org/10.52825/ocp.v1i.73

Submitted: 28 Sept. 2021 | Accepted: 13 Jan. 2022 | Published: 15 Feb. 2022

Strategies for integrating reinforcement into 3D concrete printing at TU Dresden

Egor Ivaniuk[1][https://orcid.org/0000-0002-0905-9557], Steffen Müller[1][https://orcid.org/0000-0002-0630-5441], Tobias Neef[1][https://orcid.org/0000-0002-8256-1455], and Viktor Mechtcherine[1][https://orcid.org/0000-0002-4685-7064]

[1] Technische Universität Dresden, Germany

Abstract. 3D concrete printing (3DCP) has all the chances to become the future of the construction industry, but this technology is not yet widely applicable. One of the main challenges still to be mastered is the difficulty of reinforcing printed structures. At this point, many reinforcement strategies have already been proposed, which are fully or partially capable of solving the problem. This publication provides first an overview of existing reinforcement strategies, classified according to the time of reinforcement introduction: before, during, or after 3D printing. Then the authors present the approaches developed at TU Dresden and provide readers with information on new methods that still are in the development stage.

Keywords: Digital Construction, Digital Concrete, Additive Manufacturing, 3D Concrete Printing, Reinforcement

Conference presentation video: https://doi.org/10.5446/56110

Introduction

The need for qualitative changes in the construction sector has been growing for a long time. The main reasons for this are the global technological progress, the increasing need for affordable housing, low productivity in construction works and scarcity of skilled workers in many countries [1]. While other industries such as the automotive and appliance industry have already moved to a high degree of automation, most construction projects are still carried out using manual labor. This can be changed by introducing new automated digital technologies into construction.

A number of technologies, that enable to achieve high automation of construction, have already been developed, such Smart Dynamic Casting [2], Mesh Mold [3], automated brick-laying [4], and Additive Manufacturing techniques [5] including 3D concrete printing based on layered extrusion [6], material jetting [7], and particle-bed binding [8]. At the moment 3D concrete printing technologies seem to be most promising, as can be concluded from the numerous construction projects completed worldwide [9]. They have all chances to become the future of the industry, offering faster construction, less manual work and more safety for workers, saving materials, and reducing the cost [10].

However, 3D concrete printing still has a number of problems that hinder its further development. One of the most major challenges is the absence of an ultimate solution for the reinforcement of 3D printed structures, that could be automated and would enable to sufficiently reinforce the printed structure in all required directions. Conventional reinforcement, which until now has mainly been used in 3D concrete printing projects, limits design freedom and requires manual installation and therefore does not allow for a high level of automation.

That is why researchers are currently trying to find alternative methods of reinforcement that would bring 3D printing technology to its full potential. This publication provides a brief overview of already existing approaches for reinforcement of 3D printed concrete structures and presents the state of current research at TU Dresden in this field.

Existing reinforcement strategies in 3D concrete printing

While no ultimate solution for fully automated reinforcing in 3D concrete printing has yet been developed, many reinforcement strategies have already been demonstrated; see e.g. [11]–[16]. The possibilities for reinforcement integration can greatly vary depending on the chosen digital construction process. Rather than describe the reinforcement strategies for different existing digital construction technologies, as it has been presented already in earlier publications, this paper will focus on the strategies applicable for 3D printing by layer-by-layer extrusion only. Thus, it can serve as a kind of a catalogue of existing and developing methods of reinforcement integration for this technology. The next three sections present the existing reinforcement strategies divided into three groups depending on the time of reinforcement introduction: before, during, and after 3D printing.

Introduction of reinforcement prior concrete printing

HuaShang Tengda company demonstrated the use of pre-installed steel meshes for the construction of vertical walls [17]; see Fig. 1a. Mesh reinforces a wall simultaneously in two directions, and, since this reinforcement is similar to the wall reinforcement in traditional concrete construction, this strategy can simplify the process of government approval, however, provided there are no cavities and good adhesion between the concrete and the reinforcement. The disadvantages of this reinforcement method are the need for a special printer with a huge bifurcated printhead and limited design freedom. The maximum height of the used reinforcement mesh is limited by the height of the bifurcated part, so a pause in the 3D printing process may be required to build up the mesh at the top.

A pre-installed mesh also can be used as a support for printing inclined and curved structures. The possibility of printing on meshes was proved as a part of the SCRIM project [18], where they used tightly fixed fine textile meshes for 3D printing of various patterns; see Fig. 1b.

a) b)

Figure 1. Introduction of reinforcement prior concrete printing: a) 3D printing around the steel meshes using bifurcated printhead [17] and b) extrusion-based material deposition on a fine textile mesh [18].

Reinforcement integration during concrete printing

The ability to integrate reinforcement during printing will allow 3D printing technology to fully reveal its potential in automation and construction speed, which is why much research has been being carried out in this area. So far, the following strategies for integrating reinforcement during concrete printing have been presented:

1) Reinforcement with bars:
   - Placement of bars in between the printed layers [19]; see Fig. 2a. The automated installation of long bars is difficult due to their bending and vibration.
   - Welding of short bars [20]. With the use of a twin nozzle, the bars can also be installed in the vertical direction; see Fig. 2b. Positioning of short bars is more precise than long ones, however, the automation of this technology is challenging and has not yet been implemented.
2) Placement of meshes and textiles for bi-directional reinforcement:
   - Horizontal placement of steel meshes in between the printed layers. For contour crafting 3D printing technology, where only the outer edges of the walls are printed for subsequent filling, this mesh allows the printed edges of the walls to be held together; see Fig. 2c.
   - Narrow textile mesh is installed vertically between layers, requiring the use of a special split nozzle [21]; see Fig. 2d. The diameter of wires in the used mesh must be small enough to provide the flexibility required to automate the mesh installation process.
   - Placement of textile in between the layers [22] for the production of a reinforced beam with 3D printing; see Fig. 2e.
3) Entraining of a cable into the printing layer. With this technology, the structure is reinforced only in the direction of printing, and the cable cross-section is limited since it must be sufficiently flexible. A system for the automated insertion of cables into extruded filament was presented at TU Eindhoven [23]; see Fig. 2f.
4) Penetration reinforcement to provide bond across the printed layers and available for full automation:
   - Pressing or shooting nails [24], short bars [25], [26], wire fibers [26] or staples [27] into printed layers; see Fig. 2g. These methods of introducing reinforcement, however, can damage the printed structure and can result in poor adhesion between the reinforcement and the concrete [11].
   - Insertion of screws by a combination of pressing and rotation; see Fig. 2h. The research conducted by Hass and Bos [28] showed a high quality of the bond between screws and printed concrete.
5) Short fibers dispersed within 3D printing material; see Fig. 2i. Because of their discontinuity, short fibers can hardly provide sufficient reinforcement, however, they are easy to use, protect the printed structure from cracking, and can be combined with virtually any other reinforcement technology.

a)

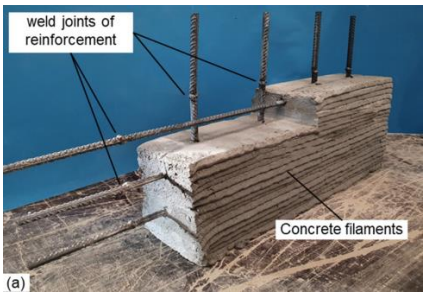

b)

c)

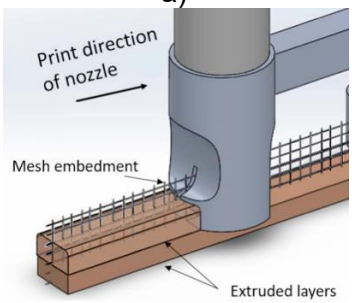

d)

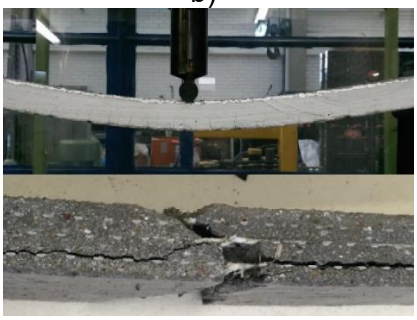

e)

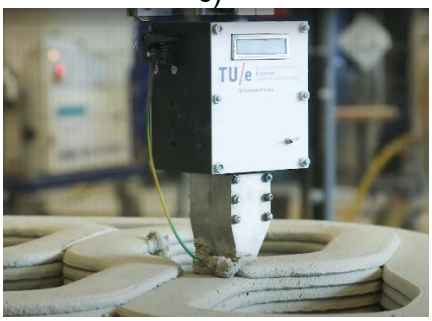

f)

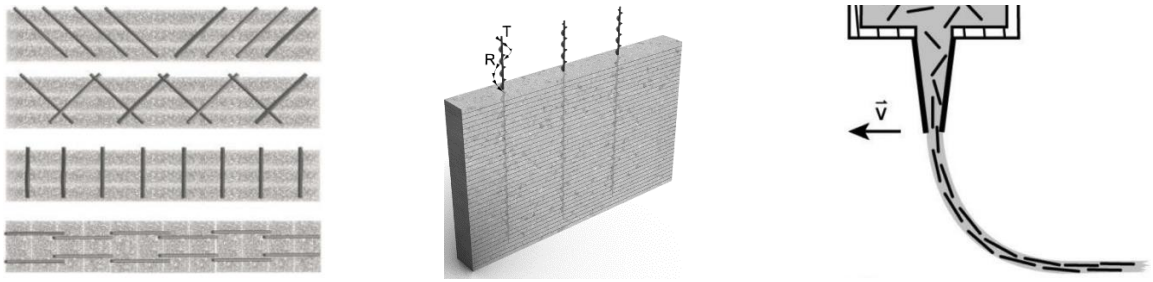

g) h) i)

Figure 2. Reinforcement integration during concrete printing with a) conventional steel bars [29], b) welding of short bars [20], c) steel mesh [30], d) textile mesh [21], e) AR-glass textile [22], f) steel cable [31], g) nails [24], h) screws [28], and i) short fibers [32].

Reinforcement integration after concrete printing

After 3D concrete printing, reinforcing bars can be placed in specially created cavities and in certain cases post-tensioned. This method was used to reinforce individual structural elements [33], or entire structures consisting of several 3D printed segments, as demonstrated in the construction of bridges [34], [35]; see Fig. 3a.

External reinforcement system is another approach developed by Asprone et al. [36]. In their study, a beam was produced from variable 3D printed modules, connected to each other by steel bars; see Fig. 3b.

Pre-fabricated cages are currently the most widely used reinforcement for the construction of columns with 3D printing. For this only the outer edge of the structure is printed that serves as a stay-in-place formwork. After that, it is possible to install a cage inside and fill the voids with concrete; see Fig. 3c.

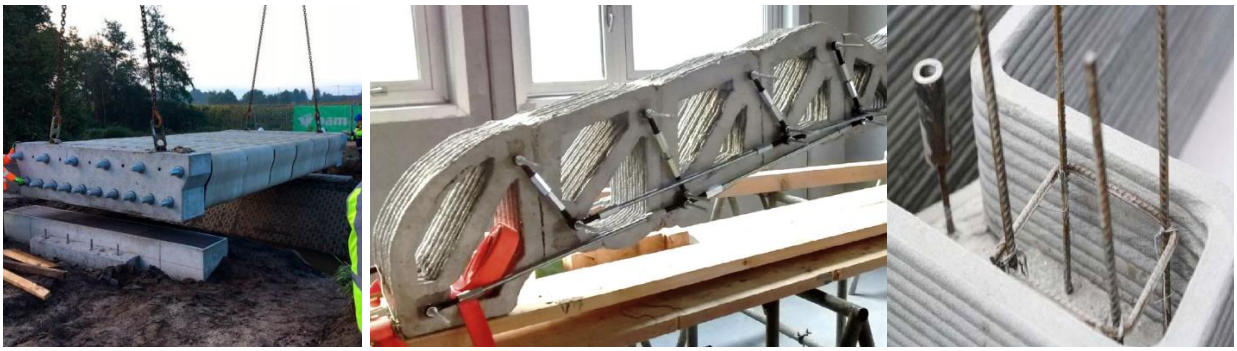

a) b) c)

Figure 3. Reinforcement integration after concrete printing with a) post-tensioned bars [34], b) external reinforcement system [36], and c) pre-fabricated cages [37].

Reinforcement strategies developed at TU Dresden

Introduction of reinforcement prior to concrete printing

A textile mesh laid on a flat surface can be used to create beams or slabs by 3D printing; see Fig. 4. Textiles do not corrode, therefore they do not require a protective layer of concrete, and the tests carried out have shown that the mesh adheres well even to relatively stiff concrete; see Fig. 4a and 4b. The advantage of this method is that reinforced beams and slabs of the required dimensions can be manufactured directly on the construction site using a 3D printer and placed in the final position after the concrete has hardened.

a) b) c)

Figure 4. a) Production of a textile reinforced beam using 3D concrete printing, b) bottom side of the beam, c) demonstration of the use of the beam: lintel with 800 *mm* span.

In addition to printing in horizontal layers, there are also interesting fields of application for the vertical printing direction. In preliminary tests for extrusion in the vertical direction on various substrates used as a support structure, it was possible to create surface evenness analogous to horizontally deposited elements and thus to prove the applicability of this printing method. When applying the layers to a standing coarse-meshed textile (fiber strand spacing 21 *mm*), a slight textile penetration was achieved (see Fig. 5a), whereby a further reinforcement variant could be derived. This variant is based on an upright reinforcement cage of conventional design, but without a simultaneous two-sided concrete application. Instead, the reinforcement cage is supplemented by a textile net installed on the horizontal bars in the middle of the wall and consequently, only one-half of the wall is printed from the side of the vertical element in the first step; see Fig. 5b. The extrusion parameters and rheological properties of the material should be selected so that the concrete does not penetrate the textile mesh, while still providing full coverage of the steel reinforcement. This method [38] allows using a much more compact printhead and provides more degrees of freedom with regard to wall thickness and curvatures.

a) b)

Figure 5. Reinforcement with standard reinforcement cage and inner textile mesh; a) penetration of textile mesh after vertical concrete depositing, b) principal process sketch [38].

Reinforcement integration during concrete printing

The technologically most demanding approach of reinforcement integration is a fully automated reinforcement implementation directly in the printing process. For steel reinforcements, a printhead extension is currently in the development phase which connects reinforcement bar sections to underlying steel elements by means of a welding process and thereby creating a continuous reinforcement element. In this case, the concrete is poured from the two opposite sides through horizontal nozzles to ensure the cleanliness of the process zone for the next welding process. A corresponding principle sketch is shown in Fig. 6a.

Another method under investigation is the printing of reinforcement in parallel with the 3D printing of concrete [39]. With Wire Arc Additive Manufacturing (WAAM) the reinforcement is gradually built up with drops of molten metal. With this technology printing of reinforcement can be fully automated, and it gives complete control over the geometry of the reinforcing bars and the ability to adjust their cross-section; see Fig. 6b. Based on the results of the studies carried out, it was found that the values of elastic modulus, yield stress and tensile strength of the printed steel bars are slightly lower than those of conventional steel bars, but they have a much higher strain capacity. Parallel use of 3D printing of steel and concrete is still under development, and issues such as slow welding speeds and high temperatures that can damage printed concrete have yet to be addressed. Currently, WAAM technology is also being investigated in several other research institutions, including TU Munich [40], TU Braunschweig [41], and TU Delft [42]. Lately, the use of 3D printing of steel in construction was demonstrated by MX3D company by printing a whole bridge, which was later installed in Amsterdam [43].

In order to improve the bond between the printed layers while placing horizontal reinforcement, at TU Dresden it was proposed to use 2.5D textiles [44]; see Fig. 6c. Such textiles can be very useful specifically when there is a pause in construction, which can lead to the formation of a cold joint. It is assumed that in the future the laying of such reinforcement can be automated by installing a spool with textiles on a 3D printer.

Figure 6. a) Principal process sketch for installing reinforcement by welding process b) 3D printed steel bars [39], and c) illustration of 2.5D textile laying process [44].

The reinforcement with continuous carbon fibers is another investigated approach. Specially developed suspension made of micro-cement, microsilica, water, and superplasticizer [45] for impregnation of continuous fibers has many advantages over polymer impregnation of the yarns [46]. A very high technological flexibility allows the geometrical freedom of additive manufacturing to be fully exploited. The impregnated yarn can be wound onto a spool and introduced into a structure during its 3D printing following two different methods:

- Contiguous process: The yarn is placed on the already printed concrete filament and overprinted, see Fig. 7a. The advantage of this process is that the number of filaments can be varied, while also overlapping of yarns for a better transfer of tensile forces can be easily implemented. The disadvantage is that the bond in the joint is disturbed by the yarn to some extent [47].
- Simultaneous process: The yarn is inserted into layers during the printing through the openings on the back of the nozzle. Thus, the reinforcement is integrated directly into the concrete filament and deposited together; see Fig. 7b. The simultaneous process saves time and does not disturb the joint. Through openings in the back of the nozzle, up to six yarns can be integrated at the same time; see Fig. 7c. It must be taken into account that, if the consistency of an extruded material is too stiff, air pockets similar to spray shadows can occur under the reinforcement [48].

a) b) c)

Figure 7. a) Yarn is placed between the layers [47], b) yarn is integrated directly into printed layer [48], and c) nozzle geometry for integrating textile yarns into printed layers.

Strain Hardening Cementitious Composites (SHCC) are materials reinforced with short fibers and showing quasi-ductile behavior under tensile loading. SHCC can reduce the need for reinforcement or in some cases even to enable doing without it completely. Ogura et al. [49] have developed SHCC suitable for 3D printing; see Fig. 8a. According to the results of tensile tests carried out during the study, the developed material with 1.5 *%* of fibers by volume of the composite has a tensile strength of approximately 5 *MPa* and a strain capacity of approximately 3 *%*; see Fig. 8b. Later on, at the Shimizu Institute of Technology, Ogura implemented this approach under the name of Laminatable Cement-based Tough Material - fiber-reinforced cement composite, that was used to print the permanent formwork for the construction of the columns with a height of 4.2 *m* [50]; see Fig. 8c. It is worth noting that investigations on printable SHCC are carried out in several research groups, the comprehensive review on the progress in this field was presented by Li et al. [51].

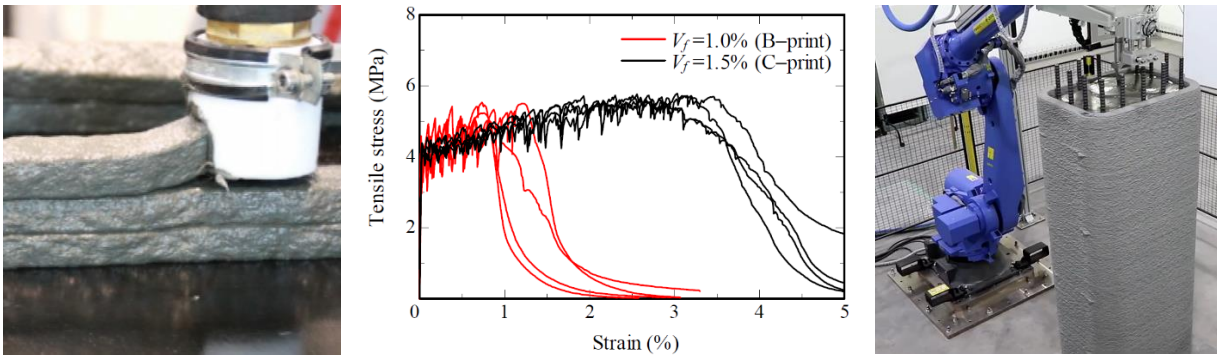

a) b) c)

Figure 8. a) 3D printing with SHCC, b) uniaxial tension tests results for a printable SHCC [49], and c) construction of a column with SHCC as a permanent formwork [50].

Reinforcement integration after concrete printing

The method of post-reinforcement of printed structures can be considered as a direct continuation of the work on the development of full-width printing technology CONPrint3D [52], but it is also suitable for contour crafting approaches. Fig. 9a presents a principle sketch. This method is technologically simple to implement, since the printing process has already been mastered, and all that remains is to place the anchors between the printed layers at certain distances. After the printed core wall has hardened, the required reinforcement can be suspended from these anchors in the form of a steel or a textile mesh; see Fig. 9b and 9c, respectively. Afterward, it can be monolithically connected to the wall by a laterally guided vertical or horizontal printing process and the final geometry of the component can be achieved. The advantage of this construction variant is due to the low demands on the machine technology and can be realized with slight adaptations with most of the printing systems com-

monly available on the market. The disadvantages are the mostly manual fastening of the reinforcement (this process can be automated though) and the need of consecutive process steps.

Figure 9. Post-printing integration of reinforcement a) principle sketch, b) steel mesh reinforcement on the printed subgrade, and c) reinforcement with a carbon textile.

Conclusion

With the development of 3D concrete printing technology, an increasing number of various strategies for reinforcement of printed structures have appeared. This publication provides a brief overview of the existing reinforcement methods and introduces various strategies developed at TU Dresden.

As in conventional construction, 3D printed walls require reinforcement in two directions. Most of the existing strategies for reinforcement integration during concrete printing cannot provide that, therefore, they must be applied in combination with other methods. Highly automated technologies that could fully cover the need for reinforcement, namely welding of short bars and 3D printing of reinforcement using Wire Arc Additive Manufacturing, are not yet ready for practical applications and still require further research. In the meantime, installing steel reinforcement before or after 3D printing is a good alternative. As examples, this article introduces both a new strategy for the installation of reinforcement before printing using fine textile mesh, which does not require a sophisticated printhead geometry, and a new strategy for reinforcement after printing, which is easy to implement as it does not involve a high degree of automation. This article also presents a new method for the production of reinforced beams and slabs directly on the construction site by printing over a textile mesh. Furthermore, some other developed approaches for reinforcement using 2.5D textile, continuous carbon fibers, and by printing of Strain Hardening Cementitious Composites are presented.

Data availability statement

Data sharing not applicable.

Author contributions

Conceptualization, E.I. and V.M.; writing – original draft, E.I., S.M., and T.N.; writing – review & editing, V.M.; funding acquisition – V.M.

Competing interests

The authors declare no competing interests.

Acknowledgement

This paper is a part of the first author's PhD dissertation. The authors would like to thank the German Research Foundation (Deutsche Forschungsgemeinschaft – DFG) for financial support of the project number 424057211 "Adaptive Concrete Diamond Construction (ACDC)", within the Priority Program "Adaptive modularized constructions made in flux" (SPP 2187) and the project number 417002380 within the framework of the projects SFB/TRR 280 "Design strategies for material-minimised carbon reinforced concrete structures – Principles of a new approach to construction".

References

1. R. Maskuriy, A. Selamat, K. N. Ali, P. Maresova, and O. Krejcar, "Industry 4.0 for the Construction Industry—How Ready Is the Industry?," Appl. Sci., vol. 9, no. 14, p. 2819, 2019, doi: https://doi.org/10.3390/app9142819.
2. E. Lloret et al., "Complex concrete structures," Comput. Des., vol. 60, pp. 40–49, 2014, doi: https://doi.org/10.1016/j.cad.2014.02.011.
3. N.. Hack, "Mesh Mould : Robotically Fabricated Metal Meshes as Concrete Formwork and Reinforcement," no. September, pp. 1–13, 2015.
4. Z. Dakhli and Z. Lafhaj, "Robotic mechanical design for brick-laying automation," Cogent Eng., vol. 4, no. 1, 2017, doi: https://doi.org/10.1080/23311916.2017.1361600.
5. R. Buswell et al., "A process classification framework for defining and describing Digital Fabrication with Concrete," Cem. Concr. Res., vol. 134, no. March, 2020, doi: https://doi.org/10.1016/j.cemconres.2020.106068.
6. R. Buswell, W. R. Leal de Silva, S. Z. Jones, and J. Dirrenberger, "3D printing using concrete extrusion: A roadmap for research," Cem. Concr. Res., vol. 112, no. October 2017, pp. 37–49, 2018, doi: https://doi.org/10.1016/j.cemconres.2018.05.006.
7. N. Hack and H. Kloft, "Shotcrete 3D Printing Technology for the Fabrication of Slender Fully Reinforced Freeform Concrete Elements with High Surface Quality: A Real-Scale Demonstrator," RILEM Bookseries, vol. 28, no. July, pp. 1128–1137, 2020, doi: https://doi.org/10.1007/978-3-030-49916-7_107.
8. D. Lowke, E. Dini, A. Perrot, D. Weger, C. Gehlen, and B. Dillenburger, "Particle-bed 3D printing in concrete construction – Possibilities and challenges," Cem. Concr. Res., vol. 112, no. November 2017, pp. 50–65, 2018, doi: https://doi.org/10.1016/j.cemconres.2018.05.018.
9. "8 Biggest Companies Building 3D Printed Houses | All3DP Pro." https://all3dp.com/2/2019-best-companies-building-3d-printed-houses/ (accessed Sep. 15, 2021).
10. T. Wangler et al., "Digital Concrete: Opportunities and Challenges," RILEM Tech. Lett., vol. 1, p. 67, 2016, doi: https://doi.org/10.21809/rilemtechlett.2016.16.
11. V. Mechtcherine et al., "Integrating reinforcement in digital fabrication with concrete: A review and classification framework," Cem. Concr. Compos., vol. 119, no. February, p. 103964, 2021, doi: https://doi.org/10.1016/j.cemconcomp.2021.103964.
12. D. Asprone, C. Menna, F. Bos, T. A. M. Salet, J. Mata-Falcón, and W. Kaufmann, "Rethinking reinforcement for digital fabrication with concrete," Cem. Concr. Res., vol. 112, no. January, pp. 111–121, 2018, doi: https://doi.org/10.1016/j.cemconres.2018.05.020.
13. V. N. Nerella, H. Ogura, and V. Mechtcherine, "Incorporating reinforcement into digital concrete construction," Annu. IASS Symp. Creat. Struct. Des., no. July, 2018.
14. F. Bester, M. van den Heever, J. Kruger, and G. van Zijl, "Reinforcing digitally fabricated concrete: A systems approach review," Addit. Manuf., vol. 37, no. September 2020, 2021, doi: https://doi.org/10.1016/j.addma.2020.101737.
15. H. Kloft, M. Empelmann, N. Hack, E. Herrmann, and D. Lowke, " Reinforcement strategies for 3D-concrete-printing ," Civ. Eng. Des., vol. 2, no. 4, pp. 131–139, 2020, doi: https://doi.org/10.1002/cend.202000022.

16. Paolini, S. Kollmannsberger, and E. Rank, “Additive manufacturing in construction: A review on processes, applications, and digital planning methods,” Addit. Manuf., vol. 30, no. October, p. 100894, 2019, doi: https://doi.org/10.1016/j.addma.2019.100894.
17. “World’s first 3D-printed house that can withstand 8.0-magnitude quake - YouTube.” https://www.youtube.com/watch?v=OloOc21_u80 (accessed Sep. 15, 2021).
18. P. Ayres, W. Ricardo, P. Nicholas, and T. J. Andersen, “SCRIM – Sparse Concrete Reinforcement in Meshworks,” Robot. Fabr. Archit. Art Des. 2018, no. September 2018, 2019, doi: https://doi.org/10.1007/978-3-319-92294-2.
19. B. Baz, G. Aouad, P. Leblond, O. Al-Mansouri, M. D’hondt, and S. Remond, “Mechanical assessment of concrete – Steel bonding in 3D printed elements,” Constr. Build. Mater., vol. 256, p. 119457, 2020, doi: https://doi.org/10.1016/j.conbuildmat.2020.119457.
20. M. Classen, J. J. , and R. Sharma, “Additive manufacturing of reinforced concrete-development of a 3D printing technology for cementitious composites with metallic reinforcement,” Appl. Sci., vol. 10, no. 11, 2020, doi: https://doi.org/10.3390/app10113791.
21. T. Marchment and J. G. Sanjayan, “Mesh reinforcing method for 3D Concrete Printing,” Autom. Constr., vol. 109, no. August 2019, p. 102992, 2020, doi: https://doi.org/10.1016/j.autcon.2019.102992.
22. W. Wang, N. Konstantinidis, S. A. Austin, R. Buswell, S. Cavalaro, and D. Cecinia, “Flexural Behaviour of AR-Glass Textile Reinforced 3D Printed Concrete Beams,” in Second RILEM International Conference on Concrete and Digital Fabrication, 2020, pp. 728–737, doi: https://doi.org/10.1007/978-3-030-49916-7_73.
23. F. Bos, Z. Y. Ahmed, E. R. Jutinov, and T. A. M. Salet, “Experimental exploration of metal cable as reinforcement in 3D printed concrete,” Materials (Basel)., vol. 10, no. 11, 2017, doi: https://doi.org/10.3390/ma10111314.
24. Perrot, Y. Jacquet, D. Rangeard, E. Courteille, and M. Sonebi, “Nailing of layers: A promisingway to reinforce concrete 3D printing structures,” Materials (Basel)., vol. 13, no. 7, 2020, doi: https://doi.org/10.3390/ma13071518.
25. T. Marchment and J. Sanjayan, “Bond properties of reinforcing bar penetrations in 3D concrete printing,” Autom. Constr., vol. 120, no. May, p. 103394, 2020, doi: https://doi.org/10.1016/j.autcon.2020.103394.
26. C. Matthäus, N. Kofler, T. Kränkel, D. Weger, and C. Gehlen, “Interlayer reinforcement combined with fiber reinforcement for extruded lightweight mortar elements,” Materials (Basel)., vol. 13, no. 21, pp. 1–17, 2020, doi: https://doi.org/10.3390/ma13214778.
27. O. Geneidy, S. Kumarji, A. Dubor, and A. Sollazzo, “Simultaneous Reinforcement of Concrete While 3D Printing,” in Second RILEM International Conference on Concrete and Digital Fabrication, 2020, pp. 895–905.
28. L. Hass and F. Bos, “Bending and Pull-Out Tests on a Novel Screw Type Reinforcement for Extrusion-Based 3D Printed Concrete,” RILEM Bookseries, vol. 28, no. July, pp. 632–645, 2020, doi: https://doi.org/10.1007/978-3-030-49916-7_64.
29. “V2 Vesta Beton-3D-Drucker baut kleines Haus.” https://3druck.com/drucker-und-produkte/v2-vesta-beton-3d-drucker-baut-kleines-haus-2846225/ (accessed Sep. 09, 2021).
30. “Rudenko 3D Printer.” http://www.totalkustom.com/gallery.html (accessed Sep. 09, 2021).
31. “3D printed concrete bridge - YouTube.” https://www.youtube.com/watch?app=desktop&v=Uzg6pilf0PI&t=275s (accessed Sep. 09, 2021).
32. M. Hambach and D. Volkmer, “Properties of 3D-printed fiber-reinforced Portland cement paste,” Cem. Concr. Compos., vol. 79, pp. 62–70, 2017, doi: https://doi.org/10.1016/j.cemconcomp.2017.02.001.
33. S. Lim, R. Buswell, T. T. Le, S. A. Austin, A. G. F. Gibb, and T. Thorpe, “Developments in construction-scale additive manufacturing processes,” Autom. Constr., vol. 21, no. 1, pp. 262–268, 2012, doi: https://doi.org/110.1016/j.autcon.2011.06.010.

34. T. A. M. Salet, Z. Y. Ahmed, F. Bos, and H. L. M. Laagland, “Design of a 3D printed concrete bridge by testing,” Virtual Phys. Prototyp., vol. 13, no. 3, pp. 222–236, 2018, doi: https://doi.org/10.1080/17452759.2018.1476064.
35. “An optimal concrete bridge — Department of Structural Engineering and Building Materials.” https://www.ugent.be/ea/structural-engineer-ing/en/research/clusters/themes/digitalfabrication/projectsdigitalfabrication/3dbridge.htm (accessed Sep. 10, 2021).
36. D. Asprone, F. Auricchio, C. Menna, and V. Mercuri, “3D printing of reinforced concrete elements: Technology and design approach,” Constr. Build. Mater., vol. 165, pp. 218–231, 2018, doi: https://doi.org/10.1016/j.conbuildmat.2018.01.018.
37. “Shanghai-based WinSun 3D Prints 6-Story Apartment Building and an Incredible Home - 3DPrint.com | The Voice of 3D Printing / Additive Manufacturing.” https://3dprint.com/38144/3d-printed-apartment-building/ (accessed Sep. 10, 2021).
38. “Patent Application: Technology for extrusions-based manufacturing of reinforced concrete elements,” 2021012014094001DE, 2021
39. V. Mechtcherine, J. Grafe, V. N. Nerella, E. Spaniol, M. Hertel, and U. Füssel, “3D-printed steel reinforcement for digital concrete construction – Manufacture, mechanical properties and bond behaviour,” Constr. Build. Mater., vol. 179, pp. 125–137, 2018, doi: https://doi.org/10.1016/j.conbuildmat.2018.05.202.
40. D. Weger et al., “Reinforced Particle-Bed Printing by Combination of the Selective Paste Intrusion Method with Wire and Arc Additive Manufacturing -- A First Feasibility Study,” in Second RILEM International Conference on Concrete and Digital Fabrication, 2020, pp. 978–987.
41. J. Müller et al., “Design and parameter identification of wire and arc additively manufactured (WAAM) steel bars for use in construction,” Metals (Basel)., vol. 9, no. 7, 2019, doi: https://doi.org/10.3390/met9070725.
42. Z. Lin, C. Goulas, W. Ya, and M. J. M. Hermans, “Microstructure and mechanical properties of medium carbon steel deposits obtained via wire and arc additive manufacturing using metal-cored wire,” Metals (Basel)., vol. 9, no. 6, 2019, doi: https://doi.org/10.3390/met9060673.
43. “MX3D Bridge | MX3D.” https://mx3d.com/industries/infrastructure/mx3d-bridge/ (accessed Sep. 20, 2021).
44. V. Mechtcherine and V. N. Nerella, “Integration der Bewehrung beim 3D-Druck mit Beton,” Beton- und Stahlbetonbau, vol. 113, no. 7, pp. 496–504, 2018, doi: https://doi.org/10.1002/best.201800003.
45. K. Schneider, A. Michel, M. Liebscher, L. Terreri, S. Hempel, and V. Mechtcherine, “Mineral-impregnated carbon fibre reinforcement for high temperature resistance of thin-walled concrete structures,” Cem. Concr. Compos., vol. 97, pp. 68–77, 2019, doi: https://doi.org/10.1016/j.cemconcomp.2018.12.006.
46. V. Mechtcherine, A. Michel, M. Liebscher, K. Schneider, and C. Großmann, “Mineral-impregnated carbon fiber composites as novel reinforcement for concrete construction: Material and automation perspectives,” Autom. Constr., vol. 110, no. September 2019, p. 103002, 2020, doi: https://doi.org/10.1016/j.autcon.2019.103002.
47. V. Mechtcherine, A. Michel, M. Liebscher, and T. Schmeier, “Extrusion-Based Additive Manufacturing with Carbon Reinforced Concrete: Concept and Feasibility Study,” Materials (Basel)., vol. 13, no. 11, p. 2568, 2020, doi: https://doi.org/10.3390/ma13112568.
48. T. Neef, S. Müller, and V. Mechtcherine, “3D-Druck mit Carbonbeton: Technologie und die ersten Untersuchungsergebnisse,” Beton- und Stahlbetonbau, vol. 115, no. 12, pp. 943–951, 2020, doi: https://doi.org/10.1002/best.202000069.
49. H. Ogura, V. N. Nerella, and V. Mechtcherine, “Developing and testing of Strain-Hardening Cement-Based Composites (SHCC) in the context of 3D-printing,” Materials (Basel)., vol. 11, no. 8, pp. 1–18, 2018, doi: https://doi.org/10.3390/ma11081375.
50. “From the Institute of Technology Succeeding to create Massive Columns Having a Free-form Curved Surface With 3D Printing The Possibilities of ‘LACTM’ Fiber-

reinforced Cement Composite | Topics | Shimizu Corporation." https://www.shimz.co.jp/en/topics/technology/item01/ (accessed Sep. 20, 2021).
51. V. C. Li et al., "On the emergence of 3D printable Engineered, Strain Hardening Cementitious Composites (ECC/SHCC)," Cem. Concr. Res., vol. 132, no. January, p. 106038, 2020, doi: https://doi.org/10.1016/j.cemconres.2020.106038.
52. V. Mechtcherine, V. N. Nerella, F. Will, M. Näther, J. Otto, and M. Krause, "Large-scale digital concrete construction – CONPrint3D concept for on-site, monolithic 3D-printing," Autom. Constr., vol. 107, no. April, p. 102933, 2019, doi: https://doi.org/10.1016/j.autcon.2019.102933.

Vision and Strategies for Reinforcing Additively Manufactured Concrete Structures

Reinforcing Methods

https://doi.org/10.52825/ocp.v1i.77

Submitted: 30 Sept. 2021 | Accepted: 10 Nov. 2021 | Published: 15 Feb. 2022

Digital Concrete Production With Vertical Textile Reinforcement

First Trials

Gözdem Dittel[1][https://orcid.org/0000-0002-8277-9251], Martin Scheurer[1][https://orcid.org/0000-0002-5193-1871], Steffen Dringenberg[1], Joaquin Velasco Jitton[1], and Thomas Gries[1][https://orcid.org/0000-0002-2480-8333]

[1] Institute for Textile Technology of RWTH Aachen University, Germany

Abstract. One major challenge preventing widespread introduction of digital concrete production is the integration of reinforcing materials. Textile grid structures offer a possible solution for this challenge.

Textile reinforced concrete (TRC) has been researched for approximately 20 years and is currently being commercialized, initially in pre-cast elements for facades and bridges. TRC enables the construction of thin-walled, strong structures with a high freedom of design, properties well suited for the integration in digital concrete production.

First trials for this integration have been performed and published. However, these studies only use short fibres mixed into the concrete matrix or textile reinforcement within the printing plane, which limits the transferred loads.

This study shows the results of preliminary tests of vertical, out-of-plane textile reinforcements for digital concrete production. The textile reinforcement is fixed vertically and the concrete printing process is performed diagonally, “through” the textile. The results of four-point bending tests are presented.

Keywords: Fibre-Based Reinforcement; 3D-Concrete Printing; Textile Reinforced Concrete; Four-Point Bending Test, Digital Concrete Production

Conference presentation video: https://doi.org/10.5446/56107

Introduction

Building structures are traditionally made using primary materials such as cement, sand, fly-ash, water and other additives. These primary materials constitute to the formation of what is popularly referred to as concrete. In cases of specific strength requirements, additional reinforcing elements such as rebars are required. The primary drawback of these structures is that they are age limited by the deterioration rate of the steel rebar reinforcing structures. Beyond a certain age, building structures have to be refurbished or rebuilt in order to maintain their structural integrity [1].

This drawback led to the development of a new, innovative building structure material. Typically referred to as Textile Reinforced Concrete or TRC, these new building materials consist of concrete with a textile based reinforcement. These kind of reinforcements comprise of an alkali-resistant fibre based material such as glass, carbon or basalt fiber embed-

ded within a cementitious matrix. The overwhelming advantage of these textile or fiber based materials is their combination of providing enhanced mechanical performance and resistance to corrosion as compared to their steel reinforced counterparts [2]. The extended life of the building structures provided through such materials has proven to possess a game changing effect on the overall economics of advanced building structures in the present day. Further, their ability to form into flexible shapes now provides architects with the freedom to design complex shapes [3].

Several manufacturing processes have been developed for manufacturing TRC based structures. As an example, textile reinforcements are produced using a warp knitting or winding process. These textiles are then coated to ensure the compatibility of the bonds between the textile and concrete mix. One of the drawbacks of such a production process is that it continues to be labour intensive.

Hence there is a need to optimize the production process for the development of such TRC based structures. This paper provides an insight into a new approach of manufacturing TRC based structures using 3D printing techniques.

With the onset of the third revolution and the inclusion of Industry 4.0 principles into the manufacturing sector, automation has become a key element of the manufacturing industry [4]. The advent of 3D printing and the introduction of digital technologies in the concrete construction sector are the result of the appropriation and adaptation of technology initially developed for other materials, such as resins and plastics [5].

State of the art

There are several approaches available for addressing the production of TRC based structures, especially in the area of the concrete printing processes. There are two technologies that exhibit promising results: extrusion- or spraying-based layer-by-layer deposition of a pre-mixed concrete solution and layer-by-layer binding by jetting a binding agent onto a previously laid solid aggregate.

Binder jetting has been used to 3D print sand moulds, but it can also be used to print concrete directly [6]. It offers a high degree of complexity in the design, such as parts connected only from above, due to the supporting surrounding unbound material. However, binding jetting has many drawbacks. For example, the binding process limits the dimensions of the printing process, such as layer height and speed of the nozzle movement. At the same time, the outermost area of the structure can receive an unreliable amount of binder. Additionally, the unbound material (cement) might not be reusable and the inclusion of reinforcement is problematic, due to the need of periodically placing new layers of unbound material.

Extrusion based deposition is the most widely used solution which was explored as early as 2004 [7]. The technical principle has been realized through different approaches, but in all of them, a pre-mixed concrete solution is continuously or discretely pressured through the opening at the end of a stiff nozzle, fixed at the tip of the print head. Its simplicity and flexibility make it an ideal option for on-site use.

The consistency of the mixture and the hardening time are the keys to the feasibility and the speed of the printing process. Hasty printing on uncured layers may deform the structure, and too slow printing may mean a weak binding between layers thus limiting the vertical printing rate. The development of technology that incorporates the reinforcement in the automated process is still in nascent stages.

In one of the approaches, the contours of the structure are printed leaving openings in which later the steel cage is inserted, and concrete is poured, in order to bind the reinforcement with the concrete [8]. A similar solution initially places a steel cage structure and then,

using a specially designed print head and nozzle, encloses the cage layer-by-layer [9]. This however is limited by the geometry of both the nozzle head and the accessibility of the steel cage structure, especially in large scale structures (Figure 1).

Figure 1. Simultaneous extrusion on both sides of the steel reinforcement cage [9].

Research significance

In order to meet the growing demands, in volume and complexity, of the global construction industry, new production processes and materials are required. The combination of TRC and digital concrete production enables material efficient, quick and safe production of complex geometries. However, the integration of reinforcing textiles into the digital concrete production is challenging and current approaches are limited to the placement of reinforcement within the printing plane [10]. This paper presents a first step towards the vertical integration of reinforcing textiles into digital concrete production, facilitating structural reinforcement and unlocking new applications of digital concrete production.

Experimental investigation

In this study the structural behaviour of 3D-printed concrete elements with vertically positioned reinforcing textile grid structure is investigated under flexural load. The results are compared with the structural behaviour of the TRC specimens produced with the traditional casting method. In the following the material properties and production and testing methods are presented.

Fibre-based reinforcement materials and concrete mixtures

The biaxial warp knitted textile grid reinforcement is realized using alkali resistant (AR) glass rovings, type Cem-FIL® 5325 manufactured by the company Owens Corning. The mesh opening in warp and weft direction is approximately 8.4 mm. The rovings are warp knitted on the machine Karl Mayer Malimo P2-2S by using the binding type counterlaid tricot. This type of binding allows an easy impregnation of the coating material into the single fibres through the oval shaped cross section of the roving. The open mesh structure enables an easy penetration of the concrete matrix through the grid structure. The used knitting yarn is polyester yarn type 167f48. The physical and mechanical properties of the roving material are listed in Table 1.

Table 1. Properties of the roving material.

Property	AR-glass roving
Filament Diameter [µm]	19
Filament tensile strength [MPa]	1700
Modulus of elasticity [GPa]	72
Elongation at break [%]	2.4
Linear density of roving [tex]	2400
Density [g/cm^3]	2.68

The warp knitted textile is coated with an epoxy based resin material. The Epoxydharz L with the corresponding hardener EPH 161, produced by the company R&G Faserverbundwerkstoffe GmbH, is used in a mixing ratio of 100:25 parts by weight (resin:hardener). The coating material with its low viscosity and high strength is suitable to create an internal compound structure between the separate filaments of the roving. The mechanical properties of the epoxy resin system are given in Table 2.

Table 2. Properties of the epoxy resin system.

Property	R&G Epoxydharz L + EPH 161
Compressive strength [MPa]	123
Tensile strength [MPa]	70
Flexural strength [MPa]	112

For the production of 3D-printed specimens, a cement-based grouting mortar Sika Grout®-551 produced by the company Sika Deutschland GmbH is used. The matrix material has a maximum grain size of 1 mm, is viscous and easily pumpable and offers a fast hardening process at the same time. The compressive strength class is C50/60 (EN 206-1/DIN 1045-2), the flexural strength after 28 days is 10 MPa and the fresh mortar density is given as 2.27 g/cm^3.

To achieve a suitable matrix consistency for the printing process, the hardening accelerator Sigunit® L-5601 AF produced by the company Sika Deutschland GmbH is added to the mortar. The end mixture is printable as desired, sufficiently flowable to penetrate the textile and still dimensionally stable to adhere to the vertical, one-sided formwork immediately after application. The mixing ratio of the final mixture is listed in Table 3.

Table 3. Composition of the printable concrete mixture.

Component	Quantity [g/kg]
Sika Grout®-551	857.54
Water	137.21
Sika Sigunit® L-5601 AF	5.25

A fine grained concrete is used to produce the reference specimens. The maximum grain size is 0.6 mm. The flexural strength of the matrix material is 7.6 MPa and the compressive strength is 74.2 MPa, determined after 28 days. The composition of the mixture is given in Table 4.

Table 4. Composition of the reference concrete mixture.

Component	Quantity [kg/m3]
Cement CEM I 52,5 N	490
Fly ash	175
Silica fume (Elkem Microsilica® 940 U)	35

Quartz flour	500
Sand 0,2 – 0,6 mm	713
Water	280
Superplasticizer	7

Production of TRC specimens for four-point bending tests

In accordance to DIN EN 1170-5:1997 six 3D-printed Sika Grout, six cast Sika Grout TRC specimens and six reference cast TRC specimens are prepared to perform four-point bending tests. The dimensions of each specimen are as in the following: Length l = 340 mm, width w = 100 mm, thickness t = 15 mm. The textile reinforcement is positioned 5 mm above of the lower specimen face. Each specimen includes equal number of rovings in longitudinal and transversal directions.

3D-printed specimen: The coated textile is positioned in a vertical rectangular frame. The solid and liquid components are continuously mixed with an electric hand mixer for three minutes. Afterwards another two minutes are needed to fill the printing pump.

Each 15 mm wide and 50 mm high layer is printed from left to right, see Figure 2. The feed rate is constant at approximate 2 cm/s. The volume flow is regulated by the rotation speed of the threaded rod in the pump. Each specimen consists of two layers of printed matrix.

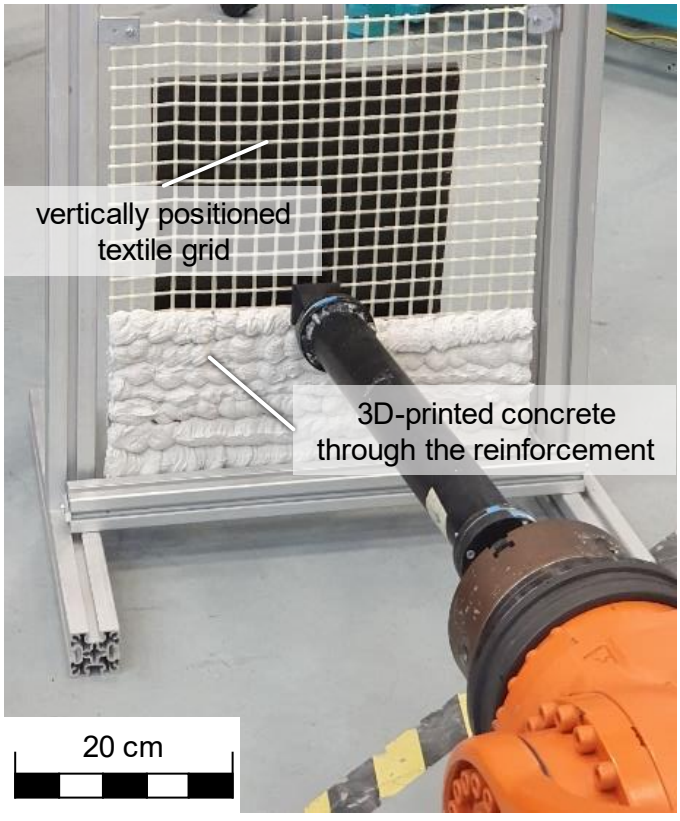

Figure 2. Demonstration of printing process.

Cast specimen: The coated textile is positioned in the same type of rectangular frame and the frame is placed horizontal to allow the casting process. The fine grained concrete mixture is poured into the formwork while applying vibration.

All specimens are cured for seven days. During the hardening process at room temperature, a foil cover protects the free matrix surfaces from water withdrawal for 24 hours. After-

wards the test specimens are removed from the formwork and stored in a water bath at room temperature for another six days until the test.

Four-point bending test: Test set-up

The four-point bending test is performed in accordance with DIN 1170–5 on a Zwick Roell testing device. The specimen is positioned on two support rollers and loaded using two load rollers in displacement controlled manner. A preload F = 1 N is applied to compensate for waviness and thickness deviations between the samples. The load rollers are moved downwards with a uniform test speed of 1.8 mm/min during which the load cell continuously determines the force. Measurements are taken up to a force drop of 70 % of the maximum force or up to a travel distance of 40 mm. Figure 3 shows the set-up of the four-point bending test.

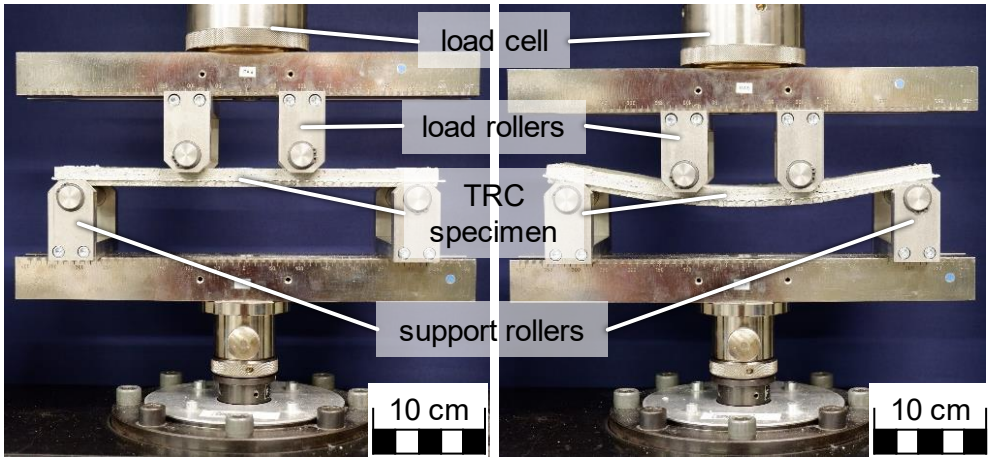

Figure 3. Experimental set-up of four-point bending test.

Experimental results and discussion

The load-deflection-curves of six 3D-printed Sika Grout TRC specimens, six cast Sika Grout TRC specimens and six reference cast TRC specimens are given in Figure 4.

The reference cast TRC specimens show a typical linear elastic response until the formation of the first crack. The cracking load values for each cast TRC specimen are between 7 to 8 MPa, which demonstrate the given flexural strength of the used fine grained concrete. Multiple micro cracks follow the first crack in the load-deflection-curves. The adhesive bond between the concrete matrix and the textile reinforcement gets damaged until approximately 10 MPa. Hereafter the textile continues to carry on the tensile stress by a residual constant friction between the internal filaments of the roving and shows a non-linear response until the average ultimate load around 22 MPa. Several macro-cracks occur on the lower face of the specimens. Beyond the ultimate load the specimen is also cracked on its upper face and the concrete matrix is completely separated into two parts. Only the longitudinal textile reinforcement absorbs the load.

The casted Sika Grout mixture specimens demonstrate an unclear behavior in the linear elastic zone. The first cracks and also a formation of multiple micro cracks are invisible. The reason for this behavior could depend on the additives in the cementitious matrix mixture. The specimens show an almost linear elastic response until the average ultimate load around 23 MPa.

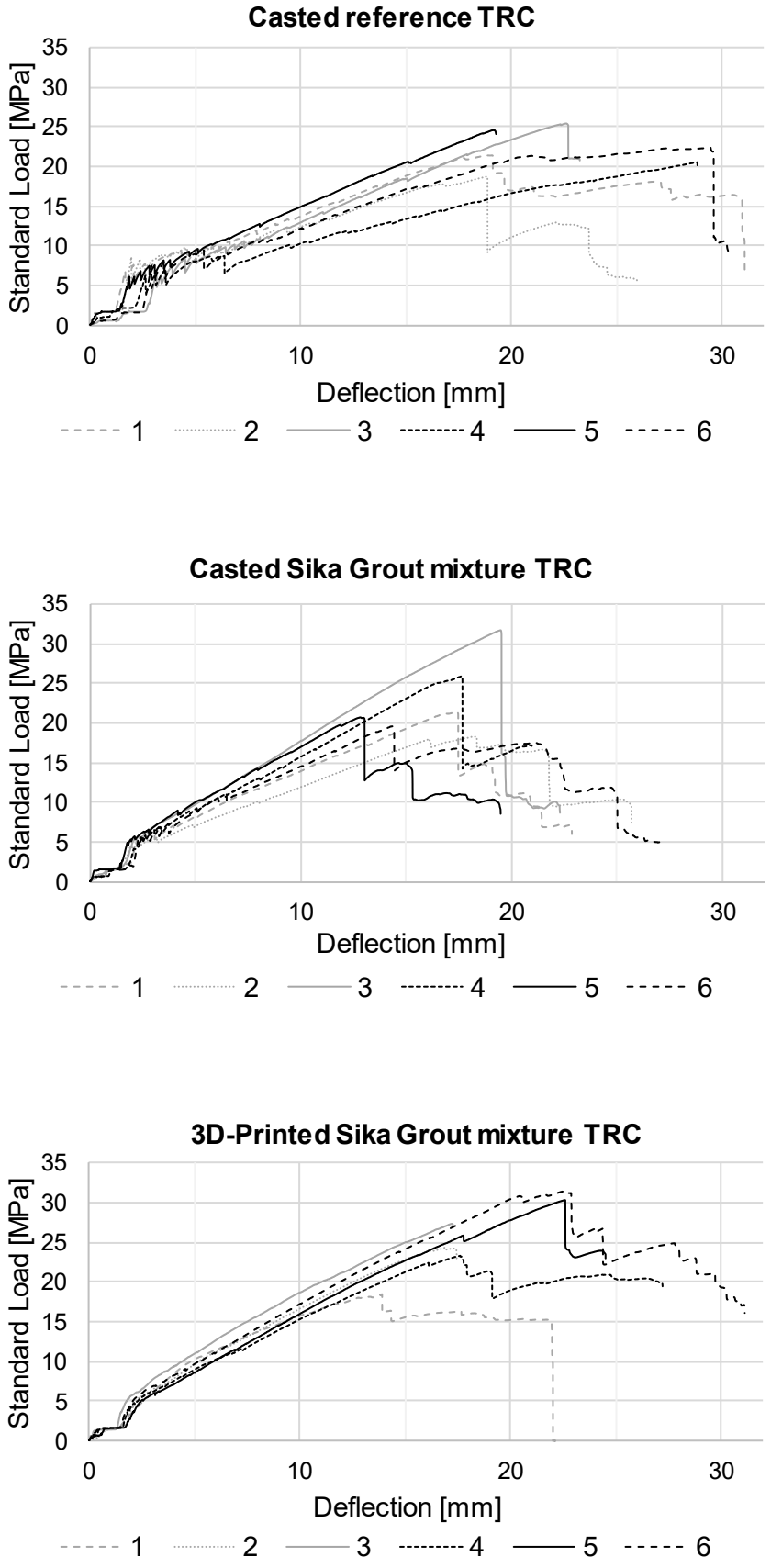

Figure 4. Load-deflection-curves of tested specimens.

The 3D-printed Sika Grout mixture specimens show an almost linear elastic response until the average ultimate load around 25 MPa. The reached ultimate load and its deflection value are similar on the basis of the relatively small sample even more preferable than these of the cast TRC specimen. The application of the cementitious matrix through the vertically positioned reinforcement grid does not affect the structural performance of the TRC elements adversely.

Conclusions

Based on the challenges in vertical reinforcement integration into the 3D concrete printing process, this study presented an alternative idea to integrate vertical reinforcement into the 3D-printed concrete structures. An experimental investigation of the effect of two different production methods for the TRC structures is presented. The AR-glass based textile grid reinforcement is positioned vertically and the concrete is printed horizontally through the textile grid. The structural behavior of the 3D-printed Sika Grout TRC specimens produced in the first trials is investigated under flexural load and compared with cast TRC specimens of the same matrix. To classify the new specialized Sika Grout mixture, there is a further comparison with traditional cast TRC specimens. Six specimens for each test series are loaded to perform four-point bending tests in accordance to DIN EN 1170-5:1997. The load-deflection behavior of all three test series are similar. In case of 3D-printed TRC the reached ultimate load is approximately 2 MPa higher than in case of the cast TRC (+9 % load). It can be concluded that the 3D-printing of the cementitious matrix through the textile grid structures has no negative effects on the structural performance of TRC elements and must be further developed.

Data availability statement

There is no relevant additional data to this article beyond the presented content.

Author contributions

Gözdem Dittel: Conceptualization, Investigation, Methodology, Visualization, Writing – original draft, review & editing. Martin Scheurer: Methodology, Writing – review & editing. Steffen Dringenberg: Investigation, Methodology, Visualization, Writing – original draft, Joaquin Velasco Jitton: Investigation, Visualization, Writing – original draft. Thomas Gries: Supervision, Writing – review & editing.

Competing interests

The authors declare no competing interests.

Acknowledgement

The authors would like to acknowledge the generous technical and material support of SIKA Deutschland GmbH and are grateful for the help of the technical staff of ITA RWTH Aachen University.

References

1. R. A. Buswell, R. C. Soar, A. G. F. Gibb, and A. Thorpe, “Freeform Construction: Mega-scale Rapid Manufacturing for construction,” Automation in Construction, vol.

16, no. 2. Elsevier BV, pp. 224–231, Mar-2007 [Online]. Available: http://dx.doi.org/10.1016/j.autcon.2006.05.002
2. T. Gries, D. Veit, B. Wulfhorst, “Textile Technology – An Introduction”, Carl Hanser Verlag GmbH Co., KG. Munich, Germany (2014).
3. T. Gries, M. Raina, T. Quadflieg, and O. Stolyarov, “Manufacturing of textiles for civil engineering applications,” Textile Fibre Composites in Civil Engineering. Elsevier, pp. 3–24, 2016 [Online]. Available: http://dx.doi.org/10.1016/B978-1-78242-446-8.00002-1
4. U. M. Dilberoglu, B. Gharehpapagh, U. Yaman, and M. Dolen, “The Role of Additive Manufacturing in the Era of Industry 4.0,” Procedia Manufacturing, vol. 11. Elsevier BV, pp. 545–554, 2017 [Online]. Available: http://dx.doi.org/10.1016/j.promfg.2017.07.148
5. D. G. Soltan and V. C. Li, “A self-reinforced cementitious composite for building-scale 3D printing,” Cement and Concrete Composites, vol. 90. Elsevier BV, pp. 1–13, Jul-2018 [Online]. Available: http://dx.doi.org/10.1016/j.cemconcomp.2018.03.017
6. J. Pegna, “Exploratory investigation of solid freeform construction,” Automation in Construction, vol. 5, no. 5. Elsevier BV, pp. 427–437, Feb-1997 [Online]. Available: http://dx.doi.org/10.1016/S0926-5805(96)00166-5
7. B. Khoshnevis, “Automated construction by contour crafting—related robotics and information technologies,” Automation in Construction, vol. 13, no. 1. Elsevier BV, pp. 5–19, Jan-2004 [Online]. Available: http://dx.doi.org/10.1016/j.autcon.2003.08.012
8. 3D printing architecture’s future, (n.d.). http://www.winsun3d.com/en (2019)
9. Chinese Construction Company 3D Prints an Entire Two-Story House On-Site in 45 Days, https://3dprint.com/138664/huashang-tengda-3d-print-house/ (2017)
10. R. Duballet, O. Baverel, and J. Dirrenberger, “Classification of building systems for concrete 3D printing,” Automation in Construction, vol. 83. Elsevier BV, pp. 247–258, Nov-2017 [Online]. Available: http://dx.doi.org/10.1016/j.autcon.2017.08.018

Vision and Strategies for Reinforcing Additively Manufactured Concrete Structures

Reinforcing Methods

https://doi.org/10.52825/ocp.v1i.78

Submitted: 1 Oct. 2021 | Accepted: 24 Jan. 2022 | Published: 15 Feb. 2022

Reinforcement Strategies for Additive Manufacturing in Construction based on Dynamic Fibre Winding: Concepts and Initial Case Studies

Stefan Gantner[1][https://orcid.org/0000-0001-6756-8942], Tom Rothe[2][https://orcid.org/0000-0001-7066-3211], Christian Hühne[2][https://orcid.org/0000-0002-2218-1223], Philipp Rennen[1], and Norman Hack[1*][https://orcid.org/0000-0002-5261-6726]

[1] Institute of Structural Design, Technische Universität Braunschweig, Pockelsstraße 4, 38106 Braunschweig, Germany

[2] Institute of Mechanics and Adaptronics, Technische Universität Braunschweig, Langer Kamp 6,38106 Braunschweig, Germany

[*] Correspondence: n.hack@tu-braunschweig.de; Tel.: +49-531-391-3580

Abstract. Whereas entire houses are reported to be built by means of 3D Concrete Printing (3DCP), the automated integration of reinforcement is still a vastly unresolved challenge and - undoubtedly - a crucial requirement for widespread adoption of 3DCP in construction practice. In this paper an automated reinforcement approach using continuous textile fibres is introduced as an alternative to the manual placement of conventional steel reinforcement. Based on a fibre winding technique, in this paper a matrix of methods and applications is presented and substantiated by initial feasibility studies on the 1:1 scale. As such, three case studies for the automated reinforcement integration are presented, addressing particle bed printing (Large Particle 3D Concrete Printing), as well as material jetting (Shotcrete 3D Printing).

Keywords: Additive Manufacturing in Construction (AMC); 3D Concrete Printing; Robotic Fibre Winding; FRP Concrete Reinforcement; Textile-Reinforced Concrete; Shotcrete 3D Printing; Large Particle 3D Concrete Printing

Conference presentation video: https://doi.org/10.5446/56109

Introduction

In view of the growing world population and the associated global demands for newly constructed habitats, global construction activity will continue to increase in the coming decades. At the same time, however, the construction industry is one of the world's most resource intensive industries, responsible for the consumption of 50% of all extracted raw materials, 12% of the overall CO_2 emissions and 55% of total waste generation [1]–[3]. New building technologies are needed to reduce this immense consumption of resources. One potential key technology for this is Additive Manufacturing in construction. Within the framework of the collaborative research centre TRR 277 Additive Manufacturing in Construction, 3D printing on construction scale is being fundamentally investigated for a variety of construction materials including concrete, steel and timber [4]. One of the biggest challenges, which is still not sufficiently investigated yet, is the automated integration of reinforcement, without which concrete components would not be able to withstand tensile forces and would therefore only be applicable for construction to a limited extent [5]–[7].

To resolve this pressing issue, and to unlock the full potential of 3D printing with concrete, the TRR 277 research project A05 “Integration of Individualized Prefabricated Fibre Reinforcement in Additive Manufacturing with Concrete” investigates automated fabrication processes for the integration of structural reinforcement for additively fabricated concrete elements. For this the Institute of Structural Design (ITE) and the Institute of Mechanics and Adaptronics (ima) of TU Braunschweig collaborate on a material and process level.

The particular focus of this project is directed towards the use of textile reinforcement as for example alkali resistant (AR) glass, aramid or carbon fibre. The main advantages of using textiles compared to conventional steel reinforcement elements are twofold: Firstly, textile reinforcement is corrosion resistant, which allows reducing the minimum required concrete cover by an order of magnitude [8]. This leads to a significant reduction in the amount of concrete required for structural components and thus to lower energy consumption along the entire value chain, as transport and assembly are also simplified. In addition, fibres as a lightweight and flexible raw material are advantageous for automated individualised manufacturing of complex force-flow-compliant reinforcement structures.

In line with that, this research project aims at developing fabrication methods for integrating textile reinforcement for all concrete related AM processes of the TRR 277, including Particle Bed 3D Printing, Concrete Extrusion, and Shotcrete 3D Printing [9]. For this, the main focus of this project is directed towards fibre winding techniques, for the reason that this fabrication process is fast, the fibres are continuous and the material properties can be varied according to the functional requirements of the building component by combining different fibre types and diameters. The investigated design and fabrication methods are validated through physical experiments, ranging from small scale test samples, middle scale case studies, to large scale demonstrators.

After a short overview of relevant research regarding non-metallic reinforcement in general as well as reinforcement integration in digital fabrication, this paper derives an overarching methodology used as the central development guideline in this project. Three novel fibre reinforcement strategies are derived from that and according feasibility studies are presented.

State of the art

Continuous fibre reinforcement in construction

The potentials of Textile-Reinforced Concrete (TRC) were realized early on by researchers from TU Dresden and RWTH Aachen, who have jointly applied for research funding for the further investigation of this topic. In 1999, the German Research Foundation approved the funding of two major Collaborative Research Centres focusing on fundamental research on textile reinforcement in concrete construction. Whereas the CRC 532 in Aachen “Textile-Reinforced Concrete - Development of a New Technology" focused on the development of novel concrete constructions, the CRC 528 "Textile Reinforcement for Structural Strengthening and Repair" focused on the application of textile reinforcement for deteriorating structures [10].

During the twelve years of funding, researchers of both initiatives developed fundamental material models, basic construction approaches, novel technological applications, new methods of calculation, as well as conducting long term surveys of the properties of TRC. Furthermore, the researchers verified the findings in several large-scale demonstrators, as for example the non-standard bridge structures in Oschatz and Kempten, as well as the research pavilions at the Kahla concrete plant and the Hypar-shell at RWTH Aachen (Figure 1) [11].

(a) (b) (c)

Figure 1: Large-Scale demonstrators from CRC 528 and 532: (a) Rottachsteg, Kempten © Nicolas Janberg, Structurae; (b) Research-Pavilion in Kahla © Ulrich van Stipriaan; (c) Hypar-shells at RWTH Aachen © Alexander Scholzen

For the fabrication of the above structures, mainly two fabrication techniques were developed. Firstly, a hand lamination process, in which pre-cut textile grids were stacked in-between thin layers of fine grain cement (Figure 2); and secondly, a conventional casting technique, where several spaced layers of textile reinforcement were placed in a custom-made formwork.

(a) (b)

Figure 2: Reinforcement of the Rottachsteg in Kempten; a) placing the prefabricated fibre mat; b) Appling the concrete in a lamination process © Dirk Jesse and Harald Michler

Even though the projects demonstrated the high flexibility of the textile formwork, as well as the material efficiency of the construction, it also became apparent that the processes are yet highly labour intensive and hence costly in production. Among others, this lack of methods to automate the integration of reinforcement can be seen as one of the reasons why TRC does not yet find a wide application in the industry.

In order to accelerate the transfer into practice, the follow-up research program ”C^3-Carbon Concrete Composite” [8], also initiated by TU Dresden and financed by the German Federal Ministry for Education and Research (BMBF) focused on issues like production optimization, recycling, safety and industrial health.

A notable approach within that research initiative is the robotically aided winding of impregnated fibres around planar rectangular steel frames [12]. Instead of cutting out openings for windows and doors from a standard carbon fibre reinforcement mat, here a winding strat-

egy is chosen to leave the regions of the openings unfilled. After the resin has cured the frame is removed and the reinforcement is placed in a standard formwork for subsequent concrete casting. This method enables the reduction of carbon fibre waste for standardized building components, like for example planar rectangular walls.

Recently a new Collaborative Research Centre, Transregio 280 “Design Strategies for Material-Minimised Carbon Reinforced Concrete Structures” has set out to investigate innovative and material efficient constructions for carbon concrete, that take reference to biomimetic principles in nature [13].

Digitally fabricated fibre reinforcement

In the research field of robotic manufacturing in architecture fibre reinforcement has been used in different material combinations leading to unique processing techniques. The Institute of Computational Design and Construction (ICD) in Stuttgart dispenses with the use of concrete in order to produce large-scale experimental structures in a lightweight design using fibre-reinforced plastic processed by their specially developed "coreless filament winding" method [14]. Further approaches in concrete construction seek to exploit synergetic functionalisation of fibre structures as formwork. By using 3D knitting, [15] was able to create individualized fabric formwork using CNC knitting machines. The resulting webs are held in place by a handcrafted cable net, which itself is stretched over an auxiliary scaffold. Finally, in a multi-step process, sprayed cement is used for stiffening and then concrete is applied in thin layers [16].

However, only few methods are known yet for integrating fibres as reinforcement in digital fabrication with concrete. Among those are, firstly, the “SCRIM” approach [17], where concrete is robotically printed onto a cage composed of regular carbon fibre reinforcement meshes (Figure 3a); secondly, the AeroCrete [18] research of ETH Zürich which uses shotcrete instead of extrusion (Figure 3b), thirdly the manual placement of a pre-cut standard reinforcement mat onto a printed layer of concrete [19]; and fourthly, a similar approach, where individualized 3D textiles are robotically placed and pressed into a fresh layer of printed concrete [20].

(a) (b)

Figure 3: (a) SCRIM - Sparse Concrete Reinforcement in Meshworks[17];
(b) Robotic AeroCrete [18]

Fibre deposit technology in aeronautics and aerospace

In view of the innovation potential, the application of fibre composites is becoming more and more established in many technical products, especially in the aerospace and wind power industries. New automated processing techniques such as Automated Fibre Place-

ment (AFP) or winding processes (Figure 4a) are driving this wider use. The winding and AFP technologies are ideally suited for the production of large-area and/or geometrically complex components. The advantages over manual production are productivity and reproducibility. Especially a combination of AFP and Additive Layer Manufacturing (ALM) with carbon continuous-fibre reinforced plastics (Figure 4b) promises a further quality increase for geometrically complex components [21].

In addition, the pultrusion process is one of the oldest processes for the production of endless fibre-reinforced plastic components and at the same time the oldest continuous process. In the classic pultrusion process, reinforcing fibres are impregnated with a matrix-like epoxy resin in a wet process and cured in a shaping tool [22]. An improvement of this process can be achieved by an in situ monitoring of the degree of cure by Resonant Ultrasonic Spectroscopy (RUS) [23]. Due to this, the degree of cure can be adjusted for the desired purpose.

These technologies used in aeronautics and aerospace were taken into account for the development of suitable reinforcement strategies with continuous fibres in construction. The case studies presented in this paper were influenced by the winding process, by AFP as well as by pultrusion. Other aspects like in situ monitoring are interesting for further process optimisation.

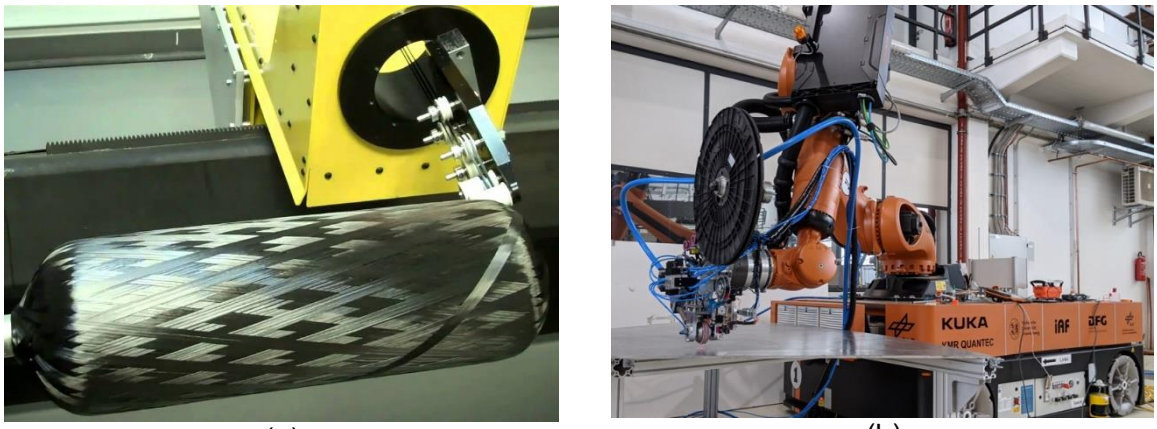

(a) (b)

Figure 4: (a) Fibre Winding on mandrel © TCR Composites (b) Integrated robotic end-effector for the combined process of AFP and ALM © Mohammad Bahar

Preliminary work

Mesh Mould

The Mesh Mould technology, developed at ETH Zurich, is a robotically fabricated construction system, which combines reinforcement and formwork into one integrative structural stay-in-place formwork system [24]. In this approach, a robot fabricates a freeform mesh, which is sufficiently dense to hold fresh concrete and is appropriately strong to act as structural reinforcement after the concrete has cured. According to the classification of Kloft et al. [6] this approach can be regarded as “reinforcement supports concrete” and hence acts as a reference to the frame winding reinforcement strategy described later in this paper. Mesh Mould was developed in two consecutive phases. In the first phase an innovative spatial printing process was developed, which allowed printing in mid-air using thermoplastics [25]. A case study demonstrator, of a mesh filled with concrete is shown in Figure 5. In preliminary studies, these meshes were additionally reinforced with continuous carbon fibre strands, that were hot-glued onto the mesh after printing.

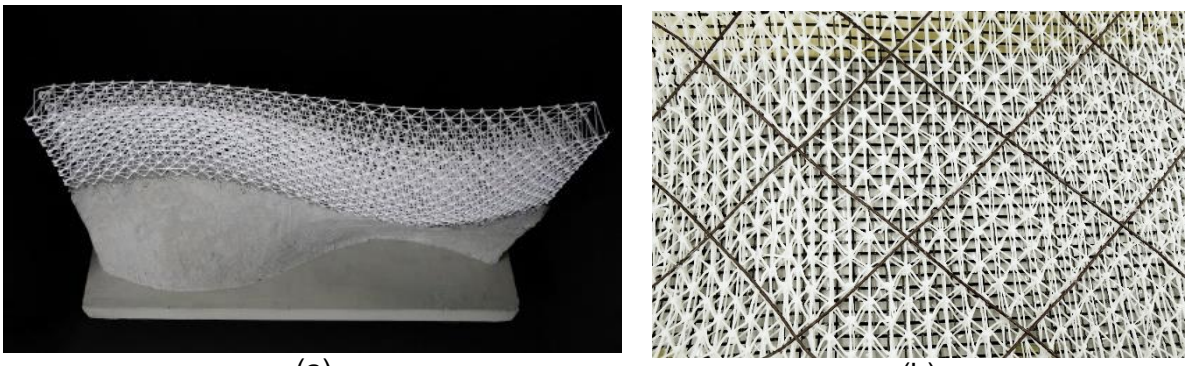

(a) (b)

Figure 5: Mesh Mould: (a) Spatially printed mesh, filled with concrete [25]; (b) Carbon fibre reinforced, spatially printed mesh © Norman Hack

In the second phase of the research project, the material system was changed from printing thermoplastics to bending, cutting and welding of 8 mm steel reinforcement. The geometric freedom and the loadbearing capacity, which are facilitated by this construction system, were recently demonstrated in the DFAB house in Zürich [26]. Here, a mobile construction robot fabricated an undulating, 12 m long steel mesh directly on the building site (Figure 6a).

The subsequent concreting process involved three consecutive steps: firstly, the mesh was filled with a commercially available fine grain concrete by pumping the material laterally into the mesh (Figure 6b); secondly, a concrete cover was applied by using a conventional shotcrete process; and finally, the surface was manually trowelled to create a smooth concrete surface of high visual quality.

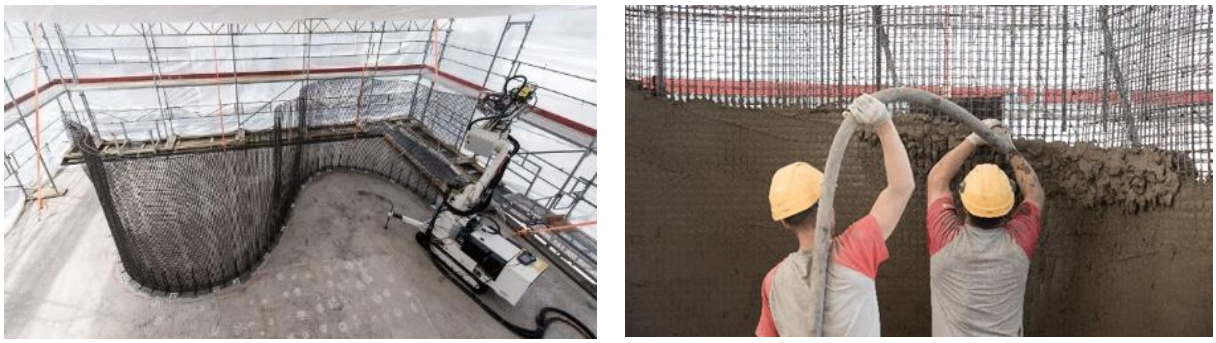

(a) (b)

Figure 6: Mesh Mould: (a) In situ fabrication of a steel mesh that acts as reinforcement and formwork; (b) Filling of the mesh by manually "printing" on and into the mesh. [24]

Fibre winding as concrete reinforcement at ITE

Previously, several methods for robotic filament processing have been developed at ITE. These techniques include for example filament winding (Figure 7a) or 3D knitting and fibre deposition. Besides developing the design algorithms and robotic control routines, additionally different robotic end effectors for an optimal fibre winding and curing process were developed. Here, a successful strategy was to soak the fibre rovings in a resin bath shortly before the filament was wound around a structure. After curing, this fibre impregnation does not only provide more structural stability, but also significantly improves the load transfer and the bonding behaviour of the textile and the concrete matrix. Several of these methods have been tested in combination with automated concrete deposition techniques, as for example Shotcrete 3D Printing (Figure 7b).

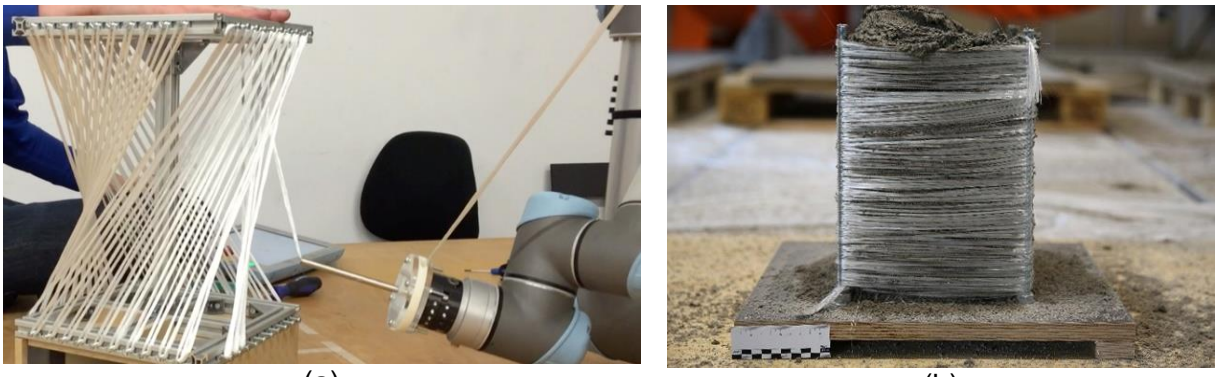

(a) (b)

Figure 7: Robotically fabricated textile reinforcement at ITE: (a) Robotic fibre winding at the ITE using custom developed end effectors, 2015; (b) Filling of a robotically wound textile reinforcement cage. © ITE

Methodology

In order to systematically explore the potentials of fibre winding for the above mentioned concrete 3D printing technologies, a matrix was developed that allows to relate part type and geometry, fibre winding technique and AM method to each other (Figure 8). In future, the schematic can be extended by further fibre processing and integration techniques. Currently, the matrix is based on fibre winding technique only, as this constitutive process is fast and provides great flexibility, which becomes evident through the specific strategies described below.

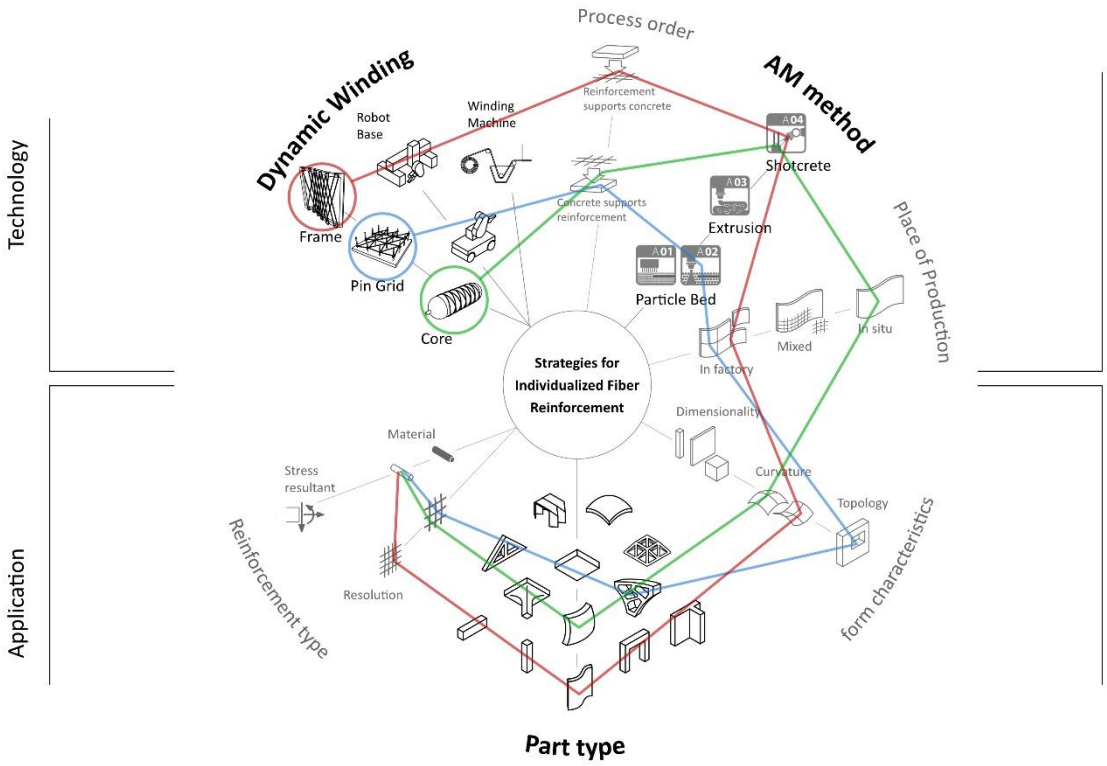

Figure 8: Diagram allowing to trace a path in order to relate part type and geometry, fibre winding technique and AM method.

In the following, three potential parts are exemplified, two for the Shotcrete 3D Printing technology, and one for the Particle Bed 3D Printing technology. The technological boundary conditions and constructive application possibilities for Particle Bed 3D Printing can be traced with the blue path, while those of Shotcrete 3D Printing are marked with a red and a green path. Although variations and other branches are possible, only three paths will be presented and explained in this paper.

The red path shows that with the Shotcrete 3D Printing technique in combination with frame winding, predominantly slender vertical building can be produced. In this process a steel frame with pins is used to wind pre-impregnated fibres to form a surface that is then covered using shotcrete. By removing the frame after curing, a discrete component with precise edges is created, promoting prefabrication. The strength of this method lies in the formation of thin elements with single or ruled curvatures. Using advanced winding techniques, double curvatures are also accessible. For a successful application of concrete, the reinforcement mesh needs to be sufficiently dense to prevent the concrete from passing through the mesh. Due to the straight fibre spans, a curved force flow in structural members cannot be mapped precisely, but the individual winding still allows density and orientation to be varied locally.

Following the blue path, the diagram shows that Pin Grid Winding is particularly suited for Particle Bed 3D Printing. It originates from the idea of a two-dimensional array of pins, which allows to produce individualized flat fibre structures by robotically winding around selected pins, so that arbitrary outlines and infill patterns can be approximated. Resulting inlays can be placed onto the particle bed in between two consecutive printed layers. Design possibilities are not restricted by the integration of fibre reinforcement, but also not enhanced like in the frame winding example. The placement of inlays seeks to adapt to the printing process with minimal interference according to the principle of “concrete supports reinforcement” [6].

So far, Particle Bed 3D Printing is clearly restricted to off-site production and most suitable for volumetric parts of limited size and high topological complexity, for example shape optimized connecting nodes of space frames. Although the described reinforcement strategy is limited to horizontal orientation, the pin grid allows for approximately arbitrary in-plane orientation and distribution of the fibres. Not only different slice contours, but also force-flow trajectories can be mapped.

Instead of forming the reinforcement in advance, fibres can also be applied after printing the core of an element. This approach, referred to as Core Winding Reinforcement (CWR), is depicted on the green path, and takes advantage of the generative nature of 3D printing by using the 3D printed concrete core as a support to fix fibre strands upon it in any orientation. As CWR fully adapts to the versatility of concrete printing, it is applicable for on-site production and does not impose inherent geometric restrictions. Therefore, this method is especially suited for spatially complex load bearing walls with irregular stress distribution.

Case studies

While in this research project other possible pathways are also being investigated, the above methods have already been studied experimentally. Three exemplary combinations are described below: firstly, Frame Winding and Shotcrete 3D Printing, secondly, Pin Grid Winding and Particle Bed 3D Printing, and thirdly, Shotcrete 3D Printing and CWR. For all tests, a custom designed Dynamic Fibre Winding Machine was used to ensure a reinforcement strand with a good mechanical bond between concrete and fibre. This machine is shown in Figure 9a and described in more detail in [27].

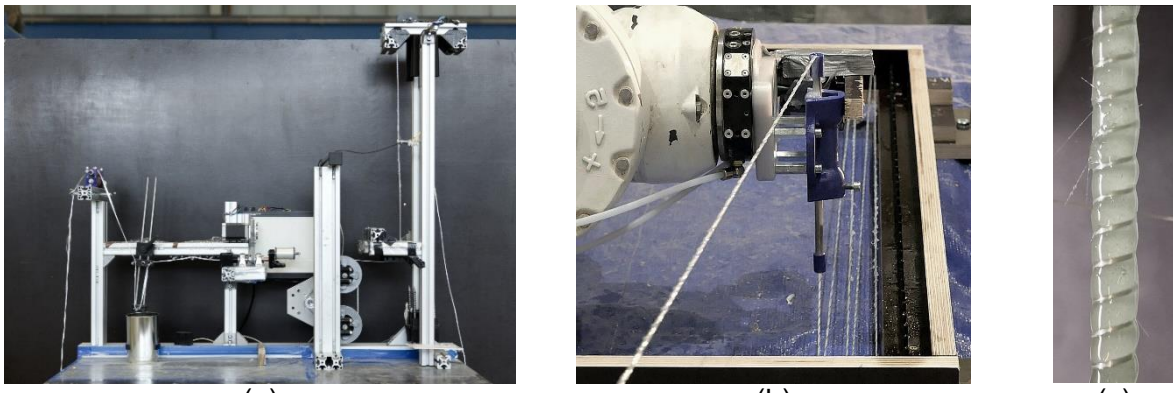

(a) (b) (c)

Figure 9: On demand production of reinforcement from glass fibre roving: (a) Dynamic Winding Machine; (b) Robotic winding end-effector; (c) Resin impregnated roving with helix profile

Frame winding and Shotcrete 3D Printing

Shotcrete 3D Printing is usually carried out by spraying concrete in horizontal layers in order to build up predominantly vertical concrete elements. However, due to the width of the shotcrete jet, elements with a width of at least 15 cm can be created [28]. With the frame winding technique, the realization of thin-walled elements was tested [27]. Here, the reinforcement structure serves as a support for the concreting process and therefore defines the resulting geometry (Figure 10).

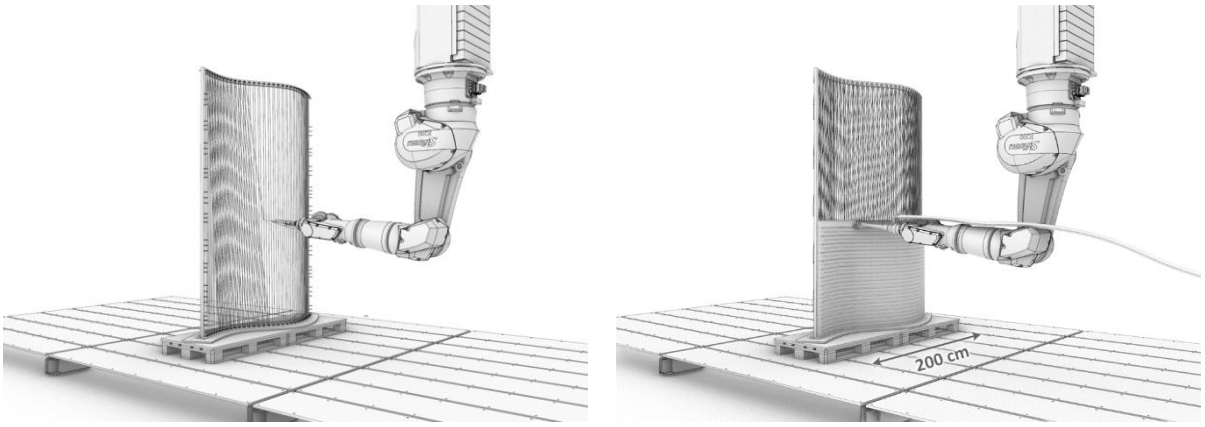

(a) (b)

Figure 10: Overall fabrication concept: (a) A robot winds a reinforcement mesh around an individualized frame; (b) concrete is applied to the mesh using the Shotcrete 3D Printing process. [27]

Firstly, rectangular frames of 1 m edge length were used for robotically winding a regular mesh with pre-treated glass fibre roving (Figure 11a). The frames remained in place during shotcreting in order to absorb the weight of the concrete (Figure 11b). In this first attempt, the spraying nozzle was aligned orthogonally to the mesh at a distance of 30 cm. The experiments resulted in a flat reinforced concrete panel shown in Figure 11c, which gave a basic proof of concept [27]. However, unresolved issues like the loss of concrete passing through the mesh without adhesion and uncovered fibres on the rear side (Figure 11c) demand for further improvement of the process. Furthermore, other paths through the schematic of Figure 8 could be tested and compared, for example replacing the concreting method by extrusion.

Figure 11: Automated manufacturing of fibre reinforced concrete element (a) robotic winding process; (b) robotic shotcreting process; (c) first results of robotically shotcreting a winded reinforcement mesh (front and rear). [27]

Pin Grid Winding with Large Particle 3D Concrete Printing

In the novel approach of Large Particle 3D Concrete Printing (LP3DCP) the integration of fibre reinforcement inlays has been tested [29]. LP3DCP is based on the concept of Selective Paste Intrusion (SPI) [30], but instead of using aggregates below 5 mm of size, here large aggregates with up to 32 mm are used. The large aggregates, that consist of recycled construction waste, are selectively bound using the Shotcrete 3D Printing method (see Figure 12a). The use of coarse recycled aggregates does not only reduce the CO_2 footprint, but can also increase the compressive strength compared to shotcrete only. [29]

Figure 12: Large Particle 3D Concrete Printing LP3DCP: (a) Process schematic with indicated reinforcement inlay; (b) final demonstrator of one cubic meter of size. [29]

In order to improve tensile load bearing capacities, two layers of prefabricated fibre-winded reinforcement were integrated at structurally relevant positions – namely in layer 12 and 26, where all contour branches meet in the sections centre (compare Figure 12a). The above-mentioned Pin Grid Winding approach was applied in a simplified manner. From the respective slice contours a planar truss layout was derived, whose node positions were used to robotically drill holes in a wooden base plate. With the help of pins an individualized grid for fibre winding was generated.

The Dynamic Winding Machine, equipped with a 2400 tex glass roving and L-285 epoxy resin for impregnation, was used to provide a helix surface profile and prepare the

fibres for subsequent winding onto the grid (Figure 13a). After curing and removing the pins, the reinforcement inlays were positioned and placed manually onto the fresh concrete after printing the respective layers (Figure 13b). By printing the next layer, the reinforcement was embedded into the structure. The manual placement of pre-fabricated fibre inlays is rapid and does not cause significant delay in the fabrication process, as it would be the case when winding the inlays in situ. Even with manual placement, a satisfactory alignment between shotcrete contour and the fibre inlay could be achieved, as both processes are based on digital fabrication.

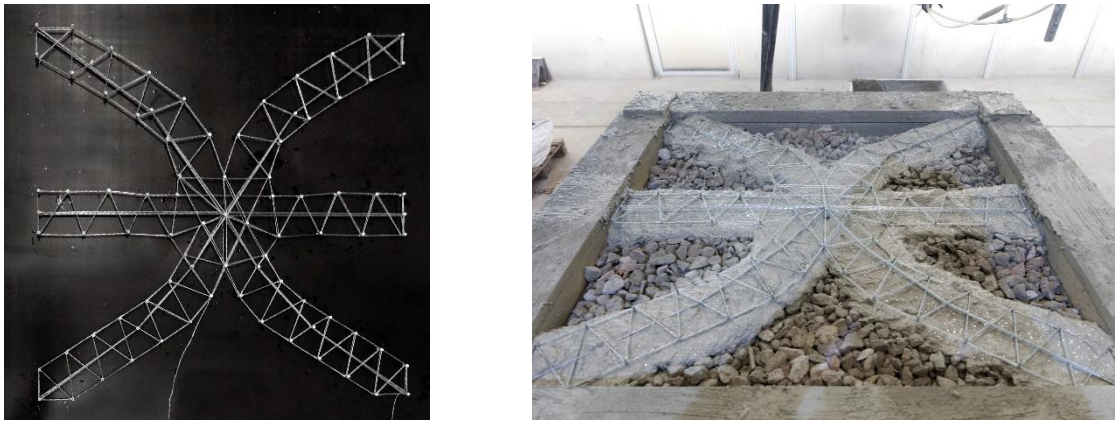

(a) (b)

Figure 13: Integration of fibre reinforcement in LP3DCP: (a) prefabricated fibre inlay on pin grid [29]; (b) placement of inlay within the printing process.

Shotcrete 3D Printing and Core Winding Reinforcement (CWR)

For CWR, the third reinforcement strategy described here, a robotic end-effector was developed (Figure 14a), which extends the fibre deposition tool by a modified stapling device, so that the reinforcement strand can be fixed to a freshly printed concrete surface at an arbitrary location and orientation. A moderately double-curved wall of 120 cm height was structurally analysed for an exemplary load case in order to retrieve a two-dimensional stress distribution (Figure 14b). Based on this, a polyline pathway along the wall's faces was derived for reinforcement deposition. The same digital model was used to define concrete printing paths, which allowed for the synchronisation of all process steps.

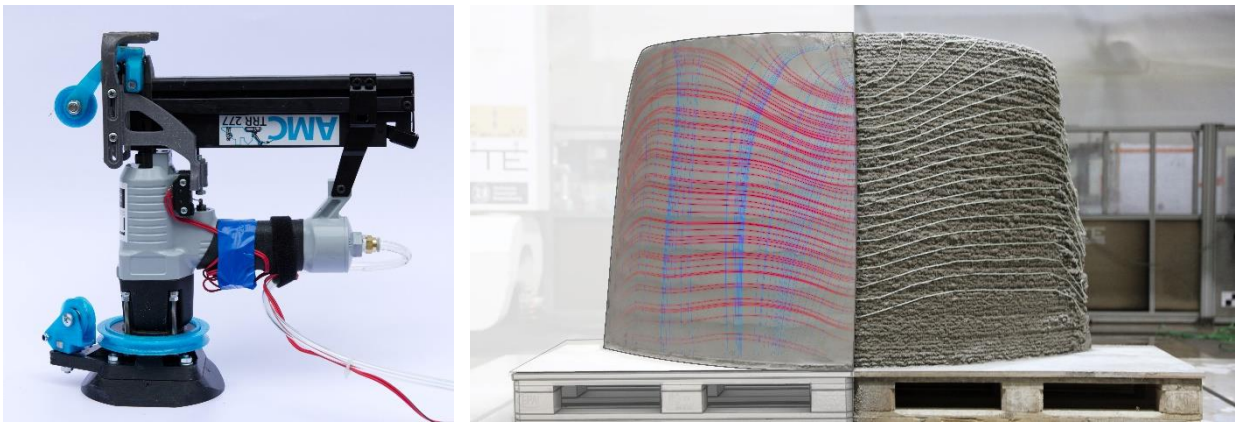

(a) (b)

Figure 14: (a) Robotic fibre deposition end-effector with incorporated staple device; (b) demonstrator wall with reinforcement layout (right) derived from structural analysis (left)

After printing a 12 cm thick core by means of SC3DP (Figure 15a), the robotic end-effector was changed to the CWR-tool and equipped with 40 mm long staples and the pre-treated 9600 tex glass fibre roving coming from the Dynamic Winding Machine. As proof of concept, the automated fibre deposition was only performed on one side of the wall (Figure 15b). In order to establish a proper compound, half of the front was covered by a layer of concrete in a second vertical shotcreting process (Figure 15c). Lastly, the wall was trowelled robotically to achieve final surface quality (Figure 15d).

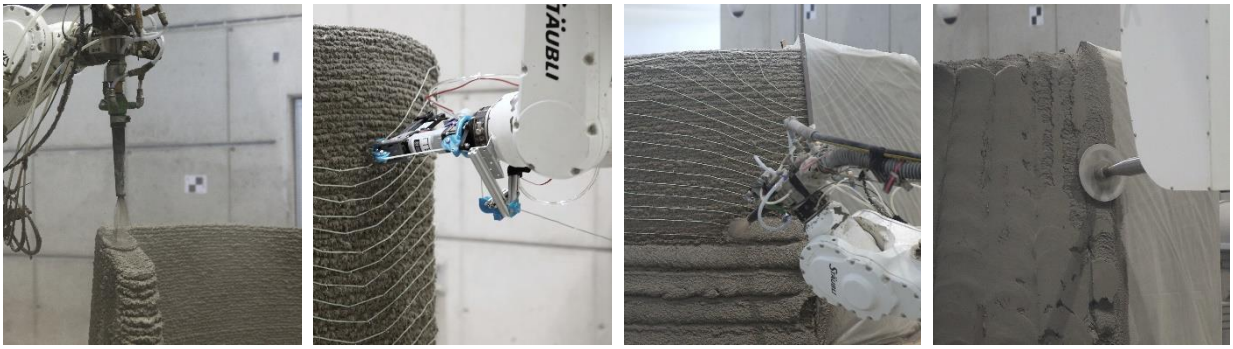

(a) (b) (c) (d)

Figure 15: Fabrication steps: (a) shotcrete printing; (b) fibre application; (c) cover printing; (d) surface finish

Despite its early development stage all process steps of this technique were performed successfully in a fully automated manner. Thus, it is worthwhile to investigate the performance of CWR more in detail regarding for example the grip of staples in fresh concrete and the compound quality between fibres and concrete.

Conclusion und outlook

In this paper, the importance of integrating reinforcement into digital fabrication with concrete was described. In particular, continuous fibres have been identified as a promising alternative to conventional steel reinforcement - mostly due to their corrosion resistance and their flexibility in processing. A methodology which helps to detect yet overlooked process combinations and which allows to compare and assess them from varied perspectives was developed. Three approaches were described in particular, providing reinforcement strategies for Large Particle 3D Concrete Printing and for Shotcrete 3D Printing. Finally, their feasibility has been proven by case studies.

These initial investigations lead to differentiated findings: due to the different functions, most importantly the compression resistance of the concrete and the tensile strength of the fibres, each building component requires a unique reinforcement layout. Moreover, it affects the form of the part itself and thus the manufacturing process. Choosing an appropriate reinforcement strategy is not a deterministic downstream process, but the most effectiveness can be achieved by involving even the design of the respective parts and their physical environment. However, by considering only the application and the ideal representation, one ends up with unproducible designs. Both the technical possibilities and the practical requirements need to be considered in a holistic manner when developing a manufacturing framework for additively concreted fibre reinforced elements. In accordance with this, the scheme in Figure 8 can be utilized as a tool to classify and assess different possible approaches.

The presented case studies are still at their early stages. In the future they will be investigated upon their geometric potential, but also upon their structural performance. Moreover, several other possible paths leading through the diagram will be investigated.

Data availability statement

There is no relevant additional data to this article beyond the presented content.

Author contributions

Stefan Gantner: Conceptualization, Investigation, Methodology, Software, Visualization, Writing – original draft, review & editing. Tom-Niklas Rothe: Conceptualization, Writing – review & editing. Christian Hühne: Conceptualization, Funding acquisition, Supervision, Writing – review & editing. Phillipp Rennen: Investigation; Norman Hack: Conceptualization, Funding acquisition, Methodology, Supervision, Visualization, Writing – original draft, review & editing.

Competing interests

The authors declare no competing interests. The funders had no role in the design of the study; in the collection, analyses, or interpretation of data; in the writing of the manuscript, or in the decision to publish the results.

Funding

The authors would like to thank the German Research Foundation (DFG), for funding the Collaborative research center TRR 277 Additive Manufacturing in Construction and the DFG Large Research Equipment, Digital Building Fabrication Laboratory (project numbers 416601133 and 414265976), as well as the Ministry of Science and Culture of Lower Saxony (MWK). Norman Hack's Junior Professorship in Digital Building Fabrication is generously funded by the Gerhard und Karin Matthäi Foundation.

References

1. Agustí-Juan and G. Habert, "Environmental design guidelines for digital fabrication," Journal of Cleaner Production, vol. 142, pp. 2780–2791, 2017, doi: https://doi.org/10.1016/j.jclepro.2016.10.190.
2. R. J. M. Wolfs and T. A. M. Salet, "Potentials And Challenges In 3D Concrete Printing." 2016.
3. Agustí-Juan, F. Müller, N. Hack, T. Wangler, and G. Habert, "Potential benefits of digital fabrication for complex structures: Environmental assessment of a robotically fabricat-ed concrete wall," Journal of Cleaner Production, vol. 154, 2017, doi: https://doi.org/10.1016/j.jclepro.2017.04.002.
4. H. Kloft et al., " TRR 277: Additive Manufacturing in Construction (AMC) ," Civil Engineering Design, Jun. 2021, doi: https://doi.org/10.1002/CEND.202100026.
5. V. Mechtcherine et al., "Integrating reinforcement in digital fabrication with concrete: A review and classification framework," Cement and Concrete Composites, vol. 119, May 2021, doi: https://doi.org/10.1016/j.cemconcomp.2021.103964.
6. H. Kloft, M. Empelmann, N. Hack, E. Herrmann, and D. Lowke, " Reinforcement strategies for 3D-concrete-printing," Civil Engineering Design, vol. 2, no. 4, pp. 131–139, Aug. 2020, doi: https://doi.org/10.1002/cend.202000022.
7. T. Wangler et al., "Digital Concrete: Opportunities and Challenges," RILEM Technical Letters, vol. 1, pp. 67–75, Oct. 2016, doi: https://doi.org/10.21809/RILEMTECHLETT.2016.16.
8. "C3: Carbon Concrete Composite e.V. – Eine neue Art des Bauens," 2017. https://www.bauen-neu-denken.de/en/homepage/#about-c3 (accessed Nov. 26, 2021).

9. TRR 277, “TRR 277 Additive Manufacturing in Construction.” https://www.tu-braunschweig.de/trr277/projects/amc-structure/a-projects (accessed Nov. 26, 2021).
10. S. Scheerer, F. Schladitz, and M. Curbach, “Textile reinforced concrete - from the idea to a high performance material,” 11th International Symposium on Ferrocement and Textile Reinforced Concrete 3rd ICTRC, pp. 15–34, 2015.
11. S. Rempel, N. Will, J. Hegger, and P. Beul, “Filigrane Bauwerke aus Textilbeton: Leistungsfähigkeit und Anwendungspotenzial des innovativen Verbundwerkstoffs,” Beton- und Stahlbetonbau, vol. 110, no. S1, pp. 83–93, 2015, doi: https://doi.org/10.1002/best.201400111.
12. F. Schladitz, S. Ritter, A. Kahnt, M. Tietze, M. Curbach, and M. Lieboldt, “Herstellung von Fertigteilen aus Textilbeton,” DE102015100438B3, 2015
13. M. Curbach and J. Hegger, “Collaborative Research Centre, Transregio 280 ‘Design Strategies for Material-Minimised Carbon Reinforced Concrete Structures,’” 2020. https://www.sfbtrr280.de/en/ (accessed Sep. 30, 2021).
14. J. Solly, N. Frueh, S. Saffarian, and M. Prado, “ICD/ITKE Research Pavilion 2016/2017: Integrative Design of a Composite Lattice Cantileve,” in Proceedings of the IASS Symposium 2018 Creativity in Structural Design, 2018, no. July, pp. 2–8.
15. M. Popescu, “KnitCrete: Stay-in-place knitted fabric formwork for complex concrete structures,” ETH Zurich, Department of Architecture, 2019.
16. M. Popescu, M. Rippmann, A. Liew, T. van Mele, and P. Block, “Concrete Shell Built Using A Cable-Net And Knitted Formwork,” Structure Published by Detail, 2019. https://www.detail.de/artikel/betonschale-aus-stahlseilen-und-gestrickter-schalung-33857/ (accessed Nov. 26, 2021).
17. P. Ayres, W. R. Leal da Silva, P. Nicholas, T. J. Andersen, and J. P. R. Greisen, “SCRIM – Sparse Concrete Reinforcement in Meshworks BT - Robotic Fabrication in Archi-tecture, Art and Design 2018,” 2019, pp. 207–220, doi: https://doi.org/10.1007/978-3-319-92294-2_16
18. N. Taha, A. N. Walzer, J. Ruangjun, E. Lloret-Fritschi, F. Gramazio, and M. Kohler, “Robotic AeroCrete A novel robotic spraying and surface treatment technology for the,” in Architecture in the Age of the 4 th Industrial Revolution, 2019, vol. 3, pp. 245–254, doi: https://doi.org/10.3929/ethz-b-000387276.
19. H. Kloft et al., “Additive manufacturing in construction: First 3-D printed reinforced concrete components using Shotcrete 3-D printing (SC3DP) technology,” Bautechnik, vol. 96, no. 12, 2019, doi: https://doi.org/10.1002/bate.201900094.
20. V. Mechtcherine and V. N. Nerella, “Incorporating reinforcement in 3D-printing with concrete (in German),” Beton- und Stahlbetonbau, vol. 113, no. 7, pp. 496–504, Jul. 2018, doi: https://doi.org/10.1002/best.201800003.
21. M. Rakhshbahar and M. Sinapius, “A Novel Approach: Combination of Automated Fiber Placement (AFP) and Additive Layer Manufacturing (ALM),” Journal of Composites Science, vol. 2, no. 3, p. 42, Jul. 2018, doi: https://doi.org/1010.3390/JCS2030042.
22. H. Lengsfeld, J. Lacalle, T. Neumeyer, and V. Altstädt, Faserverbundwerkstoffe: Prepregs und ihre Verarbeitung. Carl Hanser Verlag GmbH & Co. KG, 2015. doi: https://doi.org/10.3139/9783446440807.
23. C. Pommer and M. Sinapius, “Proof of Concept for Pultrusion Control by Cure Monitoring Using Resonant Ultrasound Spectroscopy,” Journal of Composites Science, vol. 4, no. 3, p. 115, Aug. 2020, doi: https://doi.org/10.3390/JCS4030115.
24. N. P. Hack, “Mesh Mould: A Robotically Fabricated Structural Stay-in-Place Formwork System,” ETH Zurich, 2018. doi: https://doi.org/10.3929/ethz-b-000263345.
25. N. Hack, W. V. Lauer, F. Gramazio, and M. Kohler, “Mesh-Mould: Robotically Fabricated Spatial Meshes as Reinforced Concrete Formwork,” in Fabricate: Negotiating Design & Making, 2014, pp. 224–231.
26. N. Hack et al., “Structural stay-in-place formwork for robotic in situ fabrication of non-standard concrete structures: A real scale architectural demonstrator,” Automation in Con-struction, vol. 115, p. 103197, Jul. 2020, doi: https://doi.org/10.1016/j.autcon.2020.103197.

27. N. Hack et al., “Development of a robot-based multi-directional dynamic fiber winding process for additive manufacturing using shotcrete 3d printing,” Fibers, vol. 9, no. 6, Jun. 2021, doi: https://doi.org/10.3390/fib9060039.
28. N. Hack and H. Kloft, “Shotcrete 3D Printing Technology for the Fabrication of Slender Fully Reinforced Freeform Concrete Elements with High Surface Quality: A Real-Scale Demonstrator,” RILEM Bookseries, vol. 28, pp. 1128–1137, 2020, doi: https://doi.org/10.1007/978-3-030-49916-7_107.
29. Mai et al., “Large Particle 3D Concrete Printing—A Green and Viable Solution,” Materials 2021, Vol. 14, Page 6125, vol. 14, no. 20, p. 6125, Oct. 2021, doi: https://doi.org/10.3390/MA14206125.
30. D. Lowke, E. Dini, A. Perrot, D. Weger, C. Gehlen, and B. Dillenburger, “Particle-bed 3D printing in concrete construction – Possibilities and challenges,” Cement and Concrete Research, vol. 112, pp. 50–65, Oct. 2018, doi: https://doi.org/10.1016/J.CEMCONRES.2018.05.018.

Vision and Strategies for Reinforcing Additively Manufactured Concrete Structures

Reinforcing Materials

https://doi.org/10.52825/ocp.v1i.75

Submitted: 30 Sept. 2021 | Accepted: 4 Feb. 2022 | Published: 15 Feb. 2022

Combining Wire and Arc Additive Manufacturing and Selective Paste Intrusion for Additively Manufactured Structural Concrete

Fundamental Investigations on the Effect of Heat Exposure by WAAM on the Rheological and Intrusion Behavior of Cement Paste in the Particle Bed During Selective Paste Intrusion

Alexander Straßer[1][https://orcid.org/0000-0003-0293-3392], Daniel Weger[2][https://orcid.org/0000-0003-3762-5592], Carla Matthäus[1][https://orcid.org/0000-0001-9079-8578], Thomas Kränkel[1][https://orcid.org/0000-0002-5650-3825], and Christoph Gehlen[1][https://orcid.org/0000-0002-1214-3960]

[1] Technical University of Munich; Chair of Materials Science and Testing, Germany

[2] Ingenieurbüro Schiessl Gehlen Sodeikat GmbH, Germany

Abstract: The Selective Paste Intrusion (SPI) is an additive manufacturing method in which thin layers of aggregates are bound selectively by cement paste only where the structure shall arise. In this way, concrete elements with complex geometries and structures can be produced. To meet the optimum between required layer bonding and sufficient shape accuracy, the rheological properties of the cement paste, i.e., its yield stress and dynamic viscosity, are crucial [1, 2]. The combination of the SPI process and the Wire and Arc Additive Manufacturing (WAAM) process enables the production of free-formed, high-strength reinforced concrete elements, which opens up a wide range of applications. However, the WAAM process generates high temperatures, which affect the rheological properties of the cement paste and thus the printing quality [3, 4]. Therefore, we analyzed the effect of external temperature loads on the rheological performance of cement paste over the entire SPI production period and derived a maximum acceptable temperature load for the combination of SPI and WAAM. The experiments showed decreasing viscosity and increasing yield stress values by stepwise increasing the paste temperature from 20 °C to 60 °C. Between 60 °C and 70 °C, the rheological behavior suddenly changed, and both viscosity and yield stress instantly increased to a multiple of their initial values. In a subsequent numerical simulation of the intrusion behavior of the paste in the particle bed, we could show that the high yield stress and viscosity lead to poor paste penetration and thus insufficient layer bonding, whereas paste temperatures up to 60 °C are not detrimental to the SPI process. Therefore, the results demonstrate that the combination of SPI and WAAM is possible if the WAAM process is adjusted by e.g. cooling strategies, increased distance of the welding point from the particle bed, or increased time intervals between the welding points to avoid paste temperatures exceeding 60 °C.

Keywords: Additive Manufacturing; Concrete; Particle-Bed; Selective Paste Intrusion; Reinforcement; Wire and Arc Additive Manufacturing; SPI; WAAM; Rheology; Temperature

Conference presentation video: https://doi.org/10.5446/56112

Introduction

Free and complex geometries are often expensive or impossible to realize by conventional manufacturing methods due to the complicated and sometimes even impossible construction of suitable formworks. However, introducing additive, layer-by-layer-based manufacturing techniques make such geometries possible and cheaper to build since there is no need for formwork [5]. The Selective Paste Intrusion (SPI) is such an additive manufacturing method for concrete elements. Compared to other additive manufacturing processes with concrete, such as extrusion or shotcrete, nearly any overhangs are possible [3, 5]. Thereby cement paste is applied to locally bind layers of aggregates. For good penetration behavior, the cement paste needs a constant high flowability over the entire production period. The sufficient penetration behavior is crucial for both a good layer bonding and a satisfying shape accuracy [3, 5–9]. A simple and easy-to-handle test to determine the flowability of the cement paste is the mini-slump flow [10, 11].

In order to improve the mechanical properties and the durability of the concrete components, the SPI process can be supplemented by the integration of steel reinforcement [4]. One possibility is to conventionally insert steel. However, this involves several challenges: prior placement of a reinforcement cage is not possible due to the layer-by-layer production process of SPI, the insertion of reinforcement must be aligned with the open time of the cement paste, and geometrical freedom is restricted. Instead, the reinforcement can also be created additively parallel to the SPI process, which allows the geometric freedom to be retained. Wire and Arc Additive Manufacturing (WAAM), in which molten drops of steel are welded together, can be used to produce steel bars additively with variable diameters and curved structures [12]. As the steel has to be melted for a new layer, high temperature loads are generated at the welding point affecting the surrounding particle bed and thus the intrusion behavior of the cement paste. At the welding point approx. 1500 °C are reached. The temperature decreases over the length of the rebar [4].

First preliminary investigations to determine the temperature load up to which the implementation of WAAM in the SPI process is possible were already carried out by Weger et al. [4]. The tests served as a first rough assessment of the feasibility of combining SPI and WAAM. The investigations showed that increased temperatures could contribute to the cement paste becoming less flowable. This reduces the penetration depth of the cement paste into the particle bed and thus the layer bonding. The yield stress in particular is decisive for the penetration behavior of the cement paste [3]. Therefore, it is necessary to establish improved paste mixtures optimized to almost constant yield stress values over the entire SPI production period and evaluate their yield stress development at increased temperatures. These investigations are essential primarily to enable a combined implementation of SPI and WAAM in practice and secondly for the dimensioning of cooling strategies for this combined additive manufacturing process.

Materials and Methods

Investigations were performed with a reference cement paste, consisting of an ordinary Portland cement with a strength class of 42.5 N, demineralized water, and a composite of three different polycarboxylate ether-based superplasticizers (SP). The mixture was a result of previous investigations to optimize the flowability over longer times. In the preliminary investigation, only the combination of the three SP used resulted in a constant yield stress over 180 min, which corresponds to the production period of the SPI process. The water-to-cement ratio of the paste was 0.3. Mixing was done in a laboratory mixer, operated at 2500 rpm and 4.2 Nm torque. The cement was weighed and added to the mixer. Then the water and the superplasticizer were weighed in together. The water-superplasticizer blend was added to the cement in the mixer, and the mixing process was started for 1:30 min, paused for 2:00 min, and then operated again for 1:30 min at the same speed.

Investigations by Weger [3] show that a mini-slump flow of 400 mm provides sufficiently high penetration depths for the SPI process using aggregates with an average diameter d_{50} between 1.0 mm and 2.6 mm. Therefore, the cement paste was adjusted to 400 mm ± 5 mm mini-slump flow through the dosage of SP. The mini-slump test was only used as a control measure to ensure constant initial flowability of the paste before the rheological characterization. Rheological measurements were done 15:30 min after water addition using a rotational rheometer with parallel plate measuring system.

In addition, the mini-slump flow test can be used to validate the yield stress derived from the rheometer tests [10, 11]. At 14:10 min, the cement paste was remixed with a hand mixer for 30 s so that the mini-slump test could be performed after 15:00 min. The schedule of laboratory activities is shown in Table 1.

In the presentation of results, the yield stress value of the reference cement paste at 20 °C calculated by the Herschel-Bulkley (HB) analysis is therefore compared with the yield stress according to Roussel [10, 11] at 400 mm ± 5 mm mini-slump flow.

Table 1. Schedule of laboratory operations

Time [mm:ss]	Operation
00:00	start mixing
01:30	pause mixing
03:30	start mixing
05:00	stop mixing
14:10	start remixing
14:40	stop remixing
15:00	mini-slump test
15:30	rheological measurement
15:32	stop rheological measurement

The cement paste was rheologically characterized at constant temperatures between 20 °C and 70 °C, in steps of 10 °C each. The temperature after mixing was 20 °C ± 0.5 °C for all pastes, and the temperature was increased to the desired level directly in the rheometer within a few seconds with the aid of a directly heated lower plate of the measuring system and an additional peltier hood (see Figure 1). This peltier hood also ensures a constant temperature during the measurement. Three individual tests were carried out for each temperature load.

Figure 1. Peltier hood installed in the rheometer

Figure 2 shows the used rotational measurement sequence of the rheometer. It consists of a 10 s pre-shear phase at a shear rate of 40 s^{-1} followed by gradually decreasing shear rates between 80 s^{-1} and 0.02 s^{-1}. Every single constant shear rate level lasted for 6 s. During this time, the measured shear stress converged to an almost constant value, representative for the applied shear rate. These shear rates and the corresponding converged shear stresses served for the further calculation of the rheological parameters.

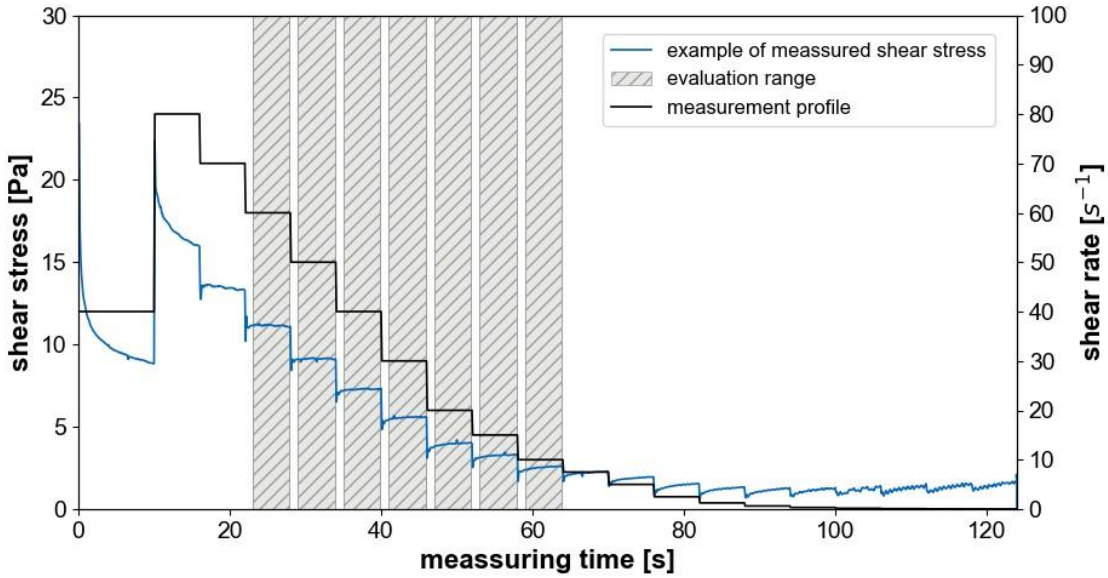

Figure 2. Measurement sequence (black line) and corresponding shear stress of a cement paste (blue line, exemplary) as well as the shear rate range for further evaluation of the rheological parameters (grey shadowed area).

The viscosity was calculated from the quotient of the measured shear stress and the measured shear rate for each measuring point. HB approach was used to calculate the yield stress τ_0, the flow index n, and the consistency index k based on the shear rates between 60 s^{-1} and 10 s^{-1} and the corresponding shear stresses using equation (1) [13, 14].

$$\tau = \tau_0 + k \cdot \dot{\gamma}^n \quad (1)$$

Parameters τ_0, n, and k were calculated in an iterative manner by minimizing the mean squared error between the calculated and the measured shear stresses. Shear rates outside 10 s^{-1} to 60 s^{-1} were excluded from further calculations since the shear stress did not converge to a constant value for the corresponding shear rate, see Figure 2. This indicates structural changes in the paste matrix (further structural breakdown at high shear and structural build-up at low shear). When calculating the mean shear stress values per step, the first and last second were neglected in order to avoid the influence of the shear rate change.

In addition to the direct rheometer measurement, the normal force between the plates was also observed. The normal force was tared at the beginning of the measurement, and the value at the end of the rotational measurement sequence was recorded.

Results and discussion

Shear stress and viscosity

Table 2 shows the measured shear stresses in the evaluated shear rate range between 10 s^{-1} and 60 s^{-1} for the investigated paste temperatures.

Table 2. Measured shear stresses for corresponding shear rates of the cement paste at paste temperatures between 20 °C and 70 °C.

Paste temperature [°C]	Shear rate [s^{-1}]						
	10	15	20	30	40	50	60
	Shear stress [Pa]						
20	2.3	3.1	4.0	5.8	8.0	10.3	13.0
30	2.1	2.7	3.3	4.8	6.5	8.4	10.5
40	2.1	2.7	3.2	4.6	6.3	8.2	10.4
50	2.1	2.5	2.9	4.0	5.3	6.9	8.7
60	2.1	2.4	2.7	3.7	4.7	6.1	7.6
70	14.9	13.4	12.4	12.8	13.3	13.6	14.2

Between 20°C and 60°C, the shear stresses of the cement paste tend to decrease with increasing temperature at the respective shear rate. Moreover, the shear stresses of the samples in that temperature range differ significantly less in the low shear rate range than in the high shear rate range. With increasing shear rate, the shear stresses, therefore, develop under proportionally with increasing paste temperature up to 60 °C, which indicates a decreasing viscosity of the cement paste with increasing temperature. This can also be seen in Figure 3, where the dynamic viscosities are shown as the ratio of applied shear rate to measured shear stress for the paste temperatures investigated.

In investigations by Lee et al. [15], this decrease in viscosity with increasing temperature attributes to increasing Brownian motion. Lee et al. [15] carried out rheological investigations with cement pastes between 5 °C and 40 °C and showed this behavior in agreement with the results presented here. The higher the temperature, the lower the viscosity. The higher the temperature, the faster the molecules can move in the cement paste suspension.

The binding forces between the molecules decreases, and in turn, the distance between the cement particles increases. Thus, the flow resistance decreases in this temperature range. [15–17]

Furthermore, the cement pastes showed slightly shear-thinning behavior in the low-shear range up to 30 s^{-1} – 40 s^{-1} and switched afterward to slightly shear thickening behavior for increased shear. This is valid for every investigated temperature up to 60 °C. The ob-

served behavior can be related to the fact that the particles in the cement paste start moving at low shear rates, and their distance to each other in shear direction increases due to steric and electrostatic repulsion as well as particle alignment. This causes shear-thinning behavior. Increasing the shear stress causes pronounced particle collisions in the cement paste so that the shear-thinning behavior gradually turns into shear-thickening behavior. [18]

Summarizing the viscosity values up to a paste temperature of 60 °C, it can be concluded that the viscosity in this range does not increase, but even decreases slightly. This corresponds to a slight improvement with regard to the requirements in the SPI process, especially for conveying the cement paste through the nozzles. Furthermore, this is an important aspect regarding the SPI process requirements of a stable and constant viscosity during the printing period.

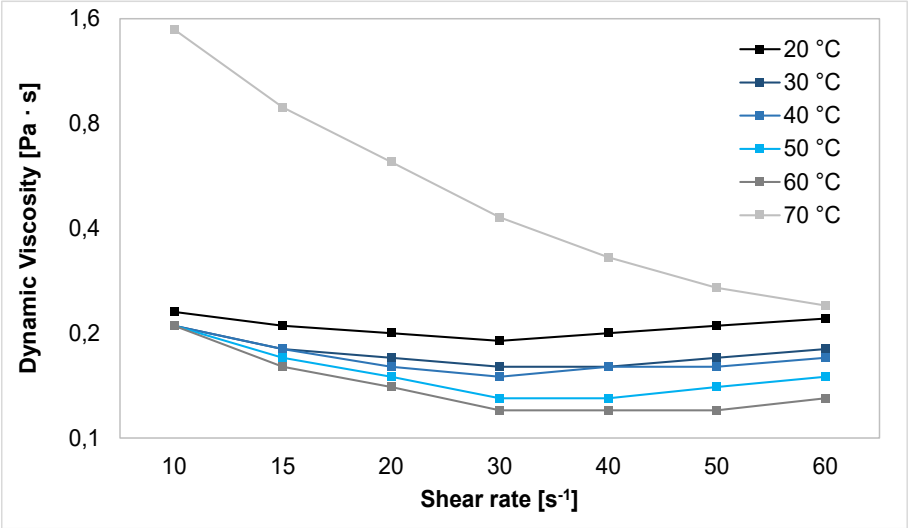

Figure 3. Viscosity curve of the cement paste at a paste temperature range from 20 °C to 70 °C.

At 70 °C, the results of the rheological measurements of the cement paste deviate from all observations made at lower temperatures. At 70 °C, the cement paste exhibits generally higher shear stresses (see Table 2) and thus shows increased dynamic viscosities (Figure 3) compared to the other mixtures at 60 °C or lower.

We assume that at a temperature increase from 60 °C to 70 °C, phase instabilities occur that lead to a change in the rheological behavior of the cement paste. At a temperature of somewhat below 70 °C, the decomposition (dehydration) of the early-built ettringite ($Ca_6Al_2(SO_4)_3(OH)_{12}\cdot 26\ H_2O$), which formed directly after the addition of water to the cement, might occur. Ettringite is known to become unstable at temperatures above approx. 50 °C [19–23], while the exact phase stability depends among others on the Al_2O_3/SO_3 ratio in the system [20, 24, 25]. Once ettringite is unstable, the sulfate and aluminum ions are probably forced to form layered double hydroxides instead of ettringite, or more specifically AFm phases, such as monosulphate. Such plate-shaped hydrates might build up a card-house structure, which could explain the sudden setting of the cement paste and thus the subsequent increase in viscosity. In addition, at 70 °C, the paste showed strong shear-thinning behavior over the entire range of shear rate evaluated. This indicates that an increased shear force is able to destroy the card-house-structure of AFm phases.

More detailed investigations to elucidate this behavior are currently being carried out. In further research, the interactions of the SP will also be investigated and a non-reactive, blank sample will be tested.

Normal force

In addition to the rheological parameters, the normal force between the plates was recorded during the rheometer measurement sequence. In the case of possible evaporation of water from the cement paste at increasing temperatures, the paste volume would decrease and with it the gap between the plates. Since the gap width between the plates was kept constant during the entire measurement sequence, water evaporation is indicated by a decreasing normal force. The measured normal forces after finishing the rheometer measurement can be taken from Table 3. By taring the values at the beginning of the measurement, tensile forces are displayed as negative values.

Table 3. Normal forces after rheometer measurement as a function of paste temperature

Temperature [°C]	Normal Force [N]
20	-0.08
30	-0.09
40	-0.07
50	-0.11
60	-0.17
70	-7.34

While the normal force is almost zero for all measurements conducted at temperatures up to 60°C, there is a sudden increase in tensile force from 60°C to 70°C. The pronounced tensile value at 70°C also indicates a change in the phase assemblage, as ettringite is a rather voluminous hydrate compared to AFm phases. However, the decomposition of ettringite or the transformation of ettringite to AFm phases would also cause the release of a significant amount of water. Therefore, more in-depth analyses on the amount of ettringite formed at lower temperatures and the amount of AFm phases formed at 70 °C need to be carried out in order to account for the volume of the various states of water (free water or bound water) and the volume of solid phases in the systems at various temperatures.

Calculation of yield stress, flow index, and consistency index

The calculated yield stresses, flow indices, consistency index, and related mean squared errors are presented in **Table 4**.

Table 4. Calculated Herschel-Bulkley parameter. Yield stress, flow index, consistency index, and mean squared error (MSE) for varying paste temperature.

Temperature [°C]	Yield stress $\dot{\gamma}$ [Pa]	Flow index n [-]	Consistency index k [-]	MSE [-]
20	1.4	1.38	0.040	0.006
30	1.5	1.46	0.023	0.006
40	1.6	1.52	0.017	0.004
50	1.7	1.62	0.009	0.003
60	1.8	1.66	0.006	0.002
70	13.3	4.42	0.000	3.703

To verify whether the calculated yield stresses are appropriate, the yield stress according to Roussel [10, 11] at a mini-slump flow of 400 mm ± 5 mm is compared to the yield stress according to the HB analysis at 20 °C. A mini-slump flow of 400 mm ± 5 mm corresponds according to Roussel [10, 11] to a yield stress range of 1.28 Pa to 1.45 Pa. The reference cement paste at 20 °C with 1.4 Pa is therefore in this range.

The yield stress and the flow index slightly increase with increasing temperature up to 60 °C. One possible explanation would be the evaporation of water. However, the effect on the yield stress is relatively high in relation to the small temperature increase from 60 °C to 70 °C. Therefore, this behavior could also be due to an already accelerated hydration caused

by the temperature. [26–28] However, a significant increase can be seen only at a temperature of 70 °C, which might be linked to the phase instabilities already described.

Effect of rheological parameters in the practical application of SPI

Weger and Gehlen [1] showed that an optimum between the layer thickness of the aggregates and the penetration depth of the cement paste must be found in order to achieve both sufficient material properties (strength, durability) and shape accuracy in the production of SPI structures.

The penetration depth of the cement paste into the particle bed depends on the rheological properties of the cement paste and the flow resistance of the particle bed. To avoid the effort of "trial and error" tests, Pierre et al. [7, 29] and Weger et al. [2] developed calculation and simulation models to predict the penetration depth of cement pastes in the SPI process.

Under the assumption of a particle bed with an average aggregate diameter d_{50} of 1.0 mm, 1.6 mm as well as 2.6 mm and the measured rheological parameters of the investigated cement pastes, see Table 4 the penetration depth of the cement paste can be calculated using Eq. 1 [2].

$$e = \frac{\rho_P \cdot g \cdot \frac{H_{0,eff}}{2} \cdot d_{eff} \cdot \varepsilon}{\tau_0 + \frac{\tau_{0,lim}}{\tau_0} \cdot k \cdot \dot{\gamma}^n} \tag{2}$$

Where e (m) is the penetration depth of the cement paste into the particle bed, ρ_p (kg m-3) is the density of the cement paste, g (m s^{-2}) is the gravitational constant, $H_{0,eff}$ (m) is the effective height of the cement paste determining the maximum initial hydrostatic pressure acting at the bottom of the cement paste, d_{eff} (m) is the effective diameter of the capillary pore system of the particle bed, ε is the porosity of the particle-bed, τ_0 is the Herschel-Bulkley yield stress (Pa), $\tau_{0,lim}$ is the limiting yield stress (Pa), k is the Herschel-Bulkley consistency index (-), $\dot{\gamma}$ (s^{-1}) is the shear rate of the penetrating cement paste in a pressure less capillary pore system and n (-) is the Herschel-Bulkley flow index. Figure 4 shows the predicted penetration depths following Eq. (2).

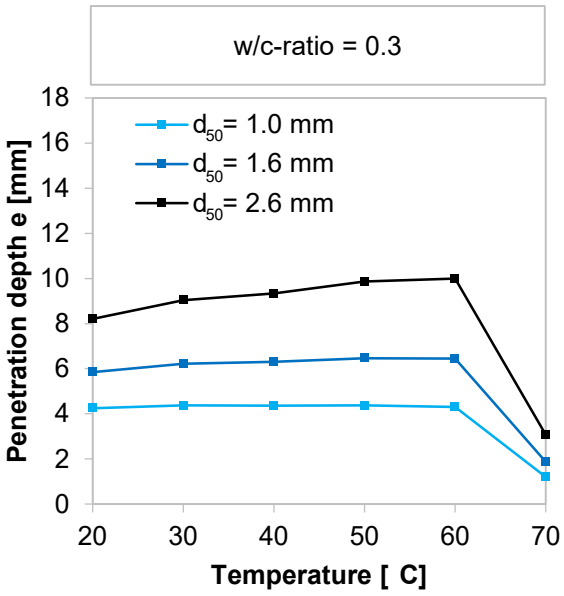

Figure 4. Penetration depth e of the cement paste in dependency of the temperature of the cement paste following Eq. 2 [2]

On the one hand, the results show an increasing penetration depth of the cement paste with increasing average diameter d_{50} of the particles in the particle bed due to a decreasing flow resistance [1–3, 5–9]. On the other hand, the results exhibit an increasing penetration depth up to a cement paste temperature of 60 °C, although the yield stress is almost constant, and the flow index n is slightly increasing. This can be explained by the simultaneously decreasing viscosity and consistency index k. Furthermore, the increase in penetration depth with temperature is more pronounced with increasing d_{50}, while the particle bed with a d_{50} of 1.0 mm exhibits a quite constant penetration depth up to 60 °C. This is probably caused by the increasing flow resistance of the particle bed and therefore limited free flow of the cement paste into the voids between the particles. This effect limits the influence of the viscosity and increases the impact of the yield stress on penetration depth [2, 3].

However, at 70 °C, the penetration depths strongly decrease at all investigated aggregate sizes. This can be explained by the strong increase of the yield stress and the apparent viscosity due to the first decomposition (dehydration) of the early-built ettringite and the related built-up of plate-shaped hydrates, which itself might build up a card-house structure (see results of apparent viscosity measurements above).

Related to a practical application, the prediction acc. Eq. (1) shows that the temperature should have an effect on the penetration depth and, therefore, on the maximum possible layer thickness in the SPI printing process. Assuming a layer thickness of 3 ± 2 mm, a sufficient layer bonding should be achieved up to a temperature of 60 °C. However, using a d_{50} of 2.6 mm shape accuracy could decrease with increasing temperature. As soon as a temperature of 70 °C is reached, the penetration depth decreases to 1.2 mm (d_{50} = 1.0 mm), 1.9 mm (d_{50}=1.6 mm) and 3.1 mm (d_{50} = 2.6 mm). Therefore, when WAAM is used at the same time, it will be essential to limit the cement paste temperature by additional cooling strategies for the printing process.

It should be noted that a printer with a nozzle diameter of 2 mm was assumed. The technology of the SPI printer is further under development, and the nozzle diameter might change in the future. It must be taken into account that the penetration behavior is, besides the cement paste rheology, also linked to the printer setting (i.e., the nozzle diameter) and the characteristics of the particle bed (i.e., particle diameter, shape, and packing density/porosity). Therefore, the calculations may have to be repeated if these parameters are changed.

Conclusions

The additive manufacturing method Selective Paste Intrusion (SPI) is combined with Wire and Arc Additive Manufacturing (WAAM) to produce a steel reinforcement in SPI elements. The WAAM process will generate heat in the reinforcing steel, transferred to the surrounding cement paste in the particle bed [4].

In the SPI process, the rheological properties of the cement paste are of high significance. They affect the printing quality of the components. Thus, yield stresses smaller than limiting yield stress, which depends on the flow resistance of the particle bed, must be aimed [3, 7]. Since external temperature loads influence the rheological properties of cement pastes, the critical temperature threshold was determined at temperatures above 60 °C. Up to this temperature, the yield stresses were between 1.41 and 1.80 Pa and should thus allow sufficient penetration depths. It can be assumed that temperature loads up to at least 60 °C are permissible. The fact that viscosity decreases with increasing temperature load is a positive side effect. However, the temperature load must not be higher than 70 °C. The range between 60 °C and 70 °C can still be investigated in further tests. The findings obtained will help to develop cooling strategies and the design of a cooling system to keep the temperature loads in the particle bed to a minimum. Furthermore, based on them, the combined SPI-WAAM process can be designed, including the distance between the welding point and the

powder bed as well as the maximum feasible speeds of the layer production, thus achieving a further step towards reinforced, high-strength concrete elements.

Outlook

Future investigations are planned to take a closer look at the critical range between 60 °C and 70 °C by starting a new series with, for example, an increment of 2 °C.

It is also conceivable to optimize the cement paste formulation. Initial discussions with producers of chemicals for the building materials industry revealed that additional additives, such as retarders or super absorbing polymers, could make the cement paste more resistant to external temperature loads.

In addition, printing tests will be carried out on the SPI printer. Here, both the performance of the cement paste and the process stability towards increased temperature loads are to be investigated and optimized.

Data availability statement

The data are not published. In case of interest, the corresponding author (alexander.strasser@tum.de) will provide the data upon request.

Author contributions

Conceptualization, A.S.; methodology, A.S.; validation, A.S.; formal analysis, A.S.; investigation, A.S.; writing—original draft preparation, A.S., D.W.; writing—review and editing, A.S., D.W., C.M., T.K.; visualization – Figures 1, 2 and 3, A.S., Figure 4, D.W.; supervision, C.M., T.K.; project administration, C.M., T.K.; funding acquisition, C.G. All authors have read and agreed to the published version of the manuscript

Competing interests

The authors declare no competing interests.

Funding

This research was funded by the Deutsche Forschungsgemeinschaft (DFG, German Research Foundation) – Project-number 414265976 – TRR 277

Acknowledgment

The authors would like to thank Prof. Alisa Machner and Dr. Anne Heisig, Chair of Mineral Construction Materials, Technical University of Munich, for their support and fruitful discussion regarding the chemical changes of cement paste at elevated temperatures.

References

1. Weger, D. and Gehlen, C. 2021. Particle-Bed Binding by Selective Paste Intrusion-Strength and Durability of Printed Fine-Grain Concrete Members. Materials (Basel, Switzerland) 14, 3. DOI: https://doi.org/10.3390/ma14030586.

2. Weger, D., Pierre, A., Perrot, A., Kränkel, T., Lowke, D., and Gehlen, C. 2021. Penetra-tion of Cement Pastes into Particle-Beds: A Comparison of Penetration Models. Mate-rials (Basel, Switzerland) 14, 2. DOI: https://doi.org/10.3390/ma14020389.
3. Weger, D. 2020. Additive Fertigung von Betonstrukturen mit der Selective Paste Intru-sion – SPI / Additive manufacturing of concrete structures by Selective Paste Intrusion - SPI. Dissertation, Munich.
4. Weger, D., Baier, D., Straßer, A., Prottung, S., Kränkel, T., Bachmann, A., Gehlen, C., and Zäh, M. Reinforced Particle-Bed Printing by Combination of the Selective Paste In-trusion Method with Wire and Arc Additive Manufacturing – A First Feasibility Study 28, 978–987. DOI: https://doi.org/10.1007/978-3-030-49916-7_95.
5. Weger, D., Gehlen, C., Lowke, D. Additive Fertigung von Betonbauteilen durch selekti-ve Zementleim-Intrusion. Proceedings of Ibausil 2018.
6. Lowke, D., Dini, E., Perrot, A., Weger, D., Gehlen, C., and Dillenburger, B. 2018. Parti-cle-bed 3D printing in concrete construction – Possibilities and challenges. Cement and Concrete Research 112, 50–65. DOI: https://doi.org/10.1016/j.cemconres.2018.05.018.
7. Pierre, A., Weger, D., Perrot, A., and Lowke, D. 2018. Penetration of cement pastes into sand packings during 3D printing: analytical and experimental study. Mater Struct 51, 1. DOI: https://doi.org/10.1617/s11527-018-1148-5.
8. Weger, D., Lowke, D., Gehlen, C. 3D Printing of Concrete Structures with Calcium Sili-cate based Cements using the Selective Binding Method - Effects of Concrete Tech-nology on Penetration Depth of Cement Paste. Proceedings of Hipermat 2016 - 4th In-ternational Symposium on Ultra-High Performance Concrete and High Performance Construction Materials 2016.
9. Weger, D., Lowke, D., Gehlen, C., Talke, D., Henke, K. Additive manufacturing of con-crete elements using selective cement paste intrusion – effect of layer orientation on strength and durability. Proceedings of RILEM 1st International Conference on Con-crete and Digital Fabricaton 2018.
10. Roussel, N. and Coussot, P. 2005. “Fifty-cent rheometer” for yield stress measurements: From slump to spreading flow. Journal of Rheology 49, 3, 705–718. DOI: https://doi.org/10.1122/1.1879041.
11. Roussel, N., Stefani, C., and Leroy, R. 2005. From mini-cone test to Abrams cone test: measurement of cement-based materials yield stress using slump tests. Cement and Concrete Research 35, 5, 817–822. DOI: https://doi.org/10.1016/j.cemconres.2004.07.032.
12. Mechtcherine, V., Grafe, J., Nerella, V. N., Spaniol, E., Hertel, M., and Füssel, U. 2018. 3D-printed steel reinforcement for digital concrete construction – Manufacture, me-chanical properties and bond behaviour. Construction and Building Materials 179, 125–137. DOI: https://doi.org/10.1016/j.conbuildmat.2018.05.202.
13. Larrard, F. de, Ferraris, C. F., and Sedran, T. 1998. Fresh concrete: A Herschel-Bulkley material. Mater Struct 31, 7, 494–498. DOI: https://doi.org/10.1007/BF02480474.
14. Mezger, T.G. 2006. Das Rheologie Handbuch. Für Anwender von Rotations- und Oszil-lations-Rheometern. Vincentz, Hannover, Germany.
15. Lee, D. K. and Choi, M. S. 2018. Standard Reference Materials for Cement Paste: Part III-Analysis of the Flow Characteristics for the Developed Standard Reference Material According to Temperature Change. Materials (Basel, Switzerland) 11, 10. DOI: https://doi.org/10.3390/ma11102001.
16. Martini, S. A. and Nehdi, M. 2009. Coupled Effects of Time and High Temperature on Rheological Properties of Cement Pastes Incorporating Various Superplasticizers. J. Mater. Civ. Eng. 21, 8, 392–401. DOI: https://doi.org/10.1061/(ASCE)0899-1561(2009)21:8(392).
17. Wang, Y., Wu, A., Ruan, Z., Wang, H., Wang, Y., and Jin, F. 2018. Temperature Effects on Rheological Properties of Fresh Thickened Copper Tailings that Contain Cement. Journal of Chemistry 2018, 1–8. DOI: https://doi.org/10.1155/2018/5082636.

18. Haist, M. 2010. Zur Rheologie und den physikalischen Wechselwirkungen bei Zementsuspensionen. Dissertation. Zugl.: Karlsruhe, Univ., Diss., 2009. Karlsruher Reihe Massivbau, Baustofftechnologie, Materialprüfung H. 66. KIT Scientific Publ, Karlsruhe.
19. Gallucci, E., Zhang, X., and Scrivener, K. L. 2013. Effect of temperature on the microstructure of calcium silicate hydrate (C-S-H). Cement and Concrete Research 53, 185–195. DOI: https://doi.org/10.1016/j.cemconres.2013.06.008.
20. Lothenbach, B., Winnefeld, F., Alder, C., Wieland, E., and Lunk, P. 2007. Effect of temperature on the pore solution, microstructure and hydration products of Portland cement pastes. Cement and Concrete Research 37, 4, 483–491. DOI: https://doi.org/10.1016/j.cemconres.2006.11.016.
21. Kjellsen, K. O. and Detwiler, R. J. 1992. Reaction kinetics of portland cement mortars hydrated at different temperatures. Cement and Concrete Research 22, 1, 112–120. DOI: https://doi.org/10.1016/0008-8846(92)90141-H.
22. Damidot, D. and Glasser, F. P. 1992. Thermodynamic investigation of the CaO-Al2O3-CaSO4-H2O system at 50°C and 85°C. Cement and Concrete Research 22, 6, 1179–1191. DOI: https://doi.org/10.1016/0008-8846(92)90047-y.
23. Perkins, R. B. and Palmer, C. D. 1999. Solubility of ettringite (Ca6[Al(OH)6]2(SO4)3 · 26H2O) at 5–75°C. Geochimica et Cosmochimica Acta 63, 13-14, 1969–1980. DOI: https://doi.org/10.1016/S0016-7037(99)00078-2.
24. Lothenbach, B., Matschei, T., Möschner, G., and Glasser, F. P. 2008. Thermodynamic modelling of the effect of temperature on the hydration and porosity of Portland cement. Cement and Concrete Research 38, 1, 1–18. DOI: https://doi.org/10.1016/j.cemconres.2007.08.017.
25. Deschner, F., Lothenbach, B., Winnefeld, F., and Neubauer, J. 2013. Effect of temperature on the hydration of Portland cement blended with siliceous fly ash. Cement and Concrete Research 52, 169–181. DOI: https://doi.org/10.1016/j.cemconres.2013.07.006.
26. Nehdi, M. and Al Martini, S. 2009. Estimating time and temperature dependent yield stress of cement paste using oscillatory rheology and genetic algorithms. Cement and Concrete Research 39, 11, 1007–1016. DOI: https://doi.org/10.1016/j.cemconres.2009.07.011.
27. Nehdi, M. and Al Martini, S. 2007. Effect of Temperature on Oscillatory Shear Behavior of Portland Cement Paste Incorporating Chemical Admixtures. J. Mater. Civ. Eng. 19, 12, 1090–1100. DOI: https://doi.org/10.1061/(ASCE)0899-1561(2007)19:12(1090).
28. Varshney, A., Gohil, S., Chalke, B. A., Bapat, R. D., Mazumder, S., Bhattacharya, S., and Ghosh, S. 2017. Rheology of hydrating cement paste: Crossover between two ag-ing processes. Cement and Concrete Research 95, 226–231. DOI: https://doi.org/10.1016/j.cemconres.2017.02.034.
29. Pierre, A., Weger, D., Perrot, A., and Lowke, D. 2020. Additive Manufacturing of Cementitious Materials by Selective Paste Intrusion: Numerical Modeling of the Flow Using a 2D Axisymmetric Phase Field Method. Materials (Basel, Switzerland) 13, 21. DOI: https://doi.org/10.3390/ma13215024.

Visions and Strategies for Reinforcing Additively Manufactured Concrete Structures

Reinforcing Materials

https://doi.org/10.52825/ocp.v1i.80

Submitted: 5 Oct. 2021 | Accepted: 29 Nov. 2021 | Published: 15 Feb. 2022

Simultaneous Integration of Continuous Mineral-bonded Carbon Reinforcement into Additive Manufacturing with Concrete

Tobias Neef[1] [https://orcid.org/0000-0002-8256-1455] and Viktor Mechtcherine[1] [https://orcid.org/0000-0002-4685-7064]

[1]Technische Universität Dresden, Germany

Abstract. 3D concrete printing is becoming more and more popular, not only in research but also in practice of construction. One of the main challenges however remains the integration of reinforcement. This publication focuses on the use of continuous fibers for this purpose. The special feature of the new type of carbon yarns applied is the mineral impregnation used instead of the conventional polymer one. Such reinforcement not only yields excellent mechanical properties, but also offers many advantages, specifically with respect to processing flexibility and is therefore very well suited for additive manufacturing. The concrete for 3D printing to be reinforced with such yarns must meet particular requirements, especially when the finest concrete filaments are printed. This is also a subject of the article at hand.

Keywords: Digital construction, digital concrete, Additive Manufacturing, 3D concrete printing, reinforcement, mineral-bonded carbon fibre

Conference presentation video: https://doi.org/10.5446/56113

Introduction

The additive manufacturing with concrete, also often called 3D concrete printing (3DCP), offers a number of advantages such as saving manpower, time and resources and thus also reducing CO_2 footprint of concrete construction [1]. The work processes are simulated and optimized in advance on a digital construction site. This is followed by implementation on the real construction site [2] or the production of prefabricated parts in a factory, which only need to be assembled on site. An example for that is the bicycle bridge in the Netherlands [3], where components were first printed in a factory and then connected to form a bridge with pre-stressed reinforcement. Formwork-free construction opens up new shape-free design possibilities, especially curves or wave shapes, as can be seen on the individual segments of the bridge.

While 3DCP develops fast towards applications in the practice of construction, the integration of reinforcement into these technologies still presents a challenge. There are a number of options with respect to materials to be used, ranging from conventional steel reinforcement [4] to short-fiber reinforcement [5], carbon reinforcement [6] or prestressed reinforcement [3]. The different variants were widely discussed in Mechtcherine et al. [7]. In this article, the focus will be on simultaneous and continuous carbon fiber reinforcement. The special feature here is that the carbon is impregnated not with a polymer, following the established technique for carbon reinforcement, but with a mineral suspension.

Mineral-bonded carbon reinforcement

Why do we use mineral impregnated fiber reinforcement?

Mineral-impregnated carbon yarns have several advantages over polymer-impregnated fiber reinforcements. The easy formability of the freshly impregnated yarn is of a particular importance for additive manufacturing applications. The yarn can be deposited in any geometry without strain, thus exploiting the full potential of the geometric freedom of 3D printing. The carbon reinforced concrete filaments can be deposited in fine and narrow paths with a small cross-section, since the carbon reinforcement requires only a very thin concrete cover. This allows the reinforcement to be integrated into the border areas of the components in a statically favorable manner. A thin cover leads to material savings and thus more environmentally friendly construction. Furthermore, the mineral impregnation shows a significantly higher temperature resistance [8] than polymeric impregnation materials and enables a very intensive bond between reinforcement and concrete. At 200 degrees, the pullout force was double [8]. Concrete components with mineral-impregnated reinforcement therefore exhibit a very finely distributed crack pattern with small crack widths when subject to bending or tensile loads. This reduces possible ingress of agrecive substances into the composite, which is beneficial to its durability.

Composition and properties of the mineral impregnation suspension

To prepare the mineral impregnation suspension, two ultrafine cements (Mikrodur R-X, Mikrodur P-U, Dyckerhoff Germany) and a microsilica suspension (EMSAC 500 SE, BASF Germany) with superplasticizer are suspended in water. 95% of all particles by weight have sizes smaller than 9 µm, so that most particles can penetrate between the carbon filaments with diameters of about 7 µm after excitation. Figure 1a shows the grading curves of the constituents of the suspension in comparison to a typical CEM I 52.5 R cement. Figure 1b shows a carbon filament with adhering suspension particles. The water-to-binder ratio of the suspension is 0.8. The viscosity is adjusted using superplasticizer "MSH flüssig" to a run-out time in the Marsh Funnel of approximately 30 seconds.

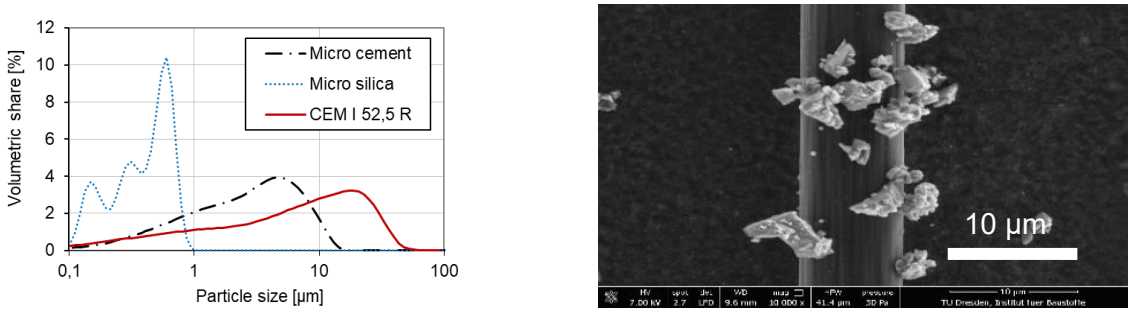

Figure 1. (a) Particle size distributions of mineral suspension and (b) micrograph of carbon fiber with adhering micro-cement with D95 < 9 µm [9].

A carbon yarn SIGRAFIL® C T50-4.4/255-E100 (SGL) was used as continuous reinforcement fiber. The yarn consists of 50,000 individual filaments with epoxy resin sizing. Complete impregnation of yarn is effectuated by multiple deflection of the yarn in the suspension. To ensure the cohesion of the filaments in the freshly impregnated yarn, the carbon yarn is spirally wrapped with a cotton thread. The carbon yarn is then wound onto a spool and fed into the additive manufacturing process. The spooled yarn can be processed for about four hours. The manufacturing process is only outlined here. A detailed description is given in Mechtcherine et al. [9].

The carbon percentage in the impregnated yarn after hardening is approximately 30 % by volume. The average diameter of a mineral-impregnated roving is approx. 3.1 mm and the corresponding cross-sectional area approximately 7.5 mm². The failure force in the uniaxial tension test (mean value) is 4.56 kN. This corresponds to a tensile strength of 581 MPa based on the total cross-section of the impregnated yarn and 2,271 MPa based on the cross-sectional area of all carbon filaments in the yarn (1.92 mm²). The modulus of elasticity related to the carbon cross-sectional area averages 249.4 GPa and is thus close to the modulus of elasticity of the carbon yarn (250 GPa).

Integration between or into concrete filaments

The additive manufacturing itself is performed with a gantry printer. The lab-scale device offers a printing space of 1.3 m x 1.3 m x 1.0 m. During production, the mixed concrete is held in a hopper. From this, the concrete is conveyed to the nozzle via an eccentric screw pump. Then it is extruded into the desired shape. There are two basic methods for integrating carbon reinforcement into the existing additive manufacturing process:

- Contiguous process: Extrusion of a concrete filament followed by deposition of the carbon rovings onto it and subsequent covering of the reinforcement yarn by extrusion of the next concrete filament [10]. The advantage of this method is that the placement of concrete and reinforcement are decoupled in time. Thus, the number of deposited reinforcements be-tween the concrete filaments can be varied according to the expected local loading. This reduces the cost of reinforcement and promotes environmentally friendly and resource-saving construction. Disadvantages are the higher time requirement if the layers are passed over twice or more times on one hand. On the other hand, the placement of the reinforcement in the joint between two concrete filaments additionally weakens this porous region. Finally, transverse tensile stresses resulting from the bond between yarn and concrete can lead to splitting along the bonded joint; see Figure 2a.
- Simultaneous process: The carbon reinforcement is embedded in the concrete filament and deposited with it. The advantages of this method are complete encasement of the yarn without weakening the joint in an efficient and time-saving manner. The disadvantage is a lacking option of having crossings and overlaps of reinforcement layers which can be favorable for transfer of forces in a print element. Note that for a simultaneous process, the degree of reinforcement in the concrete filament can be adapted using a special nozzle geometry ProfiCarb, in which up to six carbon rovings can be integrated simultaneously [6].

(a) (b)

Figure 2. Fracture pattern of a specimen produced (a) in the contiguous process, and (b) in the simultaneous process.

First studies and results

Uniaxial tension test on printed and cast specimens

In this section, results of investigations on specimens from both the simultaneous process and the conventional casting are presented. Some of the results have already been published in the journal Beton- und Stahlbetonbau [6].

For the tests, a fine-grain concrete was chosen which is often used for 3D printing processes at the Institute for Construction Materials at the TU Dresden; see e.g. [11], [12]. Portland cement, microsilica slurry and fly ash were used as binders. The maximum grain size of the aggregate was 2 mm. The composition is given in Table 1.

Table 1. Composition of printable fine-grained concrete under investigation.

Constituent	Supplier / product name	[kg/m³]
Cement CEM I 52.5 R ft	Opterra	392
Fly ash SFA	Steament H4	214
Microsilica	EMSAC 500 SE, BASF	214
Sand 0.06-0.2	BCS 413	253
Sand 0-1	Ottendorf	253
Sand 0-2	Ottendorf	759
Water	Tab water	139
Superplasticizer	Sky 593, BASF	11

To compare the mechanical performance of the specimens from the two types of production, specimens for uniaxial tension tests were produced and loaded to failure. Both the printed and the conventionally cast specimens had a length of 300 mm and a cross-section of approximately W x H = 20 mm x 40 mm. The reinforcement was arranged in the center of the cross-section at a height of 10 mm. The reinforcement consisted of three mineral-impregnated car-bon yarns placed at 10 mm distance to each other.

The two types of specimens were prepared almost simultaneously. First, the specimens were prepared using the simultaneous printing process, as shown in Figure 3. Then, additional concrete was extruded into a container and cast into a mold. The mold was first filled with concrete up to half its height; then the reinforcement was removed from the roll, put onto concrete and tightened; finally, further concrete was filled on top of it. The production of these specimens using extruded concrete was necessary since the consistency of concrete changes significantly due to the extrusion and the associated energy input. The specimens produced by the printing were complemented with load introduction regions at their ends at the specimen age of two days. Each such region had a length of 200 mm and a width of 100 mm and was grouted with self-compacting concrete. In the conventionally cast specimens, the load application area is already given by the shape of the mold; see Figure 3. Before testing, the load application regions of all specimens were ground to a thickness of 20 mm to avoid stress peaks during clamping in the Instron 8501 testing machine. The tension test was performed with a displacement rate of the crosshead of 1 mm/min until breakage. Figure 4a shows a stress-strain diagram with the results of the uniaxial tension tests.

Figure 3. Left: expansion specimen printed at the top and molded at the bottom. Right: printing process.

The conventionally produced strain plates have a higher average yarn strength of 2.078 GPa attained at 12.6‰ strain, while the scatters of strain capacity and tensile strength are greater than those recorded for the printed specimens; which yielded an average yarn strength of 1.578 GPa at a strain of 10.9‰. The reason for this difference is probably the quality of the embedment into concrete. Defects such as air inclusions can occur during or under extrusion due to insufficient conveying of material. Thus, the force transmission from the carbon yarns into concrete is disturbed. Furthermore, while the reinforcement in the conventionally produced specimens is exactly centered and stretched, this is not always the case within the printed specimens using the online process; see also cross-section analyses in the next section.

The crack initiation and crack growth were photogrammetrically recorded using a GOM ARAMIS measurement system. For this purpose, the smooth underside of the strain plate was equipped with a stochastic speckle pattern. During tension test this specimen surface was recorded at a frame rate of 1/s. In the image analysis, five distance gauges were placed equidistantly over each crack formed. The mean value of the distance gauges indicates the crack width used for further evaluation. The distance measurement between the cracks was made along the center axis of the specimens. In addition, the strain in the measurement area was determined using two virtual extensometers, which were placed close to the right and left sides of the specimen. For the evaluation, all crack widths were considered at 50% and 90% of the ultimate strain. The determined crack widths were assigned to crack classes of 0.1 mm width (example: crack class 0.2 mm contains cracks with widths > 0.1 mm and ≤ 0.2 mm). By relating the number of cracks in the measuring range to the length of the measuring range, a crack density (unit: cracks/m) can be calculated. In Figure 4b, the elements of a crack class were determined for all specimens of a production variant and converted into a crack density.

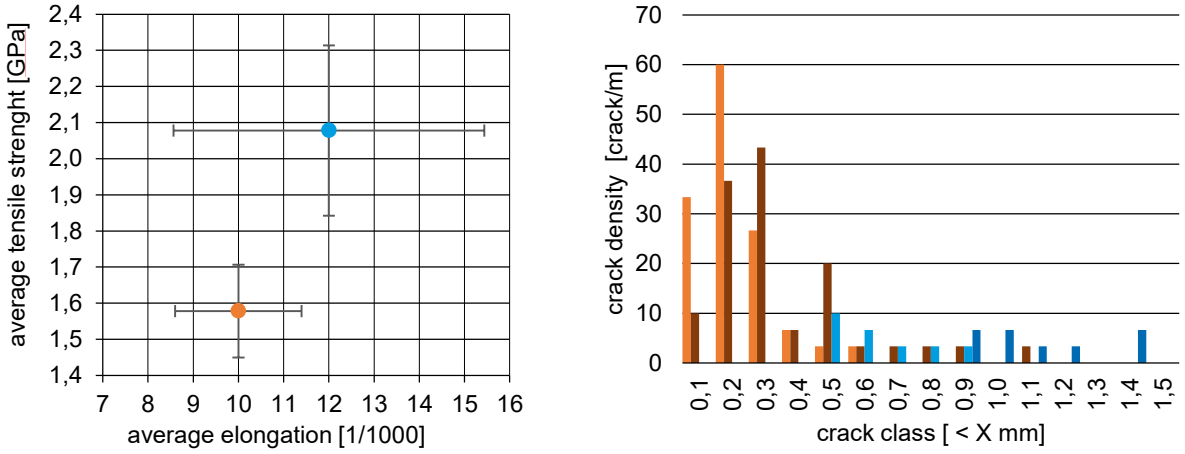

(a)

(b)

Figure 4. (a) Average tensile strength versus average elongation, (b) crack density versus crack width at different strain levels. The crack densities at 50% of the failure strain are shown in light color and at 90% failure strain with brown color. The results of specimens from the online process are shown in orange. The results of conventionally produced specimens are shown in blue.

Figure 4b shows that printed specimens have significantly more cracks with smaller crack widths. At 50% of the failure strain, the majority of the cracks have widths of up to 0.3 mm. Until 90% of the failure strain is reached, the cracks widen uniformly, and an increasing localization of deformation can be observed at one of the cracks. At this crack, tensile fracture of the composite will occur. In contrast, fewer but wider cracks appear in the conventionally

produced specimens. At 50% of the failure strain, there are few cracks with crack widths between 0.5 and 0.8 mm. Up to 90% of the failure strain, there is no further crack formation, but a uniform widening of the cracks. The reason for the greater crack density in specimens from the online process is assumed to be the rougher surface as well as fine cracks forming due to shrinkage. Stress singularities occur at these structural defects and promote crack formation or crack growth. Defects in the concrete resulting from the extrusion process have the same effect.

Visual inspection

The specimens from online and conventional production showed significant differences in failure strength and crack pattern. Imperfections during yarn placement in the online process and imperfections in concrete were assumed to be the main reasons for the differences. Thus, these features were further investigated.

One option to analyze the position of the reinforcements in the specimen is to cut the specimen along longitudinal and transverse directions and measure the position of the yarns. This destructive specimen preparation is very time-consuming when the formation of disturbing artifacts shall be reliably avoided. Furthermore, the image information can only be recorded at one section at a time.

Computed tomography (CT) offers a better alternative for non-destructive as well as three-dimensional imaging of specimen volume. In collaboration with the Institute for Parallel and Distributed Systems, University of Stuttgart, unloaded sections of strain plates (L x W x H = 50 mm x 40 mm x 20 mm) were scanned in a CT. From the data, a digital 3D model of the specimen was generated, in which the embedding of the carbon rovings and the quality of the printed concrete can be analyzed layer by layer. Figure 5 shows a horizontal section and a vertical section of a specimen produced by 3D printing. From the pictures, conclusions can be drawn about the position and orientation as well as the quality of the embedment of the yarns in the concrete.

In Figure 5b it can be clearly seen that all three carbon yarns were displaced from the specimen center, most likely by the volume flow of the concrete during extrusion. The volume flow of concrete from above pushes the yarn downwards. In the case of the central yarn, this displacement is much greater than for the yarns at the edges. A higher position of the yarn supply unit or an adjustment of the printhead nozzle could help to avoid that. It can also be seen that the carbon rovings are not always completely embedded in the concrete. During the printing process, the rovings are supplied with fresh concrete from above, so that air pockets on the underside of the yarns can prevent the formation of a uniform bond. Along the longitudinal axis of a yarn, such bonding defects can be found again and again. Note that an analogous phenomenon can occur in the production of reinforced shotcrete layers. There, an attempt is made to avoid the formation of spray shadows behind the reinforcement by spraying from different angles. In the 3D concrete printing using the method described above, only changes in nozzle geometry or a lower consistency of the fine concrete used can remedy the situation.

Figure 5a shows a longitudinal section of a print specimen. Only two out of three carbon rovings are visible here. The middle roving lies deeper and is not exposed in the selected cut; cf. also Figure 5b. The yarns exhibit slight ondulation and twisting of the filaments in the yarn. These features originate on the one hand from the wrapping of the reinforcement elements with cotton thread and on the other hand from imperfections during yarn placement in the print process. As a result, not all filaments in the yarn are exactly aligned in the direction of tensile loading. With increasing elongation, the filaments are subjected to different levels of stress and fail one after the other. This leads to a lower tensile strength of the entire yarn. However, yarn ondulation as a result of wrapping also offers advantages: Wrapped yarns

show a stronger bonding to concrete, since the latently existing material-chemical bonding components are supplemented by mechanical bonding components, so-called form closure.

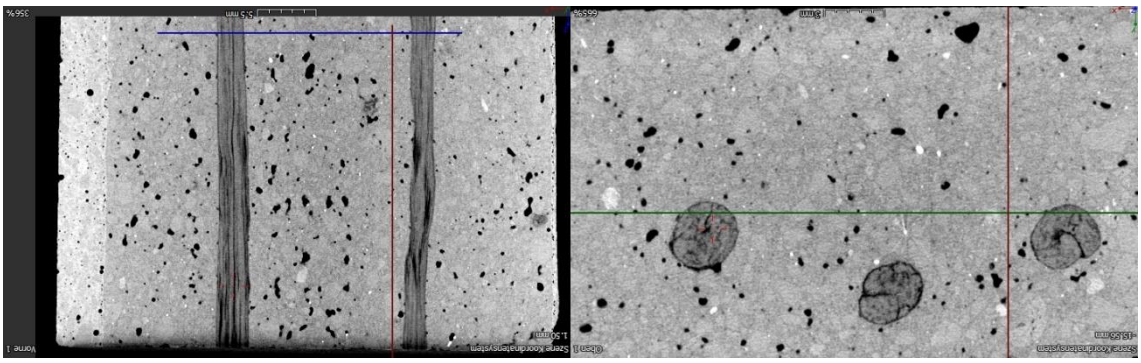

Figure 5. CT Scans of specimen made by online-method: (a) horizontal section, (b) vertical section. The colored lines mark a Cartesian system of coordinates. The sections run through their origin. Scans were made at Institute for Parallel and Distributed Systems, University of Stuttgart.

Downsizing of the concrete filament – fine filament printing

Carbon is a very high-performance material. One disadvantage, however, is that it is more expensive compared to steel reinforcement. It is therefore less suitable as reinforcement for printing solid walls (e.g., with widths ranging from 100 mm to 200 mm), since large quantity of carbonis necessary to achieve a reasonable reinforcement ratio. For this reason, research is being carried out on 3D concrete printing with fine filaments. Here, concrete filament cross-sections of 20 mm by 10 mm with an integrated mineral-impregnated carbon roving shall extruded, while high-strength concrete with a maximum aggregate size of 2 mm is used. Via a mortar pump, the previously mixed fine concrete reaches the nozzle, which is attached to the end of the robot arm. The six-axis robot arm (KUKA) serves as a manipulator and moves the extruder along the previously programmed paths to print the desired elements. The path is calculated by using a 3D-design software Rhinoceros®. The desired geometry is created and translated into the control language of robot by means of Rhinoceros®-plug-in Grasshopper.

The immense degrees of freedom in the movement of extruder through the six axes robot are advantageous. This makes it possible to approach any point in the robot's working area from different directions. This opens up the use of this manufacturing technique for geometrically complex structures such as material minimized shapes, facade elements, but also for complex components with later assembly such as ceiling elements. First examples of such

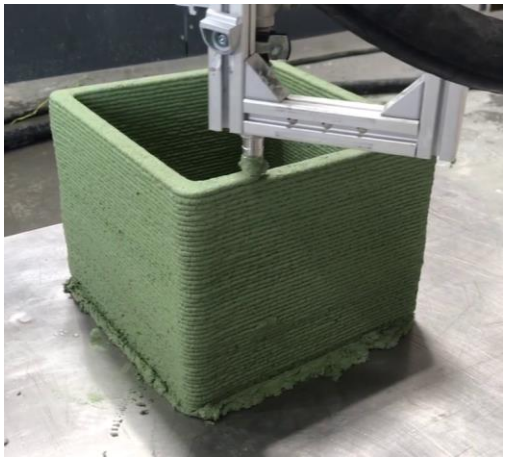

decorative elements can be seen in Figure 6.

Figure 6. Decorative elements from the fine filament 3D concrete printing.

Outlook

In the near future, not only decorative elements but also high-performance load-bearing components will be printed at the Institute for Construction Materials of TU Dresden. The research is performed within the framework of the SFB/TRR280. A particular focus is set on the integration of carbon rovings into the extruded concrete filament. Furthermore, by varying between reinforced and unreinforced concrete filaments, varying reinforcement degree appropriate to the designed load path will be introduced. This in turn leads to cost savings and conserves resources.

For an economical additive construction process, the development of a set on demand system is being implemented as well. Here, the fresh concrete is retarded and thus guarantees a long time in which it can be processed, i.e. pumped and extruded. Once it has been pumped to the nozzle, the concrete is cured in a very short time by adding and mixing in an accelerator. The curing of the concrete filament is controlled, so the printing speed and thus the construction rate can be increased. Rapid stiffening allows any construction height without the risk of collapse or buckling.

Additive manufacturing is becoming more and more important, especially in research but also for innovative companies. With excitement, we can hope for new structures with interesting designs that this new technology will produce.

Data availability statement

Data sharing is not applicable to this article.

Author contributions

Conceptualization, writing—original draft preparation Tobias Neef, writing—review and editing Viktor Mechtcherine. All authors have read and agreed to the published version of the manuscript.

Competing interests

The authors declare no conflict of interest.

Funding

The German Research Foundation (DFG) within the project SFB/TRR280 „Konstruktionsstrategien für materialminimierte Carbonbetonstrukturen – Grundlagen für eine neue Art zu bauen“ funded the research with the project number: 417002380.

References

1. G. De Schutter, K. Lesage, V. Mechtcherine, V. N. Nerella, G. Habert, and I. Agusti-Juan, „Vision of 3D printing with concrete — Technical, economic and environmental potentials“, Cem. Concr. Res., vol. 112, pp. 25–36, 2018, doi: https://doi.org/10.1016/j.cemconres.2018.06.001

2. „3D-Betondruck: Deutschlands erstes Wohnhaus wird gedruckt“. https://www.dabonline.de/2020/11/26/3d-betondruck-deutschlands-erstes-wohnhaus-wird-gedruckt-beckum-beton-peri/. [accessed: Juli 27, 2021]
3. T. A. M. Salet, Z. Y. Ahmed, F. P. Bos, and H. L. M. Laagland, „Design of a 3D printed concrete bridge by testing“, Virtual and Physical Prototyping, vol. 13, no. 3, pp. 222–236, July 2018, doi: https://doi.org/10.1080/17452759.2018.1476064
4. N. Hack and H. Kloft, „Shotcrete 3D Printing Technology for the Fabrication of Slender Fully Reinforced Freeform Concrete Elements with High Surface Quality: A Real-Scale Demonstrator“, in RILEM Bookseries, vol. 28, Springer, 2020, pp. 1128–1137, doi: https://doi.org/10.1007/978-3-030-49916-7_107
5. H. Ogura, V. N. Nerella, and V. Mechtcherine, „Developing and testing of Strain-Hardening Cement-Based Composites (SHCC) in the context of 3D-printing“, Materials (Basel)., vol. 11, no. 8, pp. 1–18, 2018, doi: https://doi.org/10.3390/ma11081375
6. T. Neef, S. Müller, and V. Mechtcherine, „3D-Druck mit Carbonbeton: Technologie und die ersten Untersuchungsergebnisse“, Beton- und Stahlbetonbau, vol. 115, no. 12, pp. 943–951, Dez. 2020, doi: https://onlinelibrary.wiley.com/doi/10.1002/best.202000069
7. V. Mechtcherine et al., „Integrating reinforcement in digital fabrication with concrete: A review and classification framework“, Cem. Concr. Compos., vol. 119, pp. 103964, Feb. 2021, doi: https://doi.org/10.1016/j.cemconcomp.2021.103964
8. K. Schneider, A. Michel, M. Liebscher, L. Terreri, S. Hempel, and V. Mechtcherine, „Mineral-impregnated carbon fibre reinforcement for high temperature resistance of thin-walled concrete structures“, Cem. Concr. Compos., vol. 97, pp. 68–77, March 2019, doi: https://doi.org/10.1016/j.cemconcomp.2018.12.006
9. V. Mechtcherine, A. Michel, M. Liebscher, K. Schneider, and C. Großmann, „Mineral-impregnated carbon fiber composites as novel reinforcement for concrete construction: Material and automation perspectives“, Autom. Constr., vol. 110, pp. 103002, 2020, doi: https://doi.org/10.1016/j.autcon.2019.103002
10. V. Mechtcherine, A. Michel, M. Liebscher, and T. Schmeier, „Extrusion-based additive manufacturing with carbon reinforced concrete: Concept and feasibility study“, Materials (Basel), vol. 13, no. 11, 2020, doi: https://doi.org/10.3390/ma13112568
11. V. N. Nerella, S. Hempel, and V. Mechtcherine, „Effects of layer-interface properties on mechanical performance of concrete elements produced by extrusion-based 3D-printing“, Constr. Build. Mater., vol. 205, pp. 586–601, 2019, doi: https://doi.org/10.1016/j.conbuildmat.2019.01.235
12. V. N. Nerella, M. Näther, A. Iqbal, M. Butler, and V. Mechtcherine, „Inline quantification of extrudability of cementitious materials for digital construction“, Cem. Concr. Compos., vol. 95, pp. 260–270, 2019 doi: https://doi.org/10.1016/j.cemconcomp.2018.09.015

Vision and Strategies for Reinforcing Additively Manufactured Concrete Structures

Reinforcing Materials

https://doi.org/10.52825/ocp.v1i.72

Submitted: 25 Sept. 2021 | Accepted: 23 Jan. 2022 | Published: 15 Feb. 2022

Interlayer Reinforcement in Shotcrete-3D-Printing

The Effect of Accelerator Dosage on the Resulting Bond Behavior of Integrated Reinforcement Bars

Niklas Freund[1][https://orcid.org/0000-0003-2392-5439] and Dirk Lowke[1][https://orcid.org/0000-0001-8626-918X]

[1] Institute of Building Materials, Concrete Construction and Fire Safety (iBMB), TU Braunschweig, Germany

Abstract. Additive manufacturing with cement-based materials has recently become increasingly common on construction site. The high degree of freedom in individual geometric shapes, the associated potential for resource-efficient designs, and the high degree of automation could make this technology a milestone in the history of construction industry. Many of the existing additive manufacturing techniques are initially based on unreinforced concrete. However, for many structural elements, the use of reinforcement is indispensable and therefore the reinforcement integration represents a prerequisite. One promising reinforcement strategy is the use of interlayer reinforcement. This method specifically uses the layered characteristic of the additive manufacturing process by integrating reinforcement between the applied layers. In combination with an adaptive path planning, it is therefore possible to manufacture force-flow-compliant reinforced elements with a minimal increase in process complexity compared to an unreinforced production. However, besides the integration process itself, material-process interactions represent an important research topic. Especially for Shotcrete-3D-Printing, the use of accelerators can significantly change the structural build-up of the applied material and thus effect the bonding ability of the sprayed concrete to the integrated reinforcement element. The present study investigates the effect of accelerator dosage on the bond properties of integrated rebars. The resulting bond is analyzed non-destructively via computer tomography and mechanically by pull-out tests according to RILEM RC6. The results show that the material compaction caused by the sprayed application leads to excellent bond properties. However, when high accelerator dosages are used, bond deteriorations can be observed.

Keywords: Additive Manufacturing in Construction; 3D Concrete Printing; Shotcrete 3D Printing, Interlayer Reinforcement Bars; Pull-out Tests; Micro Level Analysis.

Conference presentation video: https://doi.org/10.5446/56108

Introduction

Additive manufacturing techniques enable a resource-efficient and automated production of components of almost any shape. Using cement-based materials numerous techniques have been developed in recent years for the manufacturing of unreinforced concrete components [1]. To fully exploit the potential of additive manufacturing in construction, the integration of tensile strength materials represents a key challenge. Through the integration of reinforcement, load-induced tensile stresses can be transferred and a ductile failure of load-bearing concrete components can be ensured. However, the interaction between integrated reinforcement structure and concrete matrix can only work, if a good bond between these two materials is achieved. In the traditional formwork-based concrete construction, concrete is

compacted after it has been cast. Vibrating the concrete ensures that it is homogeneously bonded with the reinforcement placed in the formwork.

Looking now at additive manufacturing without formwork, the challenges of reinforcement integration become clear. The compaction of printed concretes does not seem to be a reasonable strategy. Although most concrete mixtures used for additive manufacturing typically have pronounced thixotropic properties [2], the vibration of printed layers would present a risk. The absence of a supporting formwork would result in a deviation of the target component geometry or even in a component failure. After leaving the nozzle, the applied concrete has to show a rapid structural build-up in order to bear its own load due to gravitational forces as well as the load of the layers applied on top of it [3]. Moreover, this must happen in a dimensionally stable manner [4]. A very fast structural build-up, however, counteracts a good flow of the deposited concrete around the reinforcement elements, i.e. a good form fit between concrete and reinforcement and thus a good bond.

Besides material-related challenges, there are also process-related integration challenges. The overall goal is to integrate the reinforcement without reducing geometrical freedom and without restricting the automation of the existing manufacturing methods [5]. In the current research, a number of different approaches for reinforcement integration are investigated. According to Kloft et. al [5], current approaches can be divided into the categories of (a) *concrete supports reinforcement* (CSR), (b) *reinforcement supports concrete* (RSC), and (c) *incremental* (INC), see Figure 1. The CSR category includes the integration of reinforcement bars [6], nails [7], screws [8], meshes [9], cables [10] or fibers into, between or on top of printed concrete layers [11,12]. Here, the concrete matrix acts as a supporting structure. The category RSC bundles reinforcement strategies in which the reinforcement structure is prefabricated before the printing process and thus serves as a supporting structure. Examples include the Mesh Mould process [13], the use of prefabricated reinforcement cages [14,15] or the prefabrication of a fiber winding reinforcement structure [16]. Furthermore, free formed reinforcement structures can also be prefabricated by additive gas metal arc welding, commonly known as wire-and-arc-additive-manufacturing (WAAM). These structures can then be covered by concrete in a subsequent printing process [17,18]. If the WAAM process is carried out simultaneously with the additive concrete printing process [19], it can be classified in the third category "incremental". In addition, a process-parallel joining of reinforcement elements by means of stud welding and the subsequent covering with concrete also represents a possible incremental reinforcement strategy [20].

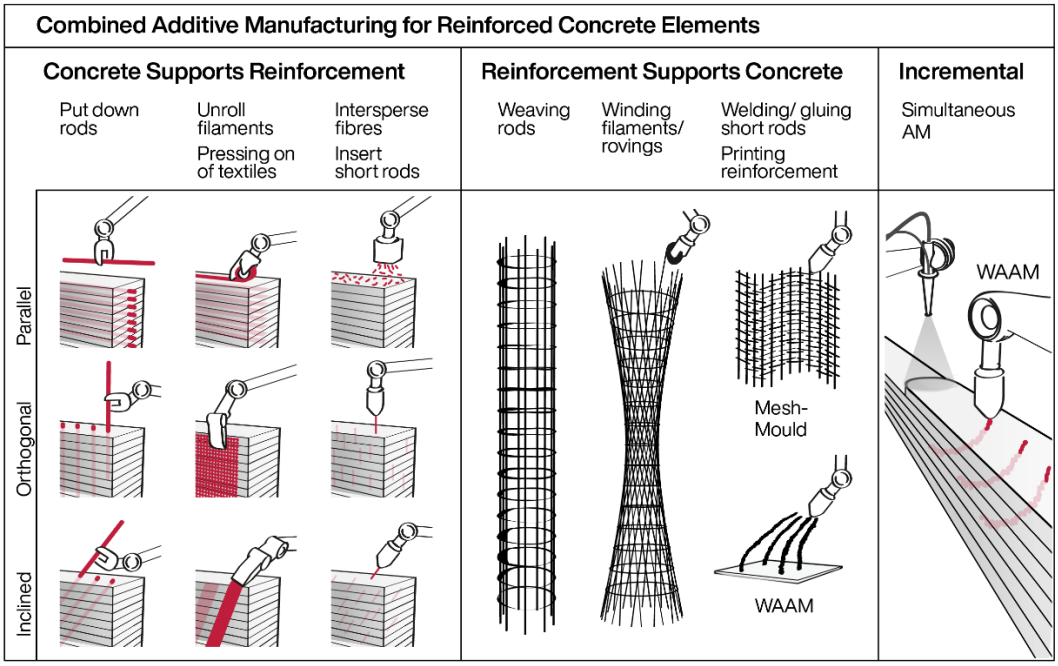

Figure 1. Reinforcement integration methods for a combined additive manufacturing of reinforced concrete elements (from [16]).

The present study addresses the integration method of interlayer reinforcement with reinforcement bars in combination with Shotcrete-3D-Printing (SC3DP). SC3DP is an additive manufacturing process that can be classified to the process sub-class “material jetting” according to [1]. SC3DP uses an additive material application based on a wet-mix shotcrete process [21].

Interlayer reinforcement in additively manufactured concrete components

The integration of reinforcement into the interlayers of the deposited strands represents a process-parallel reinforcement method. This integration method specifically uses the layered characteristic of the additive manufacturing process to place reinforcement elements in a targeted manner along with the layers' orientation. According to [5], the interlayer reinforcement method can be categorized as "concrete supports reinforcement", compare Figure 1. Besides reinforcement bars, flexible meshes, continuous steel fibers or cables could be also used as reinforcement materials [22–25].

By using adaptive path planning strategies, where the layers are not only deposited horizontally but with varying layer orientation and thicknesses due to the variation of nozzle angle and nozzle velocity, interlayer reinforcement can be used to implement force-flow-compliant reinforcement layouts [5], see Figure 2. Here, the reinforcement can be placed in an optimized arrangement along the tensile stress trajectories, while compression stresses are mainly transferred perpendicular to the layer direction. Depending on the reinforcement layout at hand, steel reinforcement bars may have to be pre-bent to match the shape of the substrate layer.

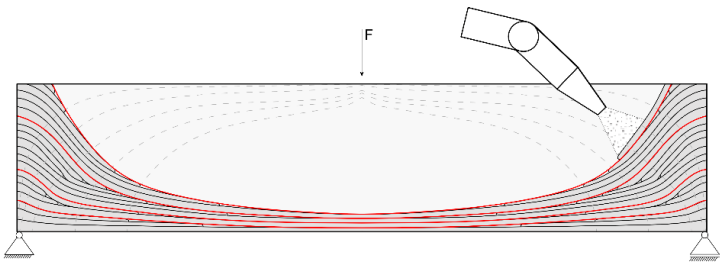

Figure 2. Manufacturing of a beam element with a force-flow-compliant reinforcement layout by using adaptive path planning in combination with interlayer reinforcement (red lines) (from [5]).

Previous studies on interlayer reinforcement in combination with extrusion 3D concrete printing demonstrated that the integration of rebars in the interlayer achieved good bond properties between the integrated bar and the surrounding concrete matrix [22,24]. However, the resulting bond properties can be affected by several material and printing parameters. For SC3DP, this can involve various parameters, such as the volume flow rates of concrete $\dot{v}_{con}$, accelerator $\dot{v}_{acc}$ or air $\dot{v}_{air}$. Furthermore, parameters of the path planning and robotic routing can also have an effect on the resulting bond behavior, e.g. nozzle to strand distance d_{nozzle}, gantry speed v, nozzle angle α_{nozzle} or the time interval Δt between printing the layers. Therefore, it is required to systematically investigate the effect of these parameters in order to know the possibilities and limitations of integrating interlayer reinforcement into SC3DP.

Scope and concept of investigations

The presented investigations focus on the bond quality between concrete and reinforcement bars that were integrated into interlayers simultaneously to the SC3DP-process. It is assumed that both, material properties as well as process parameters affect the bond properties of the manufactured reinforced specimens. Previous investigations have shown that for SC3DP, the use of accelerator has a significant effect on the structural build-up of the applied concrete and thus on the interlayer bond between the layers [26]. It is, therefore, reasonable to expect that there is also an effect on the bonding quality of rebars integrated into the interlayers. In order to systematically study the influencing factors mentioned, two main questions are to be answered:

- Does the use of accelerator affect the bond behavior of reinforcement bars that are integrated into the interlayer between two deposited layers? Therefore, interlayer-reinforced specimens are produced with varying accelerator dosages (SC3DP)
- Does the manufacturing technique itself (conventional mould casting vs. SC3DP) has an effect on the bond behavior of integrated reinforcement bars? Therefore, cast specimens and specimens produced with SC3DP are compared.

Materials and mixture preparation

Within the scope of the presented investigation, a sprayable mortar with a maximum grain size of 2 mm was used (MC Bauchemie-Müller GmbH & Co. KG). For each batch, four 25 kg bags were mixed with water in a compulsory mixer (Mader WM Jetmix 125/180). The mixing time was kept constant at 4 minutes. An overview of the mortar composition is given in Table 1.

Table 1. Mixture composition of SC3DP material.

Component	Value	Unit
Ordinary Portland Cement (CEM I 52.5 R)	500	kg/m³
Pozzolan	160	kg/m³
Silica fume	25	kg/m³
Aggregate; d=0-2 mm	1180	kg/m³
Water	266	kg/m³
Pulverized additives and micro polypropylene fibers	33	kg/m³
Alkali-free set accelerator	0, 2, 4	wt.% bwoc

As a reinforcement material for mechanical testing conventional rolled reinforcement bars with diameters of 12 mm are used (ductile B500B steel according to DIN EN 1992-1). For computer tomography analyses threaded carbon reinforcement bars (material: carbon fiber reinforced polymer) with diameters of 12 mm are additionally integrated.

Specimen preparation and reinforcement integration

Within the scope of this study, specimens were manufactured at the Digital Building Fabrication Laboratory (DBFL) [27,28]. Pullout specimens were fabricated for 0 %, 2 %, and 4 % accelerator dosage using the SC3DP-process. Furthermore, reference specimens were prepared in molds for each accelerator dosage. The geometry and placement of the rebar used in the cast pullout specimens is shown in Figure 3a. The specimens were then stored in a climate-controlled environment at 20 °C and 65 % humidity for 28 days.

For additive manufacturing using the SC3DP method, a 120 cm long base consisting of 3 layers was applied on a specimen plate. Then, four rebars were placed perpendicular to the printing direction, see Figure 3b. Three steel bars were placed for mechanical testing and

one carbon bar for µCT analysis (see section “Testing methods”). All rebars were placed on top of the substrate layer and not pressed into it. Within the SC3DP-process, the mortar was pumped to the nozzle with a concrete pump (Mader WM Variojet FU) through a 25 m long hose (inner diameter: 35 mm). The SC3DP-process was done with a concrete pump discharge rate of 0.8 m³/h, a volume air flow rate of 45 m³/h, a nozzle-to-strand-distance of 20 cm, and a gantry speed of 4.5 m/min. The bonding zone of the integrated steel rebars was limited by a plastic sleeve to 6 cm (equal to 5 times the rebar diameter), see Figure 3b. The position of the bonding zone was located in the center of the printed concrete layer. In order to avoid tilting of the rebar after placement, a height-adjustable support structure was installed on the specimen plate. This support structure was adjusted to the height of the interlayer so that the rebar was supported horizontally after placing, see Figure 3c.

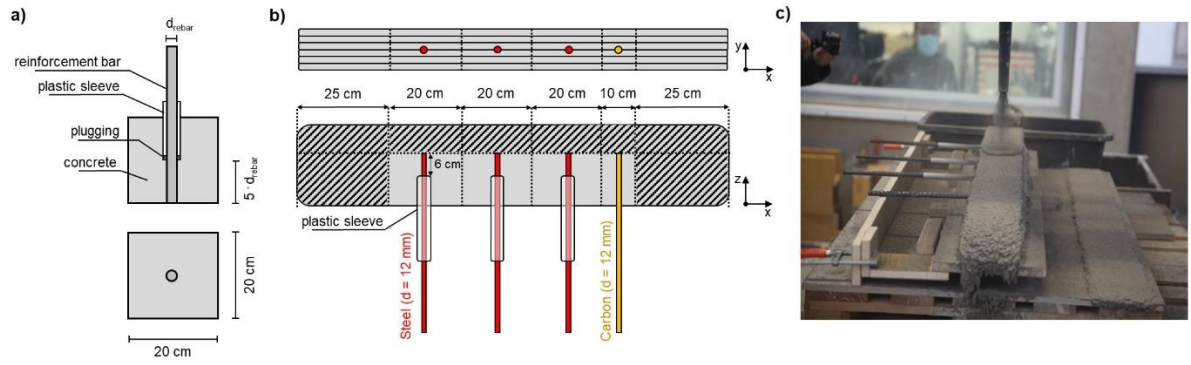

Figure 3. Specimen fabrication; a) Pull-out specimen geometry; b) Visualization of specimen manufacturing using SC3DP; c) Manufacturing process using SC3DP at the DBFL.

All additively manufactured specimens were cut in fresh state with a steel ruler, as visualized in Figure 3b. The SC3DP specimens were then left for 1 day covered with plastic foil in the working space (approx. 20 °C room temperature). In order to provide uniform specimen properties for the mechanical tests (surface for load introduction and specimen geometry), all SC3DP specimens were concreted into cube molds (edge length = 20 cm) one day after fabrication, see Figure 3a. No additional bond was created since the reinforcement bars integrated in the SC3DP process were decoupled by plastic sleeves that extended far out from the specimen, see Figure 3c. For all specimens, the bonding zone was located at the bottom of the cubes, following RILEM RC 6 [29]. The specimens were then stored in a climate-controlled environment at 20 °C and 65 % humidity for further 27 days.

Testing methods

Investigations on fresh concrete properties

In order to quantify the effect of accelerator dosage on the yield stress of the applied fresh concrete, a hand-held shotcrete penetrometer was used, see Figure 4. Measurements were taken in the vicinity of the longitudinal axis of the 25 cm long end pieces of the sprayed specimens, see Figure 3b. The penetration resistance was measured a few seconds after depositing the last layer. For each measurement, ten repetitions are conducted. The penetrometer needle used has a cylindrical height of 12.5 mm, a cone height of 2.5 mm, and a diameter of 3 mm. According to [30] the penetration resistance correlates to the yield stress of the mortar when a sufficiently large needle is used. Thus, the yield stress is calculated according to [30].

Figure 4. Testing of the printed specimen with a shotcrete penetrometer to obtain yield stress information.

Micro Computer Tomography (µCT)

In order to obtain information on the bonding zone of the inserted rebars in a non-disturbed state, µCT-images were taken for each accelerator dosage on specimens with integrated carbon bars (GE phoenix, voltage 160 kV, current: 240 µA, number of images: 1000, filter: 0.1-0.5 mm Cu, voxel size 0.09–0.12 mm). The volumetric image of each specimen is created by using a 3D reconstruction algorithm with the software phoenix datos|x2 (GE Sensing & Inspection Technologies). VG studiomax 2.2 software (Volume Graphics) is used for further analyses on the reconstructions. In addition to visual inspections of the bonding zone, the void content VC around the reinforcement bar is determined. Therefore, a circular region of interest (ROI) with a diameter of 32 mm is defined concentrically around the integrated rebar. Within this ROI, voids are identified using a gray scale value analysis. The identified void volume is then calculated over a length of $5*d_s = 60$ mm. The selected evaluation area was located in the middle of the specimen. The void content VC is defined by the ratio of the absolute void volume V_{voids} to the ROI volume V_{ROI} minus the rebar volume V_{rebar}, see formula 1.

$$VC\ [\%] = \frac{V_{voids}}{V_{ROI} - V_{rebar}} \cdot 100 \quad (1)$$

Mechanical investigations

The bond strength between the integrated rebars and the surrounding concrete was determined 28 days after fabrication by using displacement-controlled pullout tests according to RILEM RC6 [29]. A displacement rate of 0.02 mm/s was used. The mechanical tests were performed on a hydraulic testing machine (Walter + Bai AG). A schematic drawing, as well as a picture of the test setup, is shown in Figure 5.

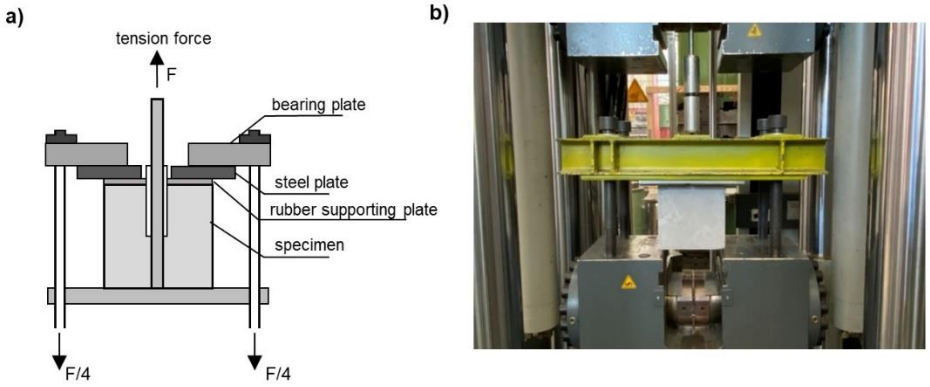

Figure 5. Pullout tests according to RILEM RC 6; a) schematic drawing of the test setup, b) test setup in the testing machine.

Results and discussion

Investigations on fresh concrete properties

By testing the manufactured concrete strands with a shotcrete penetrometer, the effect of accelerator dosage on the yield stress of the deposited concrete could be determined. All values were measured a few seconds after the addition of the accelerator at the nozzle and the subsequent deposition of the layer and thus correspond to both (a) the state of the material on which the rebar was placed and (b) the state of the material that was sprayed onto the inserted rebar. The results for 0 %, 2 %, and 4 % accelerator are shown in Figure 6.

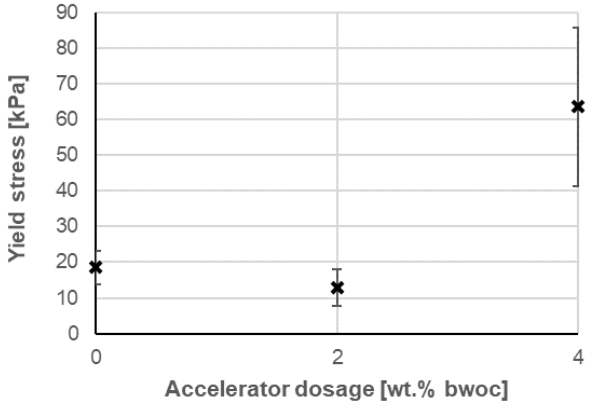

Figure 6. Yield stress values for 0 %, 2 %, and 4 % accelerator dosage measured a few seconds after depositing in the SC3DP process.

For the specimens manufactured with 0 % and 2 % accelerator, the determined yield stress is at a similar level. For 0% accelerator the yield stress was found to be 18.5 kPa (standard deviation: 4.8 kPa) and for 2 % accelerator 12.9 kPa (standard deviation: 5.2 kPa). Even though the values of 0 % and 2 % accelerator are very close to each other, it could be observed during the spraying process that the spray jet of the 2 % accelerator material seemed to be rougher. This could be due to the formation of larger agglomerates taking place already in the nozzle. However, a significantly higher yield stress of 63.6 kPa (standard deviation: 22.3 kPa) was determined for the specimen with 4 % accelerator. With regard to the interlayer reinforcement, it can thus be stated that, especially for a 4 % accelerator dosage, the rebar is placed onto and subsequently covered by a significantly stiffer concrete compared to an unaccelerated system.

Micro Computer Tomography (µCT)

Computer tomography scans are used to obtain an in-depth view of the undisturbed bonding zones for each accelerator dosage. Using grey scale value analysis, the void content (VC) could be determined for each specimen. Thus, VC provides a comparable indication for the evaluation of voids as a function of the used accelerator dosage. The estimated VC is limited to an area of 10 mm around the integrated rebar. Therefore, the focus is on the direct bonding zone close to the rebar. Thus, any further porosities in the bulk matrix are not considered in depth. Table 2 presents the values determined for VC as a function of accelerator dosage.

Table 2. Void content (VC) of reinforced specimens for 0 %, 2 % and 4 % accelerator.

Accelerator dosage	Void content (VC)
0 wt.% bwoc	2.0 vol.%
2 wt.% bwoc	2.1 vol.%
4 wt.% bwoc	4.8 vol.%

For 0 % and 2 % accelerator, VC is in a similar range at about 2 vol.%. However, looking at the specimen manufactured with 4 % accelerator, a significant increase of VC can be observed. At 4.8 vol.% VC is more than twice as high as for 0 % and 2 % accelerator. This pronounced increase from 2 % to 4 % accelerator dosage is in line with the findings of the measured fresh concrete properties, where a significant higher yield stress could be determined for an accelerator dosage of 4 % (compare section “Investigations on fresh concrete properties”). Figure 7, therefore, visualizes the void content as a function of the yield stress of the deposited shotcrete material. It can be seen that the void content tends to increase with increasing yield stress.

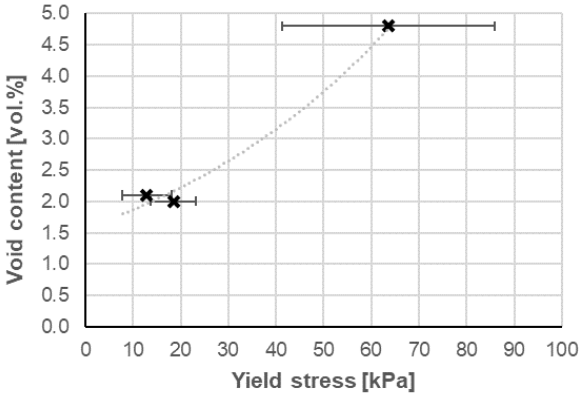

Figure 7. Void content as a function of the yield stress of the deposited shotcrete material.

Due to the rapid reaction between accelerator and cement, the deposited shotcrete material shows an increased yield stress almost instantly after leaving the nozzle. Thus, the increased stiffness of the concrete leads to a larger number of air inclusions when it is applied to the equally stiffer concrete of the previous layer [26,28]. The increased yield stress of the applied material could also lead to the formation of spray shadows below the reinforcement bar since it is more difficult for the material to flow into the shadow space below the cross-section curvature of the rebar.

In order to identify the location of the existing voids, additional visual inspections of the bonding zones were carried out, see Figure 8. Figure 8a shows a comparison of the area between the bottom of the integrated rebar, i.e. which was placed on top of the existing layer, and the rebar ribs on the top, i.e. where the subsequent layer was sprayed on. It becomes apparent that the voids are not evenly distributed around the circumference of the integrated rebar, but are increasingly identified on the bottom side. It can be clearly seen that the top side of the rebar, which was facing the nozzle, has only a few small voids, while the bottom side is characterized by a large number of imperfections. This indicates that the flowability of the sprayed concrete at 4 % accelerator dosage was too low to completely fill the shadow spaces under the rebar. This type of imperfection is also visible in the cross-sectional view in Figure 8b - a large, approx. 3 mm void as well as a small flat void immediately below the rebar.

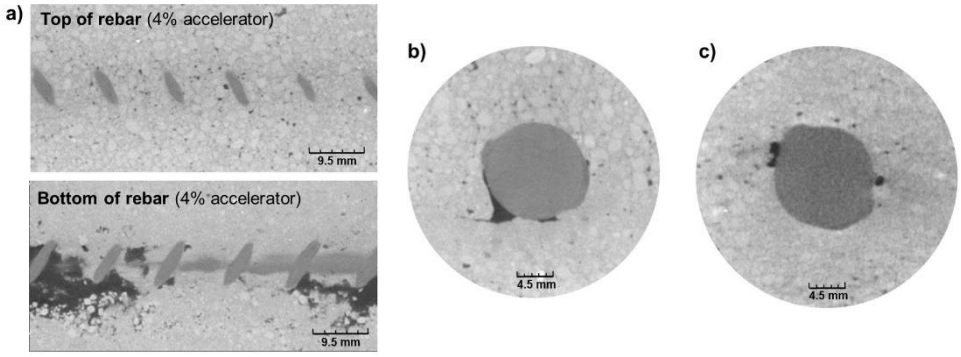

Figure 8. Computer tomography images of a) the top and bottom side of an integrated rebar with 4 % accelerator, b) voids below the integrated rebar (4 % accelerator), c) voids on the side of rebar below and above ribs (2 % accelerator).

In addition to imperfections directly under the reinforcement bars, there are also visible voids on the sides of the rebars, see Figure 8c. These are particularly found below or above ribs. Figure 8c shows this type of defect on an example of an interlayer reinforcement bar manufactured with a 2 % accelerator dosage. This imperfection may be due to a spray shadow or rebound caused by the ribs and thus the resulting inclusion of air.

Mechanical investigations

Based on pull-out tests according to RILEM RC 6, maximum pull-out forces were measured for all integrated steel reinforcement bars. The estimated maximum forces F were converted into a bond strength τ using the existing bond length l = 60 mm and the bar diameter d_{rebar} = 12 mm, see formula (2).

$$\tau = \frac{F}{\pi \cdot d_{rebar} \cdot l} \tag{2}$$

All bond strengths are shown in Figure 9. It can be seen that the additive manufactured specimens consistently show higher bond strengths than the cast specimens (compare dark and light grey columns). This could be due to the fact that the SC3DP process involves a material application with high kinetic energy, which leads to high compaction of the applied concrete.

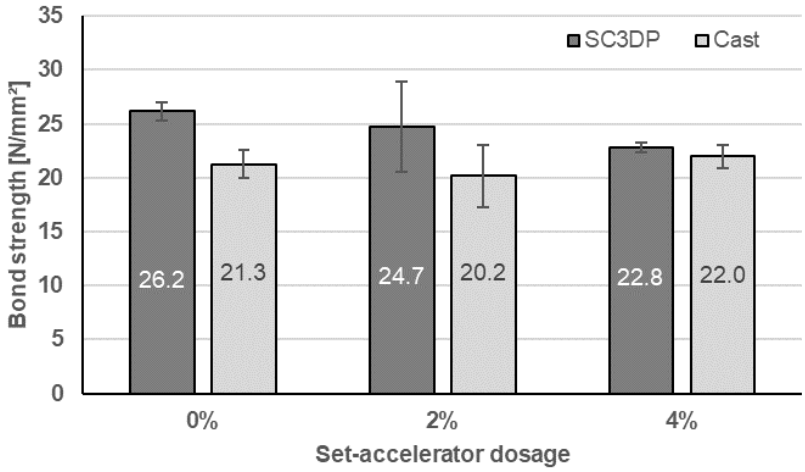

Figure 9. Bond strength of shotcrete 3D printed and conventionally cast reinforced specimens for 0 %, 2 %, and 4 % accelerator.

However, with an increase of the accelerator dosage from 0 % to 4 %, SC3DP specimens show a reduction of the bond strength by 13 % from 26.2 N/mm² to 22.8 N/mm², whereas no significant effect can be seen for the cast specimens. Assuming that all cast specimens have a homogeneous bonding zone between rebar and concrete due to concrete vibration, it can be assumed that the investigated accelerator dosages (0 – 4 wt.% bwoc) do not have a significant effect on the hardened concrete properties after 28 days. This is consistent with findings from the literature [31], where only small reductions in compressive strengths were observed after 28 days due to the use of alkali-free accelerator (even with a higher accelerator dosage).

The reduction in bond strength with increasing accelerator dosage for SC3DP specimens can be related to the previously discussed increase in void content. Figure 10 shows that the decrease in bond strength is tendentially related to an increasing void content. This can be explained by the fact that the increase of voids in the vicinity of the bar leads to a reduction of the bond area between the integrated bar and the surrounding concrete. When the bonding zone is weakened by defects, i.e. voids, the applied forces must consequently be transferred in a concentrated state over the remaining reduced bond area. This results in high local stresses, which lead to an earlier failure and thus to an overall reduced bond strength.

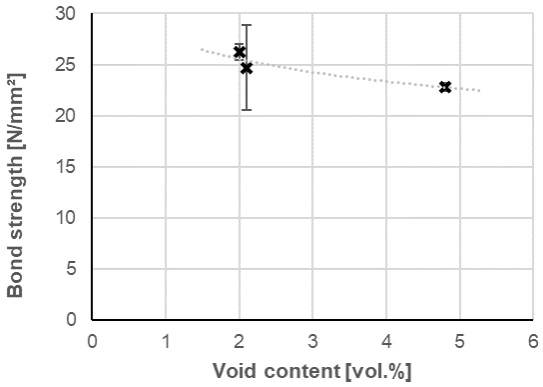

Figure 10. Bond strength as a function of void content in the vicinity of the inserted rebar.

A further explanation for the decrease in bond strength between reinforcement and concrete with increasing accelerator dosage could be a mechanical weakening of the concrete-concrete interface between to layers resulting from the process interruption required for the integration of the rebars. Especially for highly accelerated concrete, even short interruptions between the application of the layers can lead to a weakening of the interlayer bond [26,28]. As the reinforcement is applied exactly in this interlayer, a weakening of the interlayer bond automatically results in a weakening of the reinforcement bond.

Conclusion

Within the framework of this study, the integration of reinforcement bars in the interlayers of concrete strands manufactured by the Shotcrete 3D Printing process was investigated. The purpose of the investigations was to analyze the effect of increasing accelerator dosages on the resulting bond behavior.

Rheological investigations of the deposited fresh concrete using a shotcrete penetrometer showed that the yield stress for an accelerator dosage of 4 % was significantly higher than for 0 % and 2 %. Based on computer tomography analysis of the bonding zones of rebars that were integrated within the SC3DP process, the void content could be determined in the vicinity of the rebar. It could be observed that the void content increases with an increasing yield stress of the applied material. Especially for an accelerator dosage of 4 %, a higher amount of voids could be identified below the inserted rebar. This indicates that the flowabil-

ity of the sprayed concrete was too low at 4 % accelerator dosage to completely fill the shadow spaces under the reinforcement bar. Mechanical investigations using pull-out tests showed, that an increase in accelerator dosage from 0 % to 4 % leads to a reduction in reinforcement bond strength of 13 %. This supports the findings of the bonding zone analysis via µCT. Thus, it can be noted that an increase of void content results in a reduction of bond strength.

In general, this study has shown that the integration of reinforcement into interlayers represents a promising reinforcement method for SC3DP, as it can be easily integrated into the existing printing process and can provide good bond properties between concrete and reinforcement bars. By using accelerator dosages of up to 2 %, homogeneous bonding zones could be obtained. Regardless of the accelerator dosage, excellent bond strengths were achieved by the SC3DP process, even higher values than for conventionally cast concrete specimens. This phenomenon is attributed to the high compaction of the concrete in the SC3DP process, as the material is applied with high kinetic energy.

Data availability statement

The data that support the findings of this study were generated at the Institute of Building Materials, Concrete Construction and Fire Safety (iBMB), Division of Building Materials, TU Braunschweig (Germany) and are available on request from baustoffe@ibmb.tu-bs.de .

Author contributions

Conceptualization, N.F., D.L.; methodology, N.F., D.L.; validation, N.F.; formal analysis, N.F.; investigation, N.F.; resources, N.F., D. L.; data curation, N.F.; writing - original draft preparation, N.F.; writing - review and editing, N.F., D.L.; visualization, N.F.; supervision, D.L.; project administration, N.F, D.L.; funding acquisition, D.L. All authors have read and agreed to the published version of the manuscript.

Competing interests

The authors declare no competing interests.

Funding

Funded by the Deutsche Forschungsgemeinschaft (DFG, German Research Foundation) – TRR 277/1 2020 – Project number 414265976. The authors thank the DFG for the support within the CRC/ Transregio 277 - Additive Manufacturing Construction. (Project A04).

References

1. Buswell, R.A.; da Silva, W.L.; Bos, F.P.; Schipper, H.R.; Lowke, D.; Hack, N.; Kloft, H.; Mechtcherine, V.; Wangler, T.; Roussel, N. A process classification framework for defining and describing Digital Fabrication with Concrete. *Cement and Concrete Research* 2020, *134.* https://doi.org/10.1016/j.cemconres.2020.106068
2. Wangler, T.; Lloret, E.; Reiter, L.; Hack, N.; Gramazio, F.; Kohler, M.; Bernhard, M.; Dillenburger, B.; Buchli, J.; Roussel, N.*; et al.* Digital Concrete: Opportunities and Challenges. *RILEM Tech Lett* 2016, *1*, 67. https://doi.org/10.21809/rilemtechlett.2016.16
3. Reiter, L.; Wangler, T.; Roussel, N.; Flatt, R.J. The role of early age structural build-up in digital fabrication with concrete. *Cement and Concrete Research* 2018, *112*, 86–95. https://doi.org/10.1016/j.cemconres.2018.05.011

4. Buswell, R.; Kinnell, P.; Xu, J.; Hack, N.; Kloft, H.; Maboudi, M.; Gerke, M.; Massin, P.; Grasser, G.; Wolfs, R.*; et al.* Inspection Methods for 3D Concrete Printing. In *Second RILEM International Conference on Concrete and Digital Fabrication*; Bos, F.P., Lucas, S.S., Wolfs, R.J.M., Salet, T.A.M., Eds.: Springer International Publishing: Cham, 2020, pp. 790–803. https://doi.org/10.1007/978-3-030-49916-7_78
5. Kloft, H.; Empelmann, M.; Hack, N.; Herrmann, E.; Lowke, D. Reinforcement strategies for 3D-concrete-printing. *Civil Engineering Design* 2020, *2*, 131–139. https://doi.org/10.1002/cend.202000022
6. Freund, N.; Dressler, I.; Lowke, D. Studying the Bond Properties of Vertical Integrated Short Reinforcement in the Shotcrete 3D Printing Process. In *Second RILEM International Conference on Concrete and Digital Fabrication*; Bos, F.P., Lucas, S.S., Wolfs, R.J.M., Salet, T.A.M., Eds.: Springer International Publishing: Cham, 2020, pp. 612–621. https://doi.org/10.1007/978-3-030-49916-7_62.
7. Perrot, A.; Jacquet, Y.; Rangeard, D.; Courteille, E.; Sonebi, M. Nailing of Layers: A Promising Way to Reinforce Concrete 3D Printing Structures. *Materials (Basel, Switzerland)* 2020, *13*. https://doi.org/10.3390/ma13071518
8. Lucas, L.; Bos, F. Bending and Pull-Out Tests on a Novel Screw Type Reinforcement for Extrusion-Based 3D Printed Concrete. In *Second RILEM International Conference on Concrete and Digital Fabrication*; Bos, F.P., Lucas, S.S., Wolfs, R.J.M., Salet, T.A.M., Eds.: Springer International Publishing: Cham, 2020, pp. 632–645. https://doi.org/10.1007/978-3-030-49916-7_64
9. Marchment, T.; Sanjayan, J. Mesh reinforcing method for 3D Concrete Printing. *Automation in Construction* 2020, *109*. https://doi.org/10.1016/j.autcon.2019.102992
10. Bos, F.P.; Ahmed, Z.Y.; Jutinov, E.R.; Salet, T.A.M. Experimental Exploration of Metal Cable as Reinforcement in 3D Printed Concrete. *Materials (Basel, Switzerland)* 2017, *10.* https://doi.org/10.3390/ma10111314
11. Bos, F.P.; Bosco, E.; Salet, T.A.M. Ductility of 3D printed concrete reinforced with short straight steel fibers. *Virtual and Physical Prototyping* 2019, *14*, 160–174. https://doi.org/10.1080/17452759.2018.1548069
12. Ma, G.; Li, Z.; Wang, L.; Wang, F.; Sanjayan, J. Mechanical anisotropy of aligned fiber reinforced composite for extrusion-based 3D printing. *Construction and Building Materials* 2019, *202*, 770–783. https://doi.org/10.1016/j.conbuildmat.2019.01.008
13. Hack, N.; Lauer, W.V.; Gramazio, F.; Kohler, M. Mesh Mould: Robotically Fabricated Metal Meshes as Concrete Formwork and Reinforcement. *In Proceedings of the 11th International Symposium on Ferrocement and 3rd ICTRC International Conference on Textile Reinforced Concrete* 2015.
14. Kloft, H.; Hack, N.; Mainka, J.; Brohmann, L.; Herrmann, E.; Ledderose, L.; Lowke, D. Additive Fertigung im Bauwesen: erste 3-D-gedruckte und bewehrte Betonbauteile im Shotcrete-3-D-Printing-Verfahren (SC3DP). *Bautechnik (96)* 2019, 929–938. https://doi.org/10.1002/bate.201900094
15. Kloft, H.; Empelmann, M.; Oettel, V.; Ledderose, L. 3D Concrete Printing – Production of first 3D Printed Concrete Columns and Reinforced Concrete Columns. *BFT International, no. 6* 2020, 28–37.
16. Hack, N.; Bahar, M.; Hühne, C.; Lopez, W.; Gantner, S.; Khader, N.; Rothe, T. Development of a Robot-Based Multi-Directional Dynamic Fiber Winding Process for Additive Manufacturing Using Shotcrete 3D Printing. *Fibers* 2021, *9*, 39. https://doi.org/10.3390/fib9060039
17. Mechtcherine, V.; Grafe, J.; Nerella, V.N.; Spaniol, E.; Hertel, M. 3D-printed steel reinforcement for digital concrete construction - Manufacture, mechanical properties and bond behaviour. *Construction and Building Materials* 2018, 125–137. https://doi.org/10.1016/j.conbuildmat.2018.05.202
18. Müller, J.; Grabowski, M.; Müller, C.; Hensel, J.; Unglaub, J.; Thiele, K.; Kloft, H.; Dilger, K. Design and Parameter Identification of Wire and Arc Additively Manufactured (WAAM) Steel Bars for Use in Construction. *Metals* 2019, *9*, 725. https://doi.org/10.3390/met9070725

19. Weger, D.; Baier, D.; Straßer, A.; Prottung, S.; Kränkel, T.; Bachmann, A.; Gehlen, C.; Zäh, M. Reinforced Particle-Bed Printing by Combination of the Selective Paste Intrusion Method with Wire and Arc Additive Manufacturing – A First Feasibility Study. In *Second RILEM International Conference on Concrete and Digital Fabrication*; Bos, F.P., Lucas, S.S., Wolfs, R.J.M., Salet, T.A.M., Eds.: Springer International Publishing: Cham, 2020, pp. 978–987. https://doi.org/10.1007/978-3-030-49916-7_95
20. Classen, M.; Ungermann, J.; Sharma, R. Additive Manufacturing of Reinforced Concrete—Development of a 3D Printing Technology for Cementitious Composites with Metallic Reinforcement. Applied Sciences 2020, 10. https://doi.org/10.3390/app10113791
21. Kloft, H.; Hack, N.; Lindemann, H.; Mainka, J. Shotcrete 3D Printing (SC3DP) - 3D-Drucken von großformatigen Betonbauteilen. *Deutsche Bauzeitschrift* 2019, 54 - 57.
22. Baz, B.; Aouad, G.; Leblond, P.; Al-Mansouri, O.; D'hondt, M.; Remond, S. Mechanical assessment of concrete – Steel bonding in 3D printed elements. *Construction and Building Materials* 2020, *256.* https://doi.org/10.1016/j.conbuildmat.2020.119457
23. Mechtcherine, V.; Nerella, V.N. Integration der Bewehrung beim 3D-Druck mit Beton. *Beton- und Stahlbetonbau* 2018, *113*, 496–504. https://doi.org/10.1002/best.201800003
24. Matthäus, C.; Kofler, N.; Kränkel, T.; Weger, D.; Gehlen, C. Interlayer Reinforcement Combined with Fiber Reinforcement for Extruded Lightweight Mortar Elements. *Materials (Basel, Switzerland)* 2020, *13.* https://doi.org/10.3390/ma13214778
25. Gebhard, L.; Mata-Falcón, J.; Markić, T.; Kaufmann, W. Aligned Interlayer Fibre Reinforcement for Digital Fabrication with Concrete. In *Fibre Reinforced Concrete: Improvements and Innovations*; Serna, P., Llano-Torre, A., Martí-Vargas, J.R., Navarro-Gregori, J., Eds.: Springer International Publishing: Cham, 2021, pp. 87–98. https://doi.org/10.1007/978-3-030-58482-5_8
26. Dreßler, I.; Freund, N.; Lowke, D. The Effect of Accelerator Dosage on Fresh Concrete Properties and on Interlayer Strength in Shotcrete 3D Printing. *Materials,* Special *Issue "Concrete 3D Printing and Digitally-Aided Fabrication"* 2020. https://doi.org/10.3390/ma13020374
27. Neudecker, S.; Bruns, C.; Gerbers, R.; Heyn, J.; Dietrich, F.; Dröder, K.; Raatz, A.; Kloft, H. A New Robotic Spray Technology for Generative Manufacturing of Complex Concrete Structures Without Formwork. *Procedia CIRP* 2016, *43*, 333–338. https://doi.org/10.1016/j.procir.2016.02.107
28. Kloft, H.; Krauss, H.-W.; Hack, N.; Herrmann, E.; Neudecker, S.; Varady, P.A.; Lowke, D. Influence of process parameters on the interlayer bond strength of concrete elements additive manufactured by Shotcrete 3D Printing (SC3DP). *Cement and Concrete Research* 2020, *134*, 106078. https://doi.org/10.1016/j.cemconres.2020.106078
29. RILEM RC6. *Bond test for reinforcement steel*: *2. Pull-out test*, 1983.
30. Lootens, D.; Jousset, P.; Martinie, L.; Roussel, N.; Flatt, R.J. Yield stress during setting of cement pastes from penetration tests. *Cement and Concrete Research* 2009, *39*, 401–408. https://doi.org/10.1016/j.cemconres.2009.01.012
31. Paglia, C.; Wombacher, F.; Böhni, H. Influence of alkali-free and alkaline shotcrete accelerators within cement systems: hydration, microstructure, and strength development. *ACI Materials Journal 101 (5)* 2004, 353–357.

Vision and Strategies for Reinforcing Additively Manufactured Concrete Structures

Visions

https://doi.org/10.52825/ocp.v1i.83

Submitted: 24 Jan. 2022 | Published: 15 Feb. 2022

Optimizing Reinforcement

Structural Analysis, Challenges and Strategies

Adam Orlinski[1], Klaas De Rycke[2,3], and Moritz Heimrath[1]

[1] University of Applied Arts Vienna, Austria

[2] ENSAV - École nationale supérieure d'architecture de Versailles, France

[3] Bartlett School of Architecture - UCL, London

Abstract. The combination of parametric modelling with structural analysis prompted new synergies between designing and engineering. The connection of structural calculation models such as *Karamba3d* [1] to algorithmic modelling platforms such as *Grasshopper3d* allowed to embed tools for analysis and simulation into the environment of creative design processes.

This way structural analysis advanced from its single sided calculation “duty” towards participation in design language of articulated structural expression.

3d-concrete-printing serves as a great new territory to apply the potential of real-time parametric structural analysis in the built environment of rapid prototyping and robotic fabrication. While 3d-printed-concrete rapidly advanced in technology and empiric know-how, so also grew the ambition to utilize them for larger purposes and bigger building projects.

Known requirements such as structural integrity according to building code, interfaces for construction or waterproofing pose clear challenges for further realizations.

In order to develop 3d-concrete-printing to its full potential all challenges must serve as opportunities to dissect and rethink established norms and practices, and to construct a new interdisciplinary rule book for an emerging building technology. In this field working through challenges via prototypes serve as great basis for development and allows for an applied discourse within the wider community.

Furthermore to address challenges a flexible toolbox for structural analysis such as *Karamba3d* [1] offers the potential to serve as an open instrument for structural analysis and to promote 3d-concrete-printing within that interdisciplinary effort to its next level. On the one hand the tool enables to suggest customized and optimized rebar layouts which could support the development of 3D-concrete-printing further. By enabling this more customizable calculation and tailored real time feedback for complex structures, solutions can develop more structurally informed. On the other hand, recent developments with Karamba3D within our office of Bollinger+Grohmann have shown the possibility of real time feedback loops between the physical printing process and the digital calculation model.

Both developments show the potential that material systems can be optimized towards specific patterns or values of forces, or structures can be evaluated in real time for their load bearing capacity while hardening during printing.

Keywords: Optimization, Parametric Engineering, Force-Flow, 3d-Concrete-Printing

Conference presentation video: https://doi.org/10.5446/1766

Competing interests

The author declares no competing interests.

References

1. Preisinger, C. (2013), Linking Structure and Parametric Geometry. Architectural Design, 83: 110-113 DOI: https://doi.org/10.1002/ad.1564.

Visions and Strategies for Reinforcing Additively Manufactured Concrete Structures

Visions

https://doi.org/10.52825/ocp.v1i.79

Submitted: 4 Oct. 2021 | Accepted: 15 Dec. 2021 | Published: 15 Feb. 2022

Magnetic Alignment of Microsteel Fibers as Strategy for Reinforcing UHPFRC

Lukas Ledderose[1], Abtin Baghdadi[1], and Harald Kloft[1]

[1] Technische Universität Braunschweig, Institute of Stuctural Design (ITE)

Abstract. The objective of this paper is to provide an insight into current basic research at ITE for the production of resource-efficient components through the controlled, automated magnetic distribution and alignment of steel fibers in UHPFRC (Ultra-High Performance Fibre-Reinforced Concrete). The method for distributing and aligning steel fibers in UHPFRC is based on the physical phenomenon of magnetism. Since steel fibers are ferromagnetic, magnetic fields can selectively change their position in the fresh concrete and align them according to the force flow and the maxim "form follows force". The magnetic fiber alignment (MFA) process developed on this principle combines the capabilities of digital and automized component manufacturing with the potential of targeted fiber alignment to increase the material efficiency of UHPFRC. It is highlighted at four levels:

At the material level, studies were conducted on the composite properties of different brand-new and recycled microsteel fibers (MSF), formwork designs suitable for the MFA process were developed, flux densities of different magnets were simulated with special software solutions and measured in practice, and an end effector was fabricated that was implemented on 3- and 6-axis kinematics. At the process level, the interaction of the main parameters of the MFA process was evaluated by visual analysis on transparent glucose syrup-based solutions, and series of specimens were analyzed by micro-CT scans. At the component level, centric tensile tests were performed on a wide variation of dog-bones to provide an assessment of the potential increase in tensile performance of UHPFRC by the MFA process. At an economic and environmental evaluation level, the results from the tensile tests were used to assess and quantify the potential savings from reducing the fiber content and using recycled steel fibers.

Keywords: UHPFRC, magnetic fiber alignment, sustainability

Conference presentation video: https://doi.org/10.5446/56111

Introduction

Lightweight and thin concrete components made of UHPFRC require tight manufacturing tolerances and high material efficiency due to their low wall thickness and filigree nature. This can be achieved in terms of the material quality of the concrete matrix and the fiber content. In terms of fiber distribution and orientation, the precision and efficiency is missing: In expectation of a uniform distribution of fiber contents in the component, the microsteel fibers (MSF) are added to the matrix during the mixing process and poured into the forms as a complete mixture. To ensure a certain concentration of effective fibers in UHPFRC components, the overall quantity of all fibers is increased, with the consequence of poorer workability of the fresh concrete. Thus, a considerable amount of microsteel fibers that are not effective for bearing capacity are used inefficiently. In the course of the development of UHPFRC, MSF with a tensile strength of at least 2000 MPa in particular have proven to be effective due

to their strong bond with the concrete matrix [1].

The goal of the research described is to provide the foundation for the production of resource-efficient components using controlled, automated magnetic distribution and alignment of MSF in UHPFRC. In principle, three strategies for a more sustainable use of MSF can be pursued with the MFA process. First, starting from a given fiber content, an increase in ultimate load can be achieved by transferring the individual fibers into a more efficient position and orientation. Second, while maintaining a desired material strength, the fiber content can be reduced through targeted orientation. Third, the higher strengths of the fiber-matrix system achieved by the MFA process provide the opportunity for a leaner design of UHPFRC components and thus for a reduction in matrix and deadweight. Which of these three goals should be pursued by the MFA process must be decided on a case-by-case basis.

Extensive research on the magnetic alignment of MSF has been conducted at ITE over the past decade. For example, UHPFRC components have already been developed in projects of the DFG Priority Program 1542 "Concrete Light" [2], which were treated with the MFA process in first probing tests [3]. In addition, studies and experiments on the topic of magnetic fiber alignment in UHPFRC have been continuously conducted at ITE since 2014. These investigations addressed key aspects of this research project and provided concrete indications on the potentials of automized magnetic alignment and distribution of MSF. In particular, the influence of different magnetic fields on the alignment and movement of MSF was investigated experimentally in small test specimens. For this purpose, different gels were used in addition to the UHPC matrix, which, as transparent concrete substitutes, allowed direct observation of the effects. Other published preliminary investigations dealt with the automation of more complex reinforcement structures [4, 5]. For example, robotic path-based modeling of intersecting fiber strands was investigated as they could be reasonably arranged in the tension zone of biaxially flexurally stressed slabs [6].

Materials and applications

Matrix

The process of magnetic alignment of MFA in UHPFRC places specific requirements on the matrix, particularly with regard to its composition and workability. As in previous investigations [7], a fine-grained concrete based on the ready-mix NANODUR® Compound 5941 gray developed by Dyckerhoff was used in these component tests (Tab. 1). The used formulation showed a high reproducibility of the rheological properties of the fresh concrete and the mechanical properties of the hardened UHPC (Tab. 2).

Table 1. Mix design of used UHPC

Ingredient	**Weight [kg/m³]**
NANODUR® Compound 5941, grey	1100
Quartz sand H33	1012
Superplasticizer (GRACE ADVA® Flow 375)	21
Shrinkage reducer (GRACE Eclipse® Floor)	7
Water	159

Table 2. Material properties of used UHPC

Characteristic	Mean value
cube compressive strength (l = 100 mm)	120 MPa
Uniaxial tensile strength (min.)	3 MPa
Modulus of elasticity	45 GPa

Microsteel fibers (MSF)

MSF are particularly tightly bound into the very dense, strong and homogeneous structure of the fine-grained UHPC matrix. This allows high bond stresses to be transferred. In addition, the ductilizing effect of the fibers is based on the fact that in the case of cracks in the matrix, the bond friction between the matrix and the fibers is overcome without the fibers themselves cracking [8].

MSF of different lengths (4, 6, 8 and 11 mm) and different diameters (0.13 and 0.17 mm) and a fiber mix (MSF Mix) consisting of the fiber types MSF 4, 6 and 8 in equal weight proportions were analyzed and examined in experimental component tests for their suitability for the MFA process. All MSF were manufactured in accordance with DIN EN 10025-2 [9] as a hot-rolled product from mild steels in wet drawing processes and are certified in accordance with DIN EN 14889-1 [10]. They were brass coated for increased corrosion resistance. Due to the high impermeability of the UHPC structure, however, the near-surface corrosion of the fibers has no adverse effect on the durability of the components anyway [11].

The manufacturing process accounts for the very high tensile strength. Own investigations of the maximum tensile strength at fiber break resulted in values of 3400 MPa for fibers of diameter 0.13 mm and over 3900 MPa for fibers of diameter 0.17 mm. This high tensile strength compared to rebars (340 to 540 MPa) results from work hardening, which takes place during cold forming in the wire drawing process, accompanied by a simultaneous decrease in toughness.

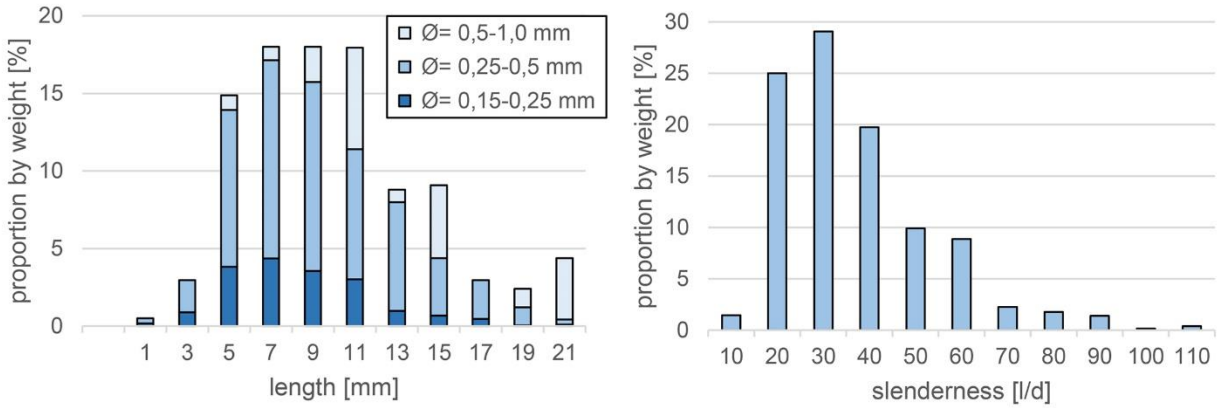

Figure 1. Distribution of lenghts and diameters (fiber type Rec) (left);

Distribution of slenderness (fiber type Rec) (right)

In addition, recycled fibers (fiber type Rec) were also investigated and used. The possible application as concrete reinforcement of this so-called srap-tire steel has already been investigated in some approaches [12, 13]. The fibers used here were provided by Genan, a company specialized in recycling scrap tires [14]. These uncertified fibers were inconsistent in geometry, some had adhesions of rubber, and most were not brass coated. Their tensile strengths were determined in own tensile tests and were 3800 MPa on average.

To determine the distribution of their geometrical properties such as length, diameter, slenderness and straightness, a sample weighing 10 grams and consisting of about 2500 individual fibers was examined. Figure 1 (left) shows the distribution of lengths and diameters, Figure 1 (right) the distribution of fiber slenderness.

Table 3 shows comparatively the most important geometrical properties of all fiber types. Three correlations between fiber geometry and fiber number should be pointed out here, each related to the same sample weight:

- As can be seen in the comparison between the fiber types MSF 4,6 and 8, the fiber slenderness, i.e. the ratio of fiber length to fiber diameter, increases for the same diameter but rising fiber length. At the same time, the number of individual fibers is reduced.
- The fiber type Rec shows a comparatively low number of individual fibers and a small total surface area due to its on average quite short and thick fibers.
- Compared with the 0.17 mm thick MSF 11, the 0.13 mm thick MSF 8 shows, despite comparable slenderness, a more than 2.3-fold higher number of individual fibers and a total surface area (contact area with the matrix) that is about one third larger.

Table 3. Comparison of the geometric properties of MSF

fiber type	fiber length l [mm]	diameter d [mm]	Slenderness (l/d)	count per g [pcs.]	surface per g [cm²]
MSF 4	4	0,13	30,1	2400	39,2
MSF 6	6	0,13	46,2	1600	39,2
MSF 8	8	0,13	61,5	1200	39,2
MSF Mix	5,3 (Ø)	0,13	42,5 (Ø)	1734	39,2
MSF 11	11	0,17	64,7	510	30,0
Rec	6,3 (Ø)	0,32 (Ø)	36,9 (Ø)	257	15,0

Two different fiber types were selected for the centric tensile tests shown below: First, MSF 8, which had proven to be the best performing fiber type within the group of MSF mentioned above. Its advantages, resulting from the high number of slender individual fibers with a large total surface area in relation to the sample weight, was also proven in bending tensile tests. Secondly, the fiber type Rec, which is geometrically inferior to MSF 8 but impresses with its economic and ecological benefits.

Magnets

The selection of the magnets was essentially based on two methods: The analysis of different magnetic fields using a FEMM software solution (Finite Element Method Magnetics, [15]) and the real measurements on selected single magnets and magnet combinations.

With the aid of the FEMM simulations, it was possible to visualize and evaluate the complex magnetic field geometry of both individual permanent magnets and their combinations as well as electromagnets. Although the simulations could be used for the specific selection of suitable magnets, the real magnetic flux densities had to be validated due to inaccuracies resulting from the simplified simulation in two-dimensional space. Thus, measurements in 2-millimeter steps up to 30 mm at and between the magnet poles were performed with a calibrated magnetometer. The exclusively used sintered NdFeB - magnets (neodymium-iron-boron) are currently the strongest permanent magnets [16]. They are characterized in particular by a very high energy density in relation to their volume and are classified according to their maximum energy product, which refers to the powers of the magnetic flux per unit volume (N 35 to N 52).

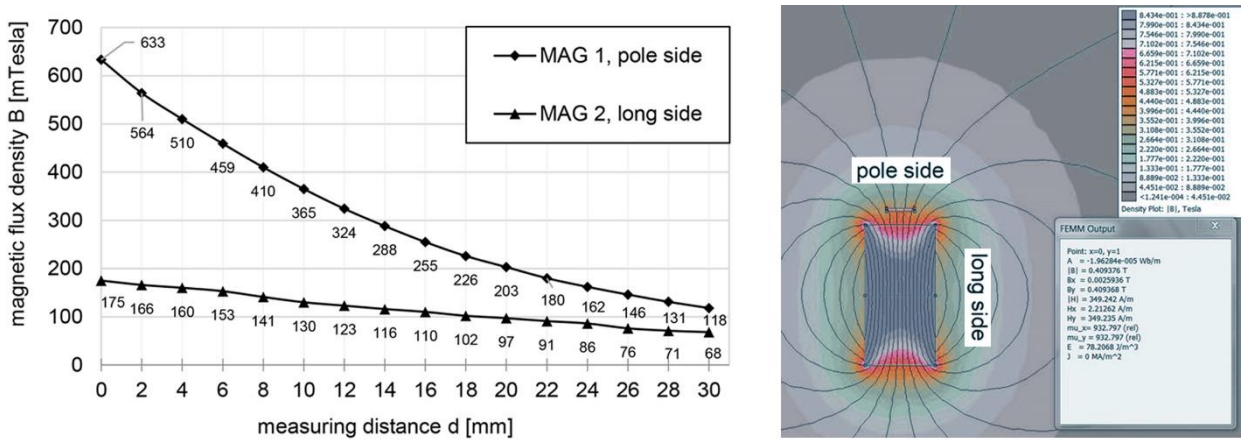

Figure 2. Flux density of MAG 1 and MAG 2 (left); Magnetic field lines of MAG 1 (right)

Figure 2 (left) shows the rapid decrease of the magnetic flux density with increasing distance to the magnet surfaces at the example of the two NdFeB magnets MAG 1 and MAG 2 used here. Figure 2 (right) illustrates the lower flux density between the poles (long side) and the elongated course of the field lines here. In contrast, the flux density is highest directly at the poles, while the field lines are more curved.

End effectors

Various magnets were applied in the research project, which were attached to individual holders (end effectors) on different robot models and CNC systems. Figure 3 shows the end effector used here. It basically consisted of a spring-mounted structure made of aluminum and 3D-printed plastic parts. The stiff parallelogram mechanism of the suspension allowed a defined contact pressure of the magnets, which was controlled by hydraulic shock absorbers. It was capable of alternating two different magnets and corresponding magnetic field geometry. A pneumatically initiated swiveling movement was triggered by a command stored in the machine code, thus enabling the use of two magnets without a conventional tool change. One of the two magnets was attached to a DC motor, which provided continuous and controllable rotation of the MAG 2 about its longitudinal axis when required. For the experiments shown here, the end effector was equipped with the MAG 1 and MAG 2 magnets; the rotation function was not used for the purely linear movements carried out here.

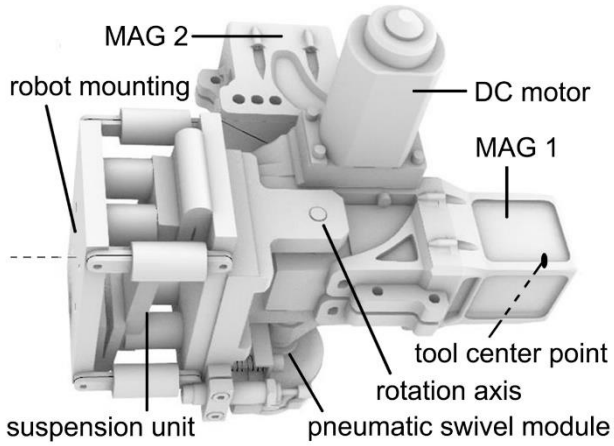

Figure 3. Visualization of the end effector with integrated magnet changer

Experiments

Efficiency increase of the fiber content

Decisive for the efficiency of the individual MSF in the UHPFRC matrix are the fiber geometry, the bond behavior and the local distribution and orientation [17, 18]. In particular, only that fiber portion is relevant for the transmission of tensile forces that is located in a component parallel or in a moderate deviation to the direction of the occurring tensile stresses. Also, only those locations are of importance where tensile stresses actually occur [19]. Thus, in a component with random distribution of fibers, not even half of the fibers used are relevant for the transmission of tensile forces. They are the only fibers that lead to the required load-transmitting crack bridging in the cracked state of the component, as well as to the resulting failure indication and possible increase in post-crack load-bearing capacity [20]. In contrast, fibers are not effective for the transmission of compressive forces, and the fiber content that is oriented approximately in parallel to the compressive forces occurring in a component remains ineffective [21].

Figure 4 (left) shows the probability of a randomly oriented single fiber deviating from a tensile trajectory. For a small deviation of 0-15° it is only 3.4%. In the range of moderate deviations it is 10.0% (15-30°) and 15.9% (30-45°). On the one hand, this geometric correlation between fiber orientation and fiber effectiveness illustrates the large unused fiber content of about 70%, which can be omitted in components with clear tensile load directions. However, it also shows the narrow spectrum that must be maintained for a directed fiber alignment. Figure 4 (right) clearly shows the difference between a magnetically aligned fiber strand and a random fiber alignment in relation to a defined tensile direction. While the probability distribution of the fiber alignment parallel to the main tensile direction (= 0°) strongly decreases in the case of a random fiber alignment (blue dashed line), the predominant fiber portion of a magnetically treated specimen lies in the range of 0 - 45° (red line), which is relevant for the transmission of tensile forces. In addition, the random, average fiber orientation without reference to a main tensile direction is also shown (black dotted line).

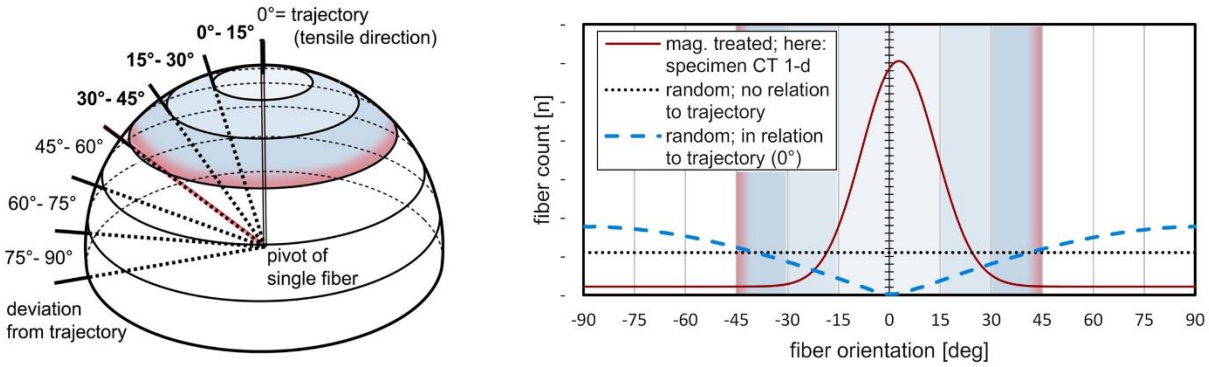

Figure 4. Deviation of fiber orientation from the trajectory (left);

Distribution of fiber orientation relative to the trajectory (right)

Bond behavior

The design principle of fiber-reinforced concrete differs fundamentally from the fiber-based design principles of nature and the construction methods derived from it, such as fiber-reinforced plastics. While the tensile strengths of these structures are largely based on long, thin fibers oriented in the direction of tension, the composite behavior between fibers and matrix plays a crucial role in short-fiber composites such as UHPFRC. There are two reasons for reinforcing concretes with short fibers. On the one hand, the mixing process of fiber-

reinforced concretes requires a certain dimensional stability of short fibers and their uniform distribution in the matrix; on the other hand, they are mainly required for ductile material behavior, which is achieved by pulling them out of the cracked matrix rather than by tearing them apart. Here, the bond behavior in interaction with the fiber properties as well as the pull-out direction of the fibers is decisive [22, 23].

In the case of straight fiber pull-out, micro-interlocking and adhesion provide the largest contributions to the maximum transmittable fiber tensile forces, friction plays a minor role. Due to fiber deformation at the deflection point, even higher tensile forces can usually be transmitted by the fiber in the case of an angled fiber pull-out. However, the formation of breakout cones at larger angles can affect the deformation capacity of the UHPFRC and lead to a more brittle mode of failure [24]. To gain deeper insight into the composite behavior of the fiber-matrix combination used here, pull-out tests were performed on straight and angled fibers.

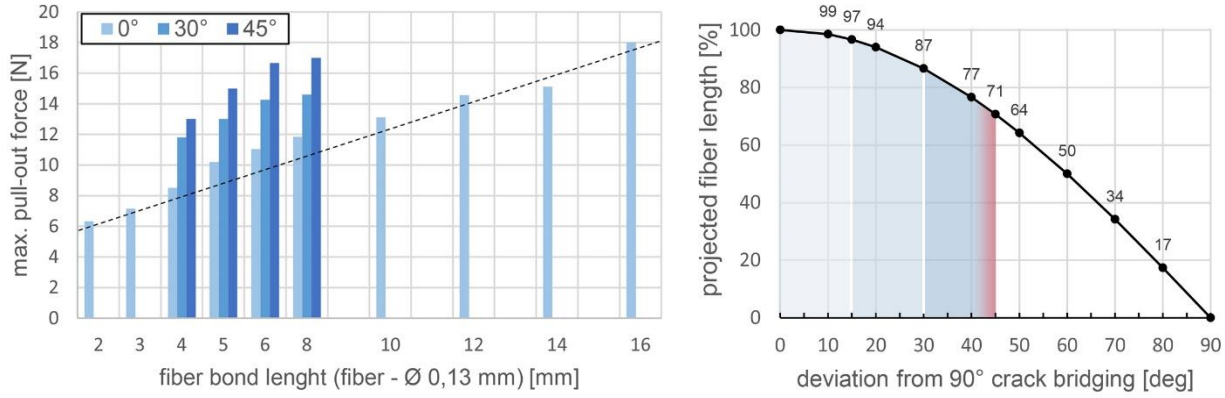

Figure 5. Results of pull-out test of individual fibers (left);

Fiber orientation and probability of crack bridging (right)

Figure 5 (left) shows the maximum pull-out forces in relation to the bond length as well as the angle of fiber pull-out. The fiber pullout forces at 30° and 45° angles and a bond length of 4 mm increased by 38% and 52%, with increasing damage to the matrix at the pullout location.

However, as shown in Figure 5 (right), increasing deviation of the fiber orientation parallel to the main tensile direction is coupled with a shortening of the projected fiber length and a decrease in the probability of crack bridging. The ratio of the projected length to the bond length is called the fiber orientation coefficient η. While the projected fiber length is hardly reduced at moderate deviations from the main tensile direction, it already drops to 50% at a deviation of 60°.

The two counteracting effects on fiber effectiveness can therefore partially neutralize each other. Although this expands the range of effective fiber orientation, it makes it more difficult to specify a narrow fiber angle spectrum. However, the tensile load-bearing behavior of UHPFRC cannot be directly derived from the bond behavior of single fibers, since further effects from scattering of the local fiber distribution and the bond behavior of fiber groups cannot be quantified in a universally valid way [25]. Nevertheless, it is a general principle that a fiber orientation parallel to the tensile direction causes an almost linear force decrease in the fiber pull-out phase, and a fiber inclination up to about 45° keeps the tensile forces longer due to fiber redirection - with increased damage to the matrix. A fiber inclination of 45° and above makes crack-bridging force transmission more difficult and faces the risk of being abruptly terminated by fiber rupture [26].

Process parameters

The analyses presented above demonstrate that, in addition to the selection of a suitable

fiber-matrix combination, fine adjustment of the process parameters of the MFA process is also necessary to achieve a significant increase in the performance of UHPFRC components.

These process parameters were investigated at ITE using two main experimental methods.

A transparent substitute for the liquid UHPC matrix based on glucose syrup was developed to allow immediate visual control of the influence of the magnetic fields on the movement of the fibers. The formulation was adapted to the consistency of the liquid UHPC using modified penetration tests of needles according to Vicat [27] and in spreading tests with the Hägermann cone. Although these two test methods are originally used for the determination of the setting time and yield stress, they could serve here for an approximation of the substitute to the used UHPC: The vacuum-deaerated mixture of glucose syrup 43° and 45° in the mixing ratio 23:77 corresponded to the UHPC matrix at a temperature of 20°C in both test methods with a deviation of penetration time (weight: 300 g, steelball, diameter: 10mm; travel: 40 mm) and slump flow spread (meassurement after 8 min.) of ± 4% each. This substitute replaced a previously used ultrasonic gel based hydrogel and could be used to to narrow the process parameters.

The second method was based on the capabilities of 3D image processing. In a parameter study on 27 UHPFRC specimens, the three most important process parameters of travel speed, magnetic field strength and component thickness were investigated. Micro-computed tomography (µCT) was used to acquire the MSF in the cuboid specimens (40 x 40 x 15/20/30 mm). The use of the Amira-Avizo 3D [28] and Fiji [29] software solutions allowed the accurate and automated analysis of the MSF in terms of their distribution, location and orientation in the specimens, allowing the interaction of the three process parameters to be assessed and quantified. Special attention was paid to the evaluation of the mentioned fiber orientation coefficient, which describes the influence of the orientation on the effectiveness of the fiber in a certain axial direction [30], as well as the fiber distribution along the cross-section of the specimens.

As mentioned, two magnets were used in the experiments: MAG 1 had dimensions of 40 × 40 × 80 mm and grade N 45. The north and south poles of the magnet were located at the end of the long central axis, respectively. In a first step, its strong pole side was used to move the randomly distributed MSF from the specimen cross-section toward a cross-section side. The intensity of the fiber movements could be controlled with the travel speed of the end effector. With its edge length of 50 mm, the cube magnet MAG 2 generates a broader magnetic field than the pole side of Mag 1. Its long side could be used in a second step to rotate the locally concentrated MSF into an angular range parallel to the formwork face. In this way, reinforcement layers could be designed in the tensile zones of specimens whose individual fibers, arranged along the tensile trajectories, lay in an angular range of 0°- 45°. In this way, reinforcement layers could be designed in the tensile zones of specimens whose individual fibers, arranged along the tensile trajectories, lay in an effective angular range of 0°- 45°. The angular range could even be limited to 0°- 15° by adjusting the parameters, and the strands could be compacted down to a fiber content of 10% by volume (Figure 6 (left)). A numerical approach to include this fiber distribution, which is not nonhomogeneous across the cross section, in the calculation of the flexural strength is explained in [3, 31].

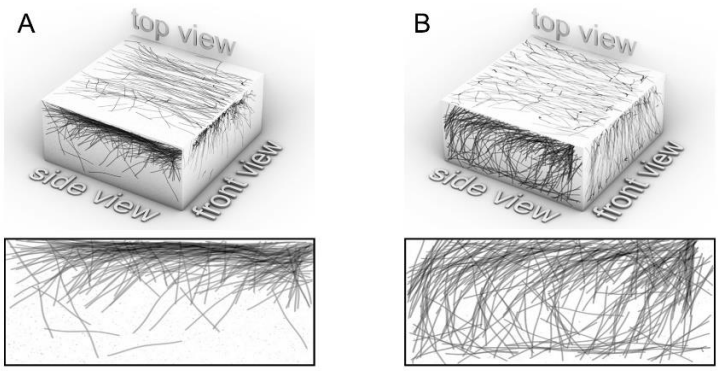

Figure 6. Visualization of µCT images of A: concentrated fiber strand (left);

B: fiber strand distributed over the entire cross-section (right)

For component thicknesses of or below 30 mm, such as the dog-bones investigated, an alignment uniformly distributed over the cross-section was achieved with fiber angles deviating only moderately from the tensile direction (Fig. 6 (right)). By fine tuning the parameters of traverse speed, magnet spacing and magnet change, homogeneous and efficient fiber strands could be modeled, especially at higher fiber contents from 2.5% by volume. The gaps between parallel strands could be reduced to 20% of the magnet widths without pronounced mutual interference between the parallel strands during modeling. In these gaps, the formation of three-dimensional transverse ribs could be observed, which formed an arc- or s-shaped bond between the strands depending on the path directions. Since the magnetic field strength of the used magnets at a distance of 30 mm is only about 39% (long side) or 19% (pole side) of the magnet surface (see Figure 2, left), a magnetic treatment on both sides is suitable for components with cross sections larger then 30mm.

Production of the test specimens

All UHPFRC mixtures were produced with a planetary mixer using a flat paddle mixer. The horizontal formworks were filled with shovels from above. In order to exclude the influence of a dominant flow direction and to achieve a fiber concentration as homogeneous as possible without local imperfections, overlapping portions of about 100 ml each were poured in. After a five-minute venting period under low-frequency vibration, the formwork was closed with screws. This was followed by the automated MFA, also in a horizontal position, within a maximum of 35 minutes after the end of mixing. Hardening of all test specimens took place in an upright position at about 20 °C. They were stripped after 48 hours and stored in a moist place until they were tested after 28 days. For the consistency test, the target mini slump flow spread of 270 ± 10 mm was checked with the Hägermann cone without shocks in parallel with the filling of the formwork. In case of deviations, the formworks were cleared and a new mix was prepared.

Centric tensile tests

The effect of near-surface fiber concentration can be used for components that are exposed to a one-sided bending load. For this, detailed experimental and numerical investigations have already been carried out at ITE [3]. However, in order to perform measurements cleaned from this effect regarding the actual tensile load capacities, an experimental setup for centric tensile tests was developed for UHPFRC components of small thickness. Figure 7 (left) shows the geometry of the dog-bones with a linear robot path (red dashed line), the articulated sliding supports on both sides for fixation during the tensile test (center), and the modular design of the formwork (right). The MFA procedure was carried out on one side with the formwork lying flat. In order to quantify the influence of the formwork edges on the fiber orientation and thus the expected increase in tensile strength described in [32], dog-bones of

three different thicknesses were investigated. The tensile tests were performed on a tensile testing machine of the IAM, TU Braunschweig with a 50 kN load cell (accuracy class 0.5 ISO 7500-1) at a speed of v = 0.15 mm/min and a measuring rate of about 10 Hz. Machine force and the machine path were recorded.

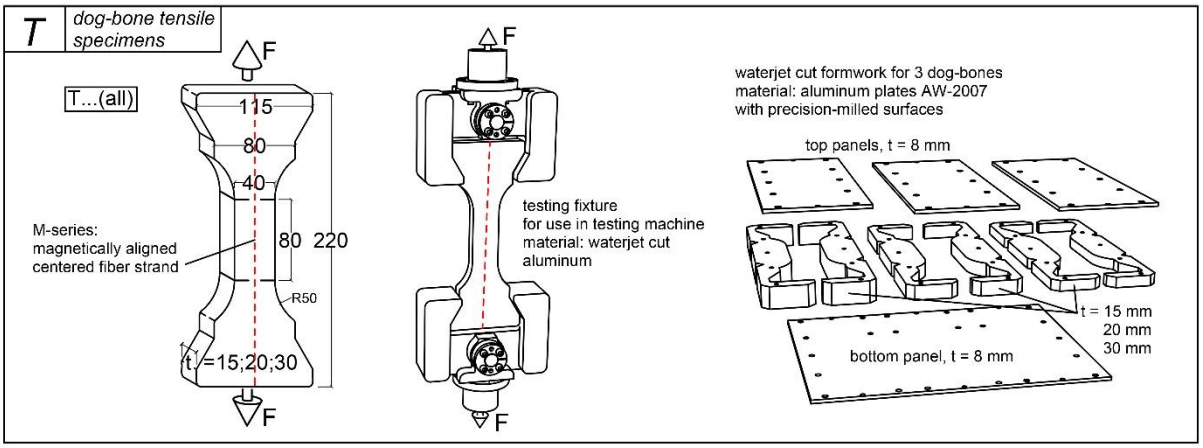

Figure 7. Shape and dimensions of the dog-bones (left), testing fixture (middle)

and construction of the formwork (right)

In this series of tests, a total of 24 dog-bones were tested. Three different thicknesses of dog-bones, four different fiber contents, two different fiber types, as well as dog-bones treated with the MFA process (M) and not treated (R) were varied. Table 4 lists all the specimens, as well as the results on the measurements performed. There are nine pairs of magnetically treated and non-treated dog-bones, whose measured values were directly compared in the lines *increase [%].*

Table 4. Measured values from the tensile tests and comparative performance increase

T	reinforcement quantity [Vol%] and (type)*	type R or M **/ increase M to R	specimen thickness t [mm]								
			15			20			30		
			stress σM [MPa]	strain εM [%]	w to (εM) [kJ]	stress σM [MPa]	strain εM [%]	w to (εM) [kJ]	stress σM [MPa]	strain εM [%]	w to (εM) [kJ]
no.1-	1,0 (MSF 8)	R	4,1	1,4	1,8	4,1	0,9	1,0	4,7	0,8	1,9
2-		M	4,3	1,7	2,1	4,2	1,4	2,5	5,8	1,3	3,8
		increase [%]	**7**	**21**	**14**	**1**	**55**	**159**	**23**	**63**	**97**
3-	1,75 (MSF 8)	M	7,6	1,9	4,0	6,4	1,3	6,9	6,3	1,6	6,1
4-	2,5 (MSF 8)	M	8,0	1,1	2,4	9,3	2,6	2,1	7,7	1,5	5,5
5-	3,5 (MSF 8)	R	5,9	1,7	1,8	8,6	1,6	5,0	6,0	1,1	3,3
6-		M	14,3	2,0	6,2	14,5	2,5	11,5	15,5	3,5	29,9
		increase [%]	**42**	**18**	**237**	**68**	**56**	**128**	**157**	**218**	**800**
7-	4,5 (Rec)	R	6,0	1,2	1,7	7,0	0,8	1,8	7,0	1,1	5,1
8-		M	8,3	1,4	2,5	7,3	1,7	3,9	8,5	1,7	7,6
		increase [%]	**38**	**17**	**49**	**4**	**113**	**112**	**21**	**55**	**49**
24 specimens, e.g. name 1-a: T 1,0 R (t 15)			*a*			*b*			*c*		

** MSF 8: micro steel fibers, 8mm; Rec: recyceled steel fibers*

*** R: random fiber distribution and orientation; M: magnetically controlled fiber distribution and orientation*

Since the focus of the investigations was on the performance increase due to the MFA process, the tests were carried out with reduced measurement technology. Therefore, no further measurement data was collected with strain gauges or optical measurement. And since only one dog-bone type was produced at a time and the test results of UHPFRC specimens are generally subject to large scatter, no generally valid conclusions for construction practice can be derived from the measurements shown here. Nevertheless, there were the following clear

trends:

- All specimens treated with the MFA procedure showed higher maximum tensile stress (σM), strain (εM) and work (w up to εM) than the non-treated specimens at the same fiber content and MSF type.
- The measurements of the maximum tensile stresses did not show a clear correlation with the dog-bone thickness and thus of an influence of the formwork edges.
- The measured values of the series with the recycled fibers "4.5 (REC) M" are on average similar to those of the series "2.5 (MSF 8) M", which in this case would mean an increase of the fiber content of the Rec fibers by about 80% compared to the MSF 8.
- All measured values of the "2.5 (MSF 8) M" series are clearly above those of the "3.5 (MSF 8) R" series. Thus, in this case, at least 1% by volume, or a fiber content of 40%, could be saved by the MFA process. This level of savings potential is also basically in agreement with the results of previous bending tensile tests [3].

Figure 8 (left, right) compares the series "1.0 (MSF 8) M", "1.0 (MSF 8) R", "3.5 (MSF 8) M" and "3.5 (MSF 8) R". The marked average max. tensile stresses of the respective series illustrate the increasing effect of the MFA process with increasing fiber content. The measured maximum tensile stresses of the "3.5 (MSF 8) M" series are higher than all measurement results of comparable tests on UHPFRC dog-bones listed in [33]. CT scans of the dog-bone T 3.5 M (t30) confirmed the particularly high homogeneous and parallel fiber alignment and distinct multicrack formation.

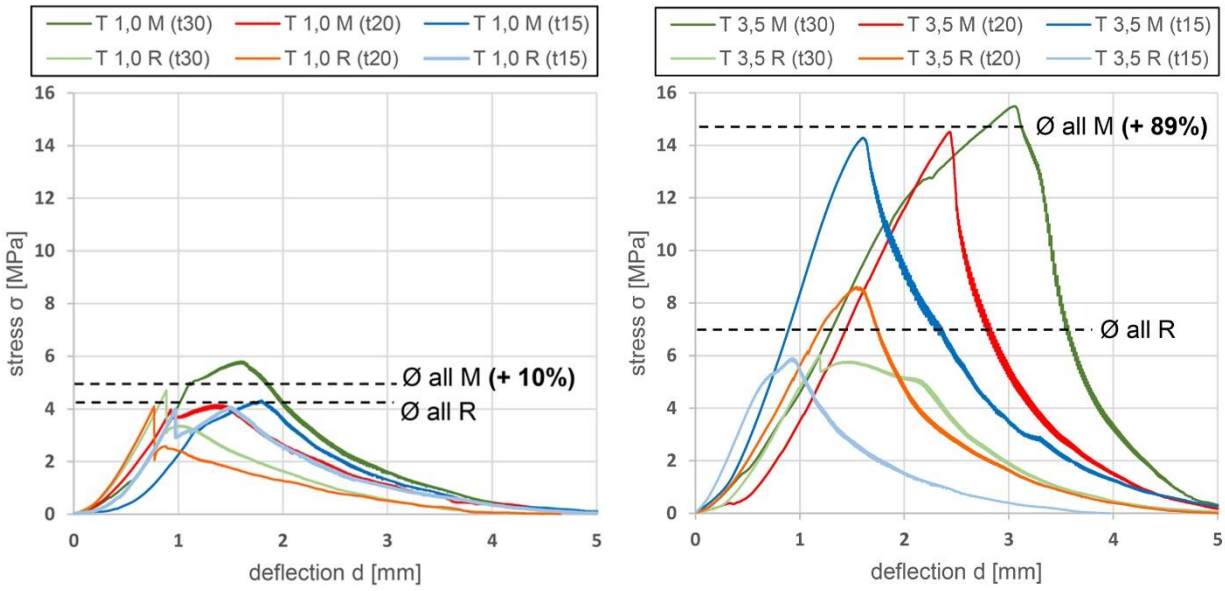

Figure 8. Stress-elongiation diagram of M and R series, fiber content 1% by volume (left);

stress-strain diagram of M and R series, fiber content 3.5% by volume (right)

Figure 9 shows the maximum tensile stresses reached in all 24 dog-bones tested in relation to the fiber content. It indicates that the fiber effectiveness of the M series treated with the MFA process (MSF 8) increases overproportionally with increasing fiber content, and that the MVA process is particularly effective with higher fiber contents. However, this does not apply to the same extent to the treated dog-bones with recycled fibers. Here, despite the high fiber content, only a smaller mean increase in the maximum tensile stresses of 21% was recorded.

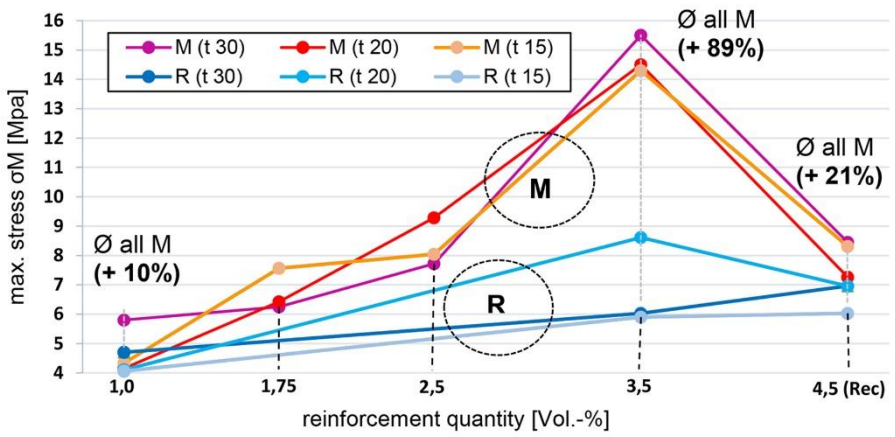

Figure 9. Maximum tensile stresses in relation to fiber content of both MFA-treated (M) and non-treated (R) dog-bones

Economic and ecological savings potential

On the basis of the centric tensile tests described above, it is possible to derive both economic and ecological savings potentials that result from the reduction of the fiber content. The magnitude of these savings depends to a large extent on the formulation of the UHPFRC under consideration. Figure 10 (left) shows the widely varying cost contribution of MSF to the concrete formulation used at a fiber content of 2.5% by volume. In the centric tensile tests, MSF of Scenario 1 (Stratec) and 4 (Genan) were used. In Scenario 2 and 3, the costs of comparable products from competitors were applied. The economic savings potential of the pure material costs of all four scenarios can be estimated as follows according to the test results:

The 40% reduction in fiber content achieved with the MFA process in the tests reduces the total cost of the UHPFRC by 24% in Scenario 1, 18% in Scenario 2, and 12% in scenario 3. Despite the 80% increase in recycled fiber content required for equivalent performance of the UHPFRC compared to the 2.5% by volume fiber content of brand-new MSG 8, the total cost of the UHPFRC would be reduced by 55% in scenario 1, 38% in scenario 2, and 20% in scenario 3.

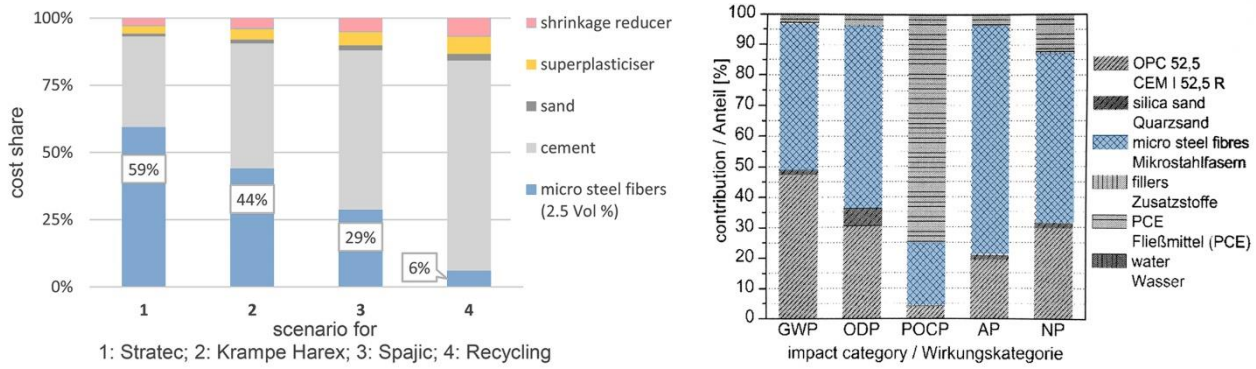

Figure 10. Cost share of 2.5% by volume of MSF from different suppliers (left); Dominance analysis for the production of an average UHPC (from [34], colorized)

Figure 10 (right) compares the shares of the individual UHPFRC ingredients of an average UHPC in different impact categories. In four of the five impact categories, the share of MSF occupies more than 50% and ranks first, even ahead of cement. Thus, the magnitude of the environmental savings potential resulting from the reduction of the fiber content is compara-

ble to the economic savings of scenario 1.

The sustainability analysis carried out in [34] divides the environmental impact of the production of MSF into the sub-processes wet drawing (40- 50%), production of the electrical steel (30-40%) and hot rolling and stranding (2 - 20%). Replacing new MSF with recycled MSF offers high environmental savings potential, as these fibers have already undergone all energy-intensive manufacturing processes. However, their non-ideal geomtrical properties in terms of length, diameter and straightness increase the necessary fiber content compared to uniform brandnew MSF. On the one hand, this resulted in poorer processability in the mixing process, and on the other hand, they therefore also showed lower performance in the transmission of tensile forces. However, since a satisfactory life cycle assessment of structures made of UHPFRC compared to structures made of normal concrete is mainly achieved by the potentially longer service life, the use of a higher fiber content is put into perspective.

Conclusion and outlook

The aim of the research described is to create the basis for the production of resource-efficient components with the aid of the controlled, automated magnetic distribution and orientation of MSF in UHPFRC. This defined arrangement of fibers significantly increases the efficiency of the fiber content used in a component and can thus lead to a large increase in performance or a significant reduction in the MFS used. As a result, in addition to improved processability of the UHPFRC, there is a large potential for saving ecological and economic resources, which can be significantly increased by using recycled MSF. In the future, the reproducible control of the process, which is to be ensured by using the latest developments in the field of automated production, will be decisive for an economical, practical construction application of the process, which has already been tested on a laboratory scale.

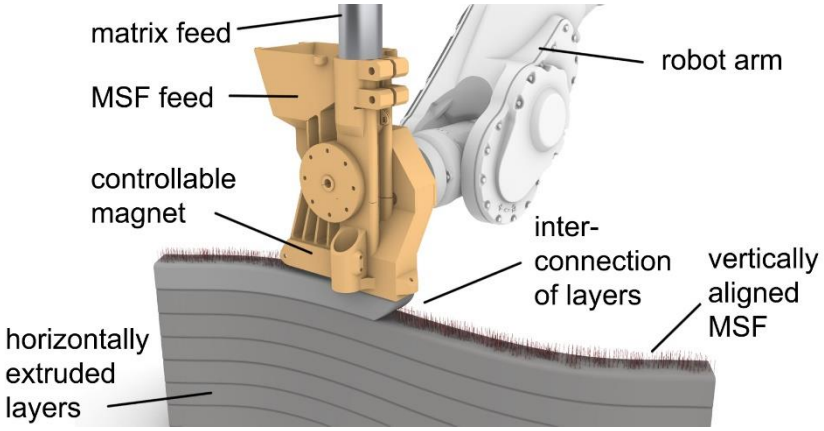

Figure 11. Illustration of a novel end effector for MFA integrated in layered extrusion

Beyond the application of the process for components made of UHPFRC cast in molds, the use of the principle of MFA in modified form is also possible in the additive manufacturing (AM) of concrete components. For example, initial trial runs of the technique in a combined process with Shotcrete 3D Printing (SC3DP) [35], developed at DBFL, have already shown promising results, providing clear indications of a possible novel reinforcement strategy for concrete components manufactured without formwork.

In addition, the application of the MFA process in other AM methods is currently being investigated at the ITE. The first end effectors for the integration of MFA into 3D concrete printing approaches based on layered extrusion and selective binding have already been produced and are now to be tested. In this context also the use of vertically oriented MSF is being investigated to avoid cold joints between extruded horizontal layers, as shown in Figure 11. One of the larger challenges in transferring the MFA process to AM construction methods without formwork is the higher viscosity of AM concrete formulations compared to fresh

UHPFRC. Therefore, an approach is presently pursued to reduce the viscosity of the matrix locally and for a short time during the printing process and thereby achieve a higher agility of the magnetically stimulated MSF.

The research field of magnetic fiber alignment thus has the potential to be extended beyond the application possibilities described to other innovative construction methods and contribute to the development of more resource-efficient concrete structures.

Data availability statement

All data generated or analysed during this study are included in this published article.

Author contributions

L. L. designed and performed the experiments, analysed the data and wrote the manusript. A. B. helped supervise the project. H. K. supervised the project.

Competing interests

The authors declare no competing interests.

Acknowledgement

The authors would like to thank the German Research Foundation (DFG) for funding the project "Fundamental investigations on robot-assisted magnetic distribution and alignment of microsteel fibers in thin-walled UHPFRC components".

References

1. M. Schmidt and E. Fehling, Eds., Entwicklung, Dauerhaftigkeit und Berechnung ultrahochfester Betone (UHPC): Forschungsbericht DFG FE 4971-1. Kassel: Kassel Univ. Press, 2005.
2. Nachrichten — SPP 1542. [Online]. Available: https://spp1542.tu-dresden.de/ (accessed: Sep. 30 2021).
3. L. Ledderose, S. Lehmberg, H. Budelmann, and H. Kloft, “Robotergestützte, magnetische Ausrichtung von Mikro-Stahldrahtfasern in dünnwandigen UHPFRC-Bauteilen,” Beton- und Stahlbetonbau, vol. 114, no. 1, pp. 33–42, 2019. https://doi.org/10.1002/best.201800083
4. Ledderose, L.; Kloft, H.: Snap-fits made of reinforced concrete: From advanced manufacturing to novel applications. Conference: Proceedings of the IASS Symposium “Creativity in Structural Design”. 16.-20.7.2018, Boston, 2018.
5. Ledderose, L.; Kloft, H.: Preliminary Investigations for Magnetic rearrangement of Steel Fibers in UHPFRC. Conference: Proceedings of the IASS Symposium „Shells, Membranes and Spatial Structures: Footprints.“, 15.-19.9.2014, Brasil, 2014.
6. Ledderose, L.; Kloft, H.: Robot-aided rearrangement of steel fibres in UHPFRC via magnetic forces. Conference: Future Visions – Proceedings of the IASS Symposium 2015 & ISOFF Symposium, 17.- 20.8. & 16.- 17.8.2015, Amsterdam, 2015, paper No. IASS2015-517423, S. 12 – ISBN: 9789053630426.
7. S. Lehmberg, L. Ledderose, F. Wirth, H. Budelmann, and H. Kloft, “Von der Bauteilfügung zu leichten Tragwerken: Trocken gefügte Flächenelemente aus UHPFRC,” Beton- und Stahlbetonbau, vol. 111, no. 12, pp. 806–815, 2016, doi: https://www.doi.org/10.1002/best.201600053.

8. F. Fingerloos, J.-D. Wörner, and K. Bergmeister, Eds., Beton-Kalender 2013: Lebensdauer und Instandsetzung, Brandschutz. Berlin: Ernst & Sohn, 2013.
9. DIN EN 10025-2:2019-10, Warmgewalzte Erzeugnisse aus Baustählen_- Teil_2: Technische Lieferbedingungen für unlegierte Baustähle; Deutsche Fassung EN_10025-2:2019, Berlin.
10. DIN EN 14889-1:2006-11, Fasern für Beton_- Teil_1: Stahlfasern_- Begriffe, Festlegungen und Konformität; Deutsche Fassung EN_14889-1:2006, Berlin.
11. S. Heinemeyer, Zum Trag- und Verformungsverhalten von Verbundträgern aus ultrahochfestem Beton mit Verbundleisten. Dissertation, RWTH Aachen, 2011.
12. C. Achilleos, D. Hadjimitsis, K. Neocleous, K. Pilakoutas, P. O. Neophytou, and S. Kallis, "Proportioning of Steel Fibre Reinforced Concrete Mixes for Pavement Construction and Their Impact on Environment and Cost," Sustainability, vol. 3, no. 7, pp. 965–983, 2011, doi: https://www.doi.org/10.3390/su3070965.
13. G. Graeff, K. Pilakoutas, K. Neocleous, and M. V. N. Peres, "Fatigue resistance and cracking mechanism of concrete pavements reinforced with recycled steel fibres recovered from post-consumer tyres," Engineering Structures, vol. 45, pp. 385–395, 2012, doi: https://www.doi.org/10.1016/j.engstruct.2012.06.030.
14. Genan, Genan - umweltfreundliches Altreifenrecycling. [Online]. Available: https://www.genan.de/ (accessed: Sep. 28 2021).
15. FEMM, HomePage: Finite Element Method Magnetics. [Online]. Available: https://www.femm.info/wiki/HomePage (accessed: Sep. 28 2021).
16. J. N. Luo and E. G. Sheu, "Physical Properties, Toxicity, and Physiological Effects of Magnets," in Magnetic Surgery, M. Gagner, Ed., Cham: Springer International Publishing, 2021, doi: https://doi.org/10.1007/978-3-030-73947-8
17. G. Bertram, Zum Verbund- und Querkrafttragverhalten von Spannbetonträgern aus ultra-hochfestem Beton. Zugl.: Aachen, Techn. Hochsch., Diss., 2012, 1st ed. Aachen: Eigenverl., 2012.
18. B. Frettlöhr, Bemessung von Bauteilen aus ultrahochfestem Faserfeinkornbeton (UHFFB). @Stuttgart, Univ., Diss., 2011. [Online]. Available: http://nbn-resolving.de/urn:nbn:de:bsz:93-opus-71514
19. J. Bonzel and M. Schmidt, Verteilung und Orientierung von Stahlfasern im Beton und ihr Einfluß auf die Eigenschaften von Stahlfaserbeton. Beton 34 (1984), S. 463-470.
20. G. Bernier and M. Behloul, "Effet de l'orientation des fibres sur le comportement mécanique des BPR.," 1996.
21. T. Stengel, Effect of Surface Roughness on the Steel Fibre Bonding in Ultra High Performance Concrete (UHPC), Nanotechnology in Construction 3. Springer, Berlin, Heidelberg, 2009. 371-376, doi: https://www.doi.org/10.1007/978-3-642-00980-8_50
22. T. Pfyl, Tragverhalten von Stahlfaserbeton. Zugl.: Zürich, Eidgenössische Techn. Hochsch., Diss., 2002. Zürich: vdf Hochsch.-Verl. an der ETH, 2003.
    I. Marković, High-Performance hybrid-fibre concrete: Development and utilisation. Zugl.: Delft, Techn. Univ., Diss., 2006. Delft: DUP Science, 2006.
23. T. Stengel, P. Schießl, C. Gehlen, and J. C. Walraven, Verbundverhalten und mechanische Leistungsfähigkeit von Stahlfasern in ultrahochfestem Beton. München, Technische Universität München, Diss., 2013. München: Universitätsbibliothek der TU München, 2013.
24. S. Stürwald, Rissentwicklung bei kombiniert bewehrten UHPC Balken. Kassel: Kassel Univ. Press, 2012.
25. S. Stürwald, "Versuche zum Biegetragverhalten von UHPC mit kombinierter Bewehrung; Forschungsbericht Fachgebiet Massivbau Fachbereich Bauingenieurwesen Universität Kassel," 2011.
26. DIN EN 196-3:2017-03, Prüfverfahren für Zement_- Teil_3: Bestimmung der Erstarrungszeiten und der Raumbeständigkeit; Deutsche Fassung EN_196-3:2016, Berlin.
27. Amira-Avizo 3D Software | Thermo Fisher Scientific. [Online]. Available: https://www.fei.com/software/avizo3d/%C2%A0#gsc.tab=0 (accessed: Sep. 29 2021).
28. Fiji. [Online]. Available: https://imagej.net/software/fiji/ (accessed: Sep. 29 2021).

29. J. Schnell, K. Schladitz, and F. Schuler, “Richtungsanalyse von Fasern in Betonen auf Basis der Computer-Tomographie,” BUST, vol. 105, no. 2, pp. 72–77, 2010, doi: https://doi.org/10.1002/best.200900055
30. S. Lehmberg, “Herstellung und Eigenschaften von dünnwandigen, trocken gefügten Bauteilen aus ultrahochfestem faserverstärkten Feinkornbeton,” Dissertation, TU Braunschweig, 2018.
31. SETRA, AFAC, Bétons fibrés à ultra-hautes performances, Recommandations, Revised edition, June 2013.
32. M. M. Reichel, Dünnwandige Segmentfertigteilbauweisen im Brückenbau aus gefasertem Ultrahochleistungsbeton (UHFB). Zugl.: Graz, Techn. Univ., Diss. Graz:, (Anhang 2) 2011.
33. T. Stengel, P. Schießl, „Sustainability analysisof UHPC using inventory analysis and impact assessment“, in Nachhaltiges Bauen mit ultra-hochfestem Beton: Ergebnisse des Schwerpunktprogrammes 1182. M. Schmidt, E. Fehling, and S. Fröhlich, Eds, Kassel: Kassel Univ. Press, 2014.
34. Lindemann, H.; Gerbers, R.; Ibrahim, S.; Dietrich F.; Dröder, K.; Raatz, A.; Kloft, H.: Development of a shotcrete 3D-printing (SC3DP) technology for Additive Manufacturing of reinforced freedom concrete structures. First RILEM International Conference on Concrete and Digital Fabrication – Digital Concrete 2018, Zürich: Springer, 2018.

Vision and Strategies for Reinforcing Additively Manufactured Concrete Structures

Visions

https://doi.org/10.52825/ocp.v1i.84

Submitted: 7 Dec. 2021 | Published: 15 Feb. 2022

Felt-Concrete Composites in Architecture and Design

Mirco Becker[1][https://orcid.org/0000-0001-8488-2108]

[1] Leibniz University Hannover, Germany

Abstract. The paper explores the possibilities of a composite of needle-felt fibres and cement-based matrix for designing and fabricating architectural elements. It summarizes the longer standing design-research undertaking in needle-felting as a novel method for creating materially graded objects without the use of formwork. The work is conducted on a design prototype of a chair to emphasise the integrative nature of this material system. This approach allows the study of all aspects from the fabrication process, the function of details, structural behaviour, and user experience.

Needle fleeting has a long tradition in arts and craft for manually forming intricate objects such as figurines or applying ornaments to textile objects. The main feature of felt material is that it can bring fibrous material into a stable shape. This process has been digitized by Disney Research proposing needle felting as a way of 3D-printing fibrous material [1]. Becker et al. also proposed a robotic process for robotically 3D-printing felt shapes [2] which form the base for a material composite of felt-fibers and a cement based matrix. Their paper argues for functionally graded architectural elements where the composite of felt and cement can provide for tensile reinforcement, compressive strength, insulation, and different haptic surfaces. Based these methods here a replica of IKEA® Leifarne chair is realized, showcasing a range of felt-concrete composite applications integrated in a single object.

Keywords: Felt, Textile Concrete, Material Grading, 3D-Printing

Conference presentation video: https://doi.org/10.5446/56105

Competing interests

The author declares no competing interests.

References

1. S.E. Hudson, Printing Teddy Bears: A Technique for 3D Printing of Soft Interactive Objects, CHI'14 Proceedings of the SIGCHI Conference on Human Factors in Computing Systems, pp. 459-468, 2014, doi: https://doi.org/10.1145/2556288.2557338
2. M. Becker, Matrix application processes for RoboFelt, Proceedings of the IASS Symposium 2018, Creativity in Structural Design, July 16-20, 2018, MIT, Boston, USA